Ocean circulation and climate at the Eemian and last glacial inception

Andreas Born

Dissertation for the degree of Philosophiae Doctor (PhD)

Geophysical Institute, University of Bergen, Norway

Look again at that dot. That's here. That's home. That's us. On it everyone you love, everyone you know, everyone you ever heard of, every human being who ever was, lived out their lives. The aggregate of our joy and suffering, thousands of confident religions, ideologies, and economic doctrines, every hunter and forager, every hero and coward, every creator and destroyer of civilization, every king and peasant, every young couple in love, every mother and father, hopeful child, inventor and explorer, every teacher of morals, every corrupt politician, every "superstar", every "supreme leader", every saint and sinner in the history of our species lived there - on a mote of dust suspended in a sunbeam.

Carl Sagan: Pale Blue Dot

Acknowledgments

This thesis would not have been possible without the help of countless people. First, to my advisers at the Bjerknes Centre for Climate Research. Thank you, Kerim, for your consistent support during the last three years. Your commitment was a key to the success of this work. The value of your guidance concerning all aspects of this work is impossible to overestimate. But most importantly your positive attitude despite temporal set-backs and your availability for discussions at all times made working with you a very enjoyable experience. I am grateful also for your support, Tore, which found its way into many aspects of this thesis. And the details of proxy data analysis would still be a mystery to me if it had not been for your advice, Bjørg. Many more people at the Bjerknes Centre shared their knowledge with me: Jan Mangerud, John-Inge Svendsen, Trond Dokken, Ulysses Ninneman, Tor Eldevik and Kikki Kleiven. I am grateful to my colleagues and fellow students at the Geophysical Institute and Department of Geology for the friendly atmosphere, in particular Jürgen Bader for generous help on many occasions. Francesco, sharing an office with you made working here truly memorable.

A large part of this thesis is the result of collaborations outside the Bjerknes Centre. Masa Kageyama and Pascale Braconnot are gratefully acknowledged for hosting me at Laboratoire des Sciences du Climat et de l'Environnement and for active collaborations. I learned a lot about ice sheet modeling in discussions with Christophe Dumas, Didier Roche and Sylvie Charbit. My work also benefited from fruitful collaborations with Anders Levermann of the Potsdam Institute for Climate Impact Research, Marisa Montoya of Universidad Complutense de Madrid and Juliette Mignot of Laboratoire d'Océanographie et du Climat.

I have been lucky to be part of the Marie Curie network NICE. The three 'all-but-summer' schools and meetings are among the best memories of my dissertation. Thank you Gilles Ramstein and Céline Moncourtois for organizing what has been so much more than a network of professionals.

Last but not least, I would like to thank my family and friends, close and afar, for reminding me of the world beyond my computer screen. I would not be writing this text today without your tireless encouragement. Thank you Cristina for giving your unconditional support, for believing in me and for sharing my life. And thank you, Álvaro, for wise questions about the North Pole and why I have to spend such long hours at work to study the ice there. Johann, you joined us barely four months ago. You do not speak yet but your smiles somehow make studying ice on the North Pole seem utterly pointless. You are perfectly right. Good thing you will not be able to tell anybody until well after the defense...

Andreas Born
Bergen, July 2010

Abstract

Combining a hierarchy of climate models of varying complexity with marine proxy data, we show that the North Atlantic surface circulation played an important role for the climate of the Eemian and the last glacial inception. As insolation decreases, increasing Arctic sea ice export causes a freshwater transport into the subpolar North Atlantic. Amplified by a nonlinear response of the subpolar gyre this leads to a reorganization of the surface currents and a stronger heat transport into the Nordic Seas. The resulting warming of this region delayed Scandinavian inception. This work introduces a relatively new concept into the field of paleoceanography: the subpolar gyre as an active component of the climate system. This is based on recent advances in physical oceanography and allows for a new and physically consistent interpretation of proxy data. Moreover, the sensitivity of the subpolar gyre to different boundary conditions is discussed, improving the understanding of the underlying mechanism.

Contents

1 Introduction

Over the last 65 million years Earth has gradually cooled resulting in a climate characterized by large ice masses periodically covering high latitude continents (Zachos et al., 2001). These glaciations increased in amplitude and duration about 700,000 years ago (700 ka) with three large ice sheets over North America, Greenland and western Eurasia. Since then, glaciated periods last approximately 100,000 years, only interrupted by relatively short interglacials, when only the Greenland ice sheet is present, lasting from 10,000 to 30,000 years.

The Eemian interglacial between 130 ka and 115 ka is the last interglacial before the present. Climate is assumed to have been relatively similar to today, albeit probably 3 to 5°C warmer in high northern latitudes at its peak (126 ka) due to exceptionally high summer insolation (Fig. 1a) (Berger, 1978). As a result, the Greenland ice sheet was approximately one third smaller than today (Otto-Bliesner et al., 2006) and sea level 4 to 6 meters higher (Rostami et al., 2000; Muhs et al., 2002), with an uncertain contribution from the western Antarctic ice sheet (Scherer et al., 1998; Overpeck et al., 2006). Greenhouse gas concentrations were similar to pre-industrial levels (Fig. 1b).

Following Milankovitch's orbital theory, the transition from interglacial to glacial climate occurs in periods of low northern high latitude summer insolation, enabling snow to persist through the warm season and accumulate even more during the following winter (Milankovitch, 1941). Following the Eemian, insolation approaches a local minimum at about 115 ka, marking the beginning of the last glacial inception. However, since insolation changes are small, internal amplification by the climate system is necessary to build continental scale ice sheets.

Several lines of evidence point to the ocean as a potential amplifier of the insolation forcing (Ruddiman and McIntyre, 1975; Otterå and Drange, 2004; Risebrobakken et al., 2007). All known ice sheet nucleation sites are close to the ocean, especially the Atlantic and Arctic Oceans. Ocean currents transport large amounts of heat to high latitudes with important consequences both for

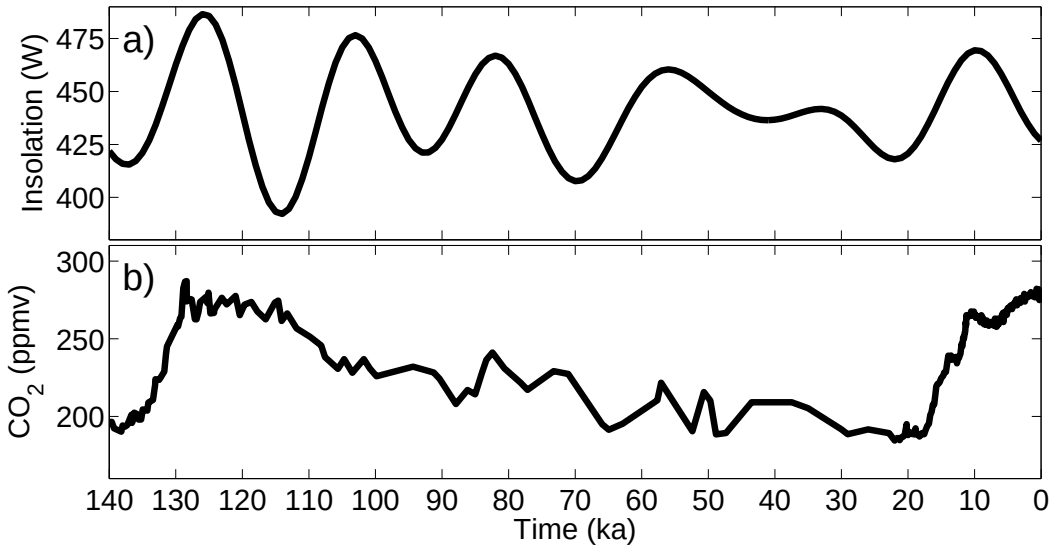

Figure 1: Summer insolation at 65°N **(a)** and atmospheric CO_2 concentration **(b)**. Insolation data by Berger and Loutre (1991), CO_2 by Petit et al. (1999); Monnin et al. (2001); Siegenthaler et al. (2005); Lüthi et al. (2008).

temperatures over coastal land and the extent of sea ice in the Arctic Ocean. The area covered by sea ice influences the amount of evaporation and thus the moisture source for ice growth. It has also been shown to impact large scale atmospheric circulation patterns (Li et al., 2005).

Hydrography and climate of the Nordic Seas and Arctic Ocean are strongly influenced by the exchanges with the Atlantic Ocean across the submarine ridge between Greenland and Scotland (Dickson and Brown, 1994; Hansen and Østerhus, 2000; Rahmstorf, 2002; Hansen et al., 2004). This ridge forms a barrier to the dense deep outflow from the Nordic Seas. Similarly, the inflow into the Nordic Seas is restricted mostly to the eastern side of the passage. Water masses flowing northward in this current are found to represent a mixture of subtropical and subpolar Atlantic waters (Hátún et al., 2005). While the contribution of subtropical water is relatively stable, the subpolar component shows pronounced variability in recent decades and probably also on millennial time scales throughout the Holocene (Thornalley et al., 2009), as a result of circulation changes of the subpolar gyre. Thus, the investigation of climatic

changes of the high latitude oceans requires a thorough understanding of the gyre circulation system.

This thesis investigates how the North Atlantic Ocean surface circulation and Arctic sea ice contribute to climate evolution of the last glacial inception. The underlying mechanisms are tested for other periods in time as well and in sensitivity experiments. The text is organized as follows: Section 2 provides an overview on orbital climate forcing, feedback mechanisms that potentially amplify the relatively weak forcing signal, and recent advances concerning the role of the subpolar gyre for climate variability. Based on this background information, the motivation for this thesis is outlined in section 3, followed by a summary of the main scientific results in section 4, and conclusions in section 5. A total of six research papers are included in this thesis and appended as manuscripts.

2 Background

2.1 Celestial mechanics and Climate, Milankovitch Theory

In theory, Earth's climate is a deterministic system that is effectually described by its boundary conditions: energy flux from the sun, dissipation of the moon's kinetic energy by tidal waves and radiochemical processes in the interior of the planet. The second is negligible, as well as the latter on all but the very longest time scales, thus making variations in solar power the most important driver of climate changes. However, besides the 11-year sun spot cycle, the sun's luminosity increases only slowly and gradually, about 10% every 1 billion years. A greater impact is caused by variations in the distribution of this energy between the equator and the poles which arise from cyclic changes in the Earth's orbit. Milankovitch first hypothesized that periodic reductions in northern high latitude summer solar irradiation (insolation) were instrumental for the growth of major ice sheets and thus the glacial-interglacial cycles

(Milankovitch, 1941). Strong support was found in the analysis of deep ocean sediment cores (Hays et al., 1976).

The complex changes in the Earth's orbit can be summarized in three fundamental cyclic movements (Fig. 2): The tilt (obliquity) of the Earth's rotational axis relative to the plane of rotation around the sun varies between 22.1°and 24.5°on a 41,000 year cycle. With greater tilt, insolation at the poles increases while it decreases at the equator, in phase in both northern and southern hemispheres.

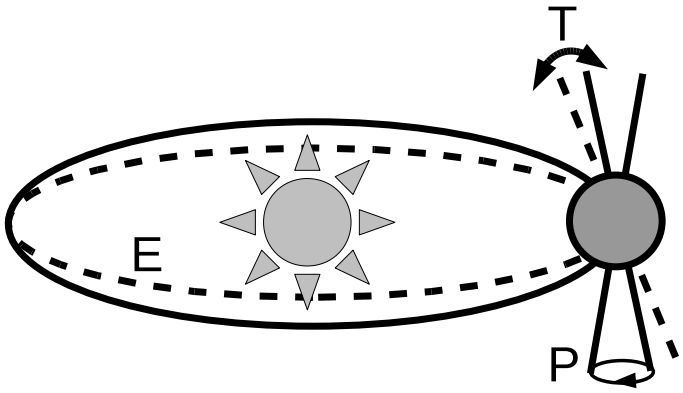

Figure 2: Variations of the Earth's orbital parameters: E denotes changes in eccentricity of the orbit, P the precession of the equinoxes and T changes in the tilt of the rotational axis.

The rotational axis is also subject to precession which does not change it's angle but the position of the equinoxes on the orbit around the sun. Since the orbit is elliptical, and distance from the sun and transition times are different for summer and winter seasons, precession modulates the length of the seasons as well as the seasonal insolation contrast. Summers are either relative cold and long, or warm and short. However, because the seasons in the two hemispheres are in exact antiphase, precession changes also have opposite sign. The period of precession of the Earth's axis is approximately 26,000 years. Precession also occurs in the orbital ellipse around the sun. This movement has the same effect on insolation and the superposition of the two effects shortens the overall cycle of precession to 21,000 years.

Table 1: Orbital parameters for the last interglacial and last glacial inception.

Time	Axial tilt (°)	Longitude of perihelion (°)	Eccentricity
126 ka	23.92	112.03	0.040
115 ka	22.40	291.72	0.041

Finally, the shape of the elliptic orbit around the sun changes with time. Increased eccentricity enhances the contrast between seasons, in antiphase for the two hemispheres, on periods of 100,000 and 400,000 years. Because the 'location' of the seasons around the orbit depends on precession, eccentricity changes can be thought of as modulating the precession cycle. With zero eccentricity, changes in precession become meaningless.

During the peak of the last interglacial at 126 ka, summer insolation at the top of the atmosphere at 65°N was at a local maximum, followed by a minimum at 115 ka (Fig. 1) (Berger, 1978). Low summer insolation at high northern latitudes is considered critical to the nucleation of large ice sheets. The decrease in summer insolation from 126 ka to 115 ka is due both to a change in precession and axial tilt (Table 1). The vernal equinox is rotated by 180°on the orbital ellipse, giving a relatively long but less intense summer season at 115 ka compensated for by a short and warm winter (Fig. 3). At the same time, the axial tilt is smaller at 115 ka, dampening the seasons mostly close to the poles and thus further cooling the northern hemisphere summer. The change in eccentricity is negligible.

2.2 Amplification of orbital forcing by feedback mechanisms

Previous model studies identified several potential feedback mechanisms amplifying the insolation signal. Retreating boreal forest over northern high latitude continents was found to increase albedo sufficiently to change local climate and favor ice growth (de Noblet et al., 1996; Meissner et al., 2003; Calov et al.,

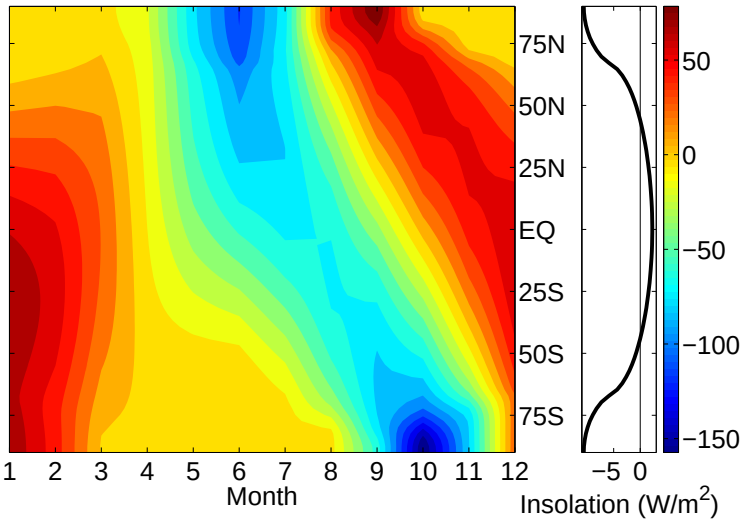

Figure 3: Incoming short wave radiation difference at the top of the atmosphere, 115 ka - 126 ka, in W/m^2. Left: Seasonal variations, right: annual average. The seasonal cycle was reduced in high northern latitudes and the Earth received less annual mean radiation poleward of 45° at 115 ka than at 126 ka.

2005; Kubatzki et al., 2006). Perennial snow cover is furthermore enhanced by an increased moisture convergence in the Arctic circle, as a result of less evaporation in a colder climate (Vettoretti and Peltier, 2003).

In addition to these mechanisms, several studies identified potential feedback mechanisms including changes in the strength of deep water formation and the Atlantic meridional overturning circulation. Realistic snow accumulation over the Canadian Arctic is only obtained in an atmospheric model with 116 ka sea surface conditions, and not with present day conditions (Yoshimori et al., 2002). Gröger et al. (2007) report that in their model experiments lower sea surface temperatures result in a higher density in the North Atlantic deep water formation regions at 115 ka and thus a more intense Atlantic meridional overturning circulation than at 126 ka. Calov et al. (2005) report a southward shift of Scandinavian land ice nucleation with a weaker Atlantic meridional overturning circulation.

Besides the direct effect of low annual average insolation at high latitudes,

the response of ocean circulation to changes in freshwater forcing has been investigated. One such study concludes that decreased sea ice melt at 115 ka yields higher salinities in the Nordic Seas sinking regions and intensifies the Atlantic meridional overturning circulation compared to 126 ka (Otterå and Drange, 2004). Similarly, less precipitation over the Arctic Ocean at 115 ka could have the same result (Khodri et al., 2003). An increasing Arctic sea ice cover as a result of a weaker Atlantic meridional overturning circulation has also been found to cool high northern latitudes and to favor accumulation of snow (Khodri et al., 2001). Proxy data studies, however, suggest that a persistent circulation might be crucial for building ice over Eurasia (Ruddiman and McIntyre, 1975; McManus et al., 2002; Risebrobakken et al., 2006).

2.3 The subpolar gyre as an active component of the climate system

While the importance of the Atlantic meridional overturning circulation in the climate system is beyond doubt, this two-dimensional simplification alone does not describe the complex system of ocean currents sufficiently. In particular, the northernmost limb of the overturning circulation, the inflow into the Nordic Seas connecting the Atlantic Ocean to the Arctic Ocean, was found to be modulated by the large scale surface circulation of the subpolar North Atlantic–the subpolar gyre (Fig. 4) (Hátún et al., 2005). This mechanism operated also on millennial time scales throughout the Holocene (Thornalley et al., 2009). Deep convection south of the Greenland Scotland ridge is directly related to the subpolar gyre (Eden and Willebrand, 2001; Levermann and Born, 2007; Lohmann et al., 2009), which has the potential to monitor AMOC changes (Häkkinen and Rhines, 2004; Böning et al., 2006; Zhang, 2008). Thus, a comprehensive understanding of climate variations clearly calls for a three-dimensional description, involving both the deep and surface circulation.

Observational estimates for subpolar gyre volume transport range from 25 Sv (Bacon, 1997) to 33.5 Sv (Clarke, 1984) (1 Sv = $10^6 m^3\ s^{-1}$), but these

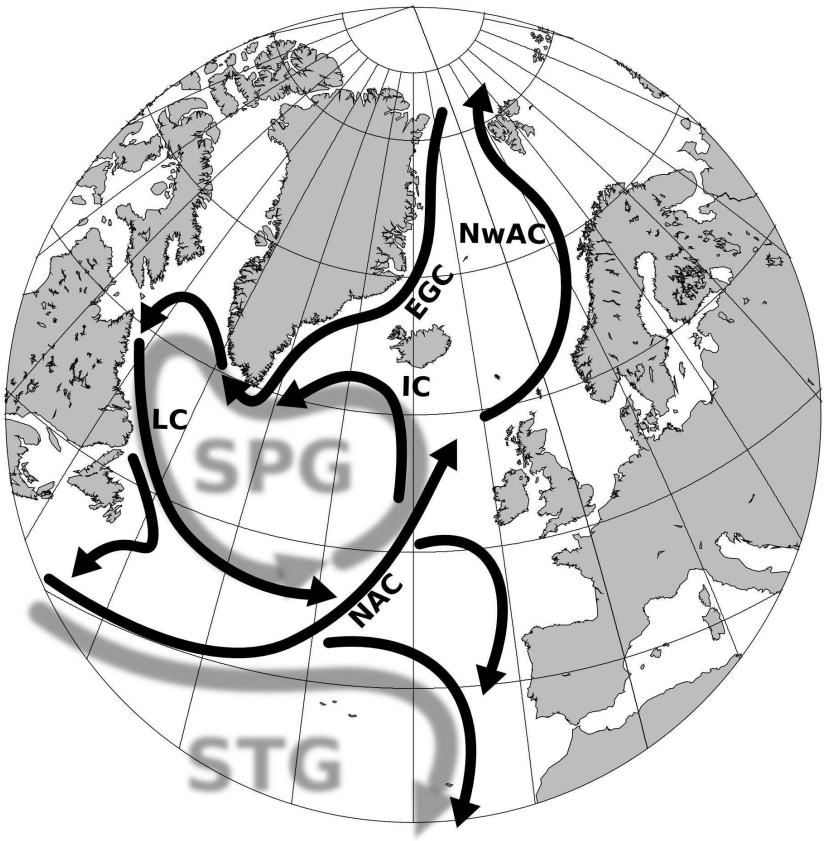

Figure 4: Map of the North Atlantic and Nordic Seas showing major ocean surface currents forming the subpolar gyre (SPG). Abbreviations: NAC, North Atlantic Current; NwAC, Norwegian Atlantic Current; EGC, East Greenland Current; LC, Labrador Current; IC, Irminger Current; STG, subtropical gyre.

likely underestimate the contribution of narrow coastal currents. High resolution models simulate a cyclonic circulation of approximately 40 Sv and more (Treguier et al., 2005). This can be compared to the overturning circulation volume transport of about 13 to 18 Sv (Ganachaud and Wunsch, 2000; Lumpkin and Speer, 2003; Talley et al., 2003; Wunsch and Heimbach, 2006; Cunningham et al., 2007).

While surface wind-stress has a large influence on its strength and variability (Curry et al., 1998; Böning et al., 2006), the subpolar gyre circulation is also controlled by baroclinic adjustments and therefore by the density structure in the subpolar North Atlantic (Mellor et al., 1982; Greatbatch et al., 1991; Myers et al., 1996; Penduff et al., 2000; Eden and Willebrand, 2001; Born et al., 2009). This has shown to have important consequences for the dynamics of the subpolar gyre, possibly leading to the existence of at least two stable circulation modes (Levermann and Born, 2007).

The underlying dynamics have been formulated conceptually in three positive feedback mechanisms (Fig. 5). First, a stronger gyre transports more tropical saline water into the subpolar region, as opposed to the Nordic Seas. This result is consistent with high-resolution model simulations (Hátún et al., 2005; Lohmann et al., 2009). Compared to a weaker gyre, less tropical waters are transported to the Nordic Seas, more recirculate in the subpolar gyre, making the center saltier. This increases the density gradient between the gyre and the relatively light exterior, sea surface elevation drops and the corresponding geostrophic response strengthens the circulation. Secondly, a stronger subpolar gyre results in stronger outcropping of isopycnals in the center of the gyre and more active deep convection. Therefore heat is removed more efficiently from the gyre's center which results in a cooling. This again increases the core density and therewith its strength.

In addition to these self-sustaining internal feedbacks, there exists an interaction with the deep outflow across the Greenland Scotland ridge. A stronger subpolar gyre reduces the salinity of the Atlantic inflow into the Nordic Seas. Thus, deep water formation north of the Greenland Scotland ridge weakens

and reduces the deep outflows. A less dense undercurrent results in stronger downwelling south of the ridge (Straneo, 2006; Spall, 2004; Deshayes et al., 2009). As a consequence, waters at the northern rim of the gyre get lighter, because they are fed by relatively light water that is formed south of the ridge as opposed to the dense overflow waters. This increases the density gradient across the gyre and enhances its strength.

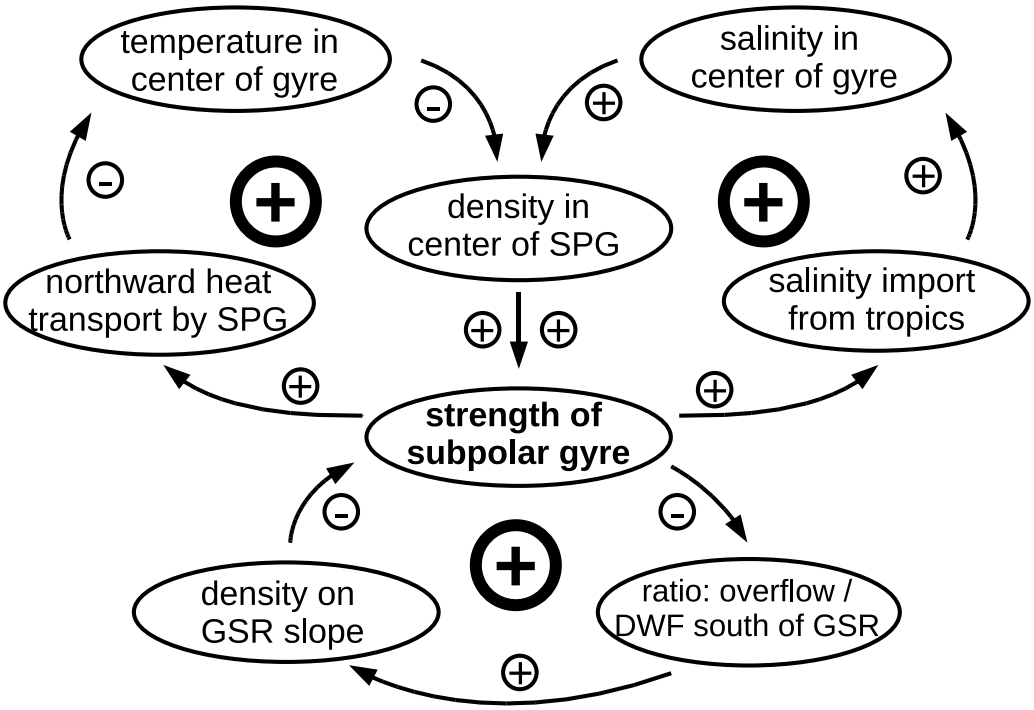

Figure 5: Three positive feedback mechanisms destabilize the subpolar gyre (Levermann and Born, 2007).

3 Motivation

This thesis addresses the role of the North Atlantic ocean circulation during the last glacial inception at 115 ka, using numerical models of varying complexity. The overall aim, however, goes beyond the simulation of specific periods of climate history into testing and advancing the relatively new hypothesis of the Atlantic subpolar gyre being an active component of the climate system. Paleoceanography has not kept up with physical oceanography in acknowledging this new understanding of the large scale surface circulation, despite the great explanatory power that this concept holds for proxy data. But benefit is mutual, as the study of past events has always brought forward the understanding of dynamic climate systems. This thesis represents an effort to narrow the gap between the two disciplines.

4 Summary of Results

The thesis is presented in six scientific papers that can be divided into two parts (see list on page 23). The first one (PAPERS I, II and III) addresses the climate evolution of the last glacial inception and the role of the ocean, combining coarse and high resolution climate modeling, ice sheet modeling, and discussion of marine and terrestrial proxy data. In accordance with the objectives outlined in the previous section, the analysis presented here is not restricted to the end of the last interglacial. The better coverage of marine proxy data for the Holocene than for the last interglacial allows for a more detailed study of the three-dimensional signature of subpolar gyre changes. In PAPER IV, a comprehensive discussion of data from the eastern and western North Atlantic, and the deep ocean is presented for the 8.2 ka event, the largest freshwater flood of the present interglacial. PAPERS V and VI investigate the driving mechanisms of the subpolar gyre under preindustrial and glacial boundary conditions, and the role of the subpolar gyre in decadal climate variability, complementing the description of its dynamics on shorter time

scales.

Based on two time slice simulations in a comprehensive coupled climate model, PAPER I establishes a causality between decreasing summer insolation at the last glacial inception and an abrupt reorganization of the subpolar surface circulation. As a direct result of weaker summer insolation, Arctic sea ice grows thicker and ice export in the East Greenland Current intensifies. The implicit freshwater transport into the subpolar North Atlantic reduces deep convection in the northwest Atlantic and thereby effectively changes the density structure of the region. This causes a nonlinear response of the subpolar gyre that amplifies freshening by sea ice.

This causal chain is reproduced in a coarse resolution coupled climate model in PAPER II. High computational efficiency of this model allows to test the physical mechanism proposed in the first paper in ensemble simulations and to expand previous work with a transient simulation of the period between 126 ka and 110 ka. The simulated temporal evolution shows that the weakening of the subpolar gyre results in a higher fraction of subtropical waters in the Atlantic inflow into the Nordic Seas and thus warming along the path of the Norwegian Atlantic Current. This mechanism is reversed when summer insolation increases again after 115 ka. Results compare favorably with marine sediment cores showing a clear late Eemian warming.

While a transient warm pulse in the Nordic Seas at the time of minimum insolation is consistent with two coupled climate models and marine proxy data, the consequence for land ice growth is still unclear. To address this question, PAPER III employs a three-dimensional ice sheet model forced by the simulated climate of the last glacial inception. The main result is that the strong heat transport into the Nordic Seas delayed glacial inception over Scandinavia. Ice started growing soon after this anomalous warm episode, in good agreement with available proxy data.

The concept of the subpolar gyre as an active component of the climate system allows for an improved understanding of proxy records beyond the last interglacial. In the example of the 8.2 ka event, addressed in PAPER IV, ac-

counting for a rapid change in the surface circulation resolves the apparent contradiction of increased freshwater inflow and enhanced deep water formation in the North Atlantic. This newly established causal relationship puts the 8.2 ka event into a new light, commonly regarded as a touchstone for the vulnerability of the Atlantic meridional overturning circulation to freshwater. While a temporary weakening of the overturning is beyond doubt, it might not have been as severe as previously thought.

The first four papers assume that the subpolar gyre is partly controlled by baroclinic adjustments and apply the resulting understanding to paleo events. Changes in wind stress are acknowledged throughout but consistently found to be negligible. In an effort to explicitly address the importance of stronger winds for the subpolar gyre, PAPER V investigates ensemble simulations with fixed observational wind stress multiplied globally by different factors between 0.5 and 2. The gyre transport is decomposed into Ekman, thermohaline, and bottom-transports. Two distinct regimes of the subpolar gyre are identified, depending on the existence of significant Greenland Scotland ridge overflows. These regimes largely correspond to the glacial and preindustrial ocean circulation pattern in this study but active overflows are also found with high wind stress amplification factors.

Finally, PAPER VI aims to identify the subpolar gyre feedbacks, originally described in a coarse resolution model, in a comprehensive coupled atmosphere ocean general circulation model. Important modifications are made to the original formulation, most notably on the characteristic time scales associated with the individual mechanisms. These delays form the basis for irregular decadal oscillations of the subpolar gyre and deep convection in its center. More intense air-sea coupling during convective events allows large scale atmospheric patterns to force the dynamical system stochastically. The analysis also suggests that the surface freshwater balance is critical for the pronounced variations of the subpolar gyre and that preindustrial climate is at a threshold defined by the feedback mechanisms. In the simulations of the Eemian and the last glacial inception with the same climate model, presented in PAPER I, the freshwater

budget of the subpolar North Atlantic is different with less and more sea ice transport compared to preindustrial climate. As a result, the strong and the weak subpolar gyre mode is stable without oscillations.

4.1 List of Papers

PAPER I

Sea ice induced changes in ocean circulation during the Eemian[1]
Born, A., K. H. Nisancioglu and P. Braconnot (2010)
Climate Dynamics, doi:10.1007/s00382-009-0709-2

PAPER II

Late Eemian warming in the Nordic Seas as seen in proxy data and climate models
Born, A., K. H. Nisancioglu, B. Risebrobakken and A. Levermann (2010)
Paleoceanography, (in revision)

PAPER III

Warm Nordic Seas delayed glacial inception in Scandinavia
Born, A., M. Kageyama and K. H. Nisancioglu (2010)
Climate of the Past, (submitted)

PAPER IV

The 8.2 ka event: abrupt transition of the subpolar gyre toward a modern North Atlantic circulation[2]
Born, A. and A. Levermann (2010)
Geochemistry Geophysics Geosystems **11**, Q06011

PAPER V

Reversed North Atlantic gyre dynamics in present and glacial climate[1]
Montoya, M., A. Born and A. Levermann (2010)
Climate Dynamics, doi:10.1007/s00382-009-0729-y

PAPER VI

The Atlantic subpolar gyre as a stochastically forced oscillator
Born, A. and J. Mignot (2010)
(manuscript in preparation)

[1]Reproduced with permission of the publisher
[2]Reproduced by permission of American Geophysical Union.

5 Conclusions and Perspective

The main conclusions of this study can be summarized in three points:

1) An improved understanding of the processes controlling the Atlantic inflow into the Nordic Seas allows for a physically consistent constraint on the advance of Scandinavian glaciers following the last interglacial. The role of the ocean for the last glacial inception over Scandinavia is investigated using coarse and high resolution climate models, an ice sheet model, and in combination with marine and terrestrial proxy data.

2) Recent advances in physical oceanography are successfully introduced into the paleoceanographic context. Rapid transitions of the large scale surface circulation, not only the deep overturning circulation, are used to improve our understanding of proxy data

3) The study of paleoclimate events and evidence for abrupt transitions of the subpolar gyre in response to known perturbations in the past improve the understanding of the underlying physical mechanisms and thresholds.

A comprehensive summary of the conclusions is found in the respective sections of the papers.

The understanding of the subpolar gyre presented is far from complete. Work presented here outlines the sensitivity of the subpolar gyre to changes in boundary conditions, as a consequence of self-amplifying feedbacks. At least two different modes of operation were identified that also differ in the strength of deep convection in the gyre's center. This indicates that thermal atmosphere-ocean coupling does not depend linearly on the background climate, but that qualitative shifts can occur, potentially decoupling a region of high atmospheric variability, the Labrador Sea, completely from the deep ocean in the case of a shut-down of deep convection. However, the question of how variability of the subpolar gyre is transferred to the deep ocean and consequences for the large scale meridional overturning circulation are not addressed here and require clarification.

Conclusions presented here are largely based on numerical models and the interpretation of proxy data with their inherent uncertainties. Comparison with instrumental observations could improve this approach significantly, but can not be used because the mechanisms highlighted work on relatively long time scales while observations cover only a few recent decades. PAPER VI represents an effort to overcome this gap and provide a hypothesis that can be tested with observations. Future work will need to address explicitly how variable atmospheric forcing, equivalent to stochastic noise from an ocean perspective, is communicated to the ocean. It is unclear how it modifies the stability of the two subpolar gyre regimes discussed here.

It was shown how the subpolar gyre evolves in response to orbital forcing at the end of the last interglacial (PAPER I and II) and that a major transition of the gyre occurred early during the present interglacial (PAPER IV). It is conceivable that variations in orbital parameters during the Holocene, albeit much smaller than at the last glacial inception, or changes in solar output influenced the gyre circulation in recent millennia. Recent analyses of marine sediments revealed that variations in subpolar gyre circulation occurred throughout the last 12,000 years, indeed, as observed in Greenland fjords (Ren et al., 2009; Kuijpers et al., 2009) and the eastern North Atlantic (Thornalley et al., 2009). A relation to the Medieval Climate Anomaly as well as with the demise of Norse colonies on Greenland was hypothesized. Our new understanding of the subpolar gyre might provide the basis for future investigations of these questions.

References

Bacon, S. (1997). Circulation and Fluxes in the North Atlantic between Greenland and Ireland. *Journal of Physical Oceanography*, 27:1420–1435.

Berger, A. (1978). Long-Term Variations of Caloric Solar Radiation Resulting from the Earth's Orbital Elements. *Quaternary Research*, 9:139–167.

Berger, A. and Loutre, M. F. (1991). Insolation values for the climate of the last 10 million years. *Quaternary Science Reviews*, 10:297–317.

Böning, C., Scheinert, M., Dengg, J., Biastoch, A., and Funk., A. (2006). Decadal variability of subpolar gyre transport and its reverberation in the North Atlantic overturning. *Geophysical Research Letters*, 33:L21S01.

Born, A., Levermann, A., and Mignot, J. (2009). Sensitivity of the Atlantic ocean circulation to a hydraulic overflow parameterisation in a coarse resolution model: Response of the subpolar gyre. *Ocean Modelling*, 27 (3-4):130–142.

Calov, R., Ganopolski, A., Petoukhov, V., Claussen, M., Brovkin, V., and Kubatzki, C. (2005). Transient simulation of the last glacial inception. Part II: sensitivity and feedback analysis. *Climate Dynamics*, 24:563–576.

Clarke, R. A. (1984). Transport through the Cape Farewell-Flemish Cap section. *Rapp. P. V. Reun. Cons. Int. Explor. Mer.*, 185:120–130.

Cunningham, S. A., Kanzow, T., Rayner, D., Baringer, M. O., Johns, W. E., Marotzke, J., Longworth, H. R., Grand, E. M., Hirschi, J. J.-M., Beal, L. M., Meinen, C. S., and Bryden, H. L. (2007). Temporal variability for the atlantic meridional overturning circulation at 26.5°n. *Science*, 317:935–937.

Curry, R., McCartney, M., and Joyce, T. (1998). Oceanic transport of subpolar climate signals to mid-depth subtropical waters. *Nature*, 391:575–577.

de Noblet, N., Prentice, I., Joussaume, S., Texier, D., Botta, A., and Haxeltine, A. (1996). Possible Role of Atmosphere-Biosphere Interactions in Triggering the Last Glaciation. *Geophysical Research Letters*, 23:3191–3194.

Deshayes, J., Straneo, F., and Spall, M. A. (2009). Mechanisms of variability in a convective basin. *Journal of Marine Research*, 67(3):273–303.

Dickson, R. R. and Brown, J. (1994). The production of North Atlantic Deep Water: Sources, rates, and pathways. *Journal of Geophysical Research*, 99:12,319–12,341.

Eden, C. and Willebrand, J. (2001). Mechanism of Interannual to Decadal Variability of the North Atlantic Circulation. *Journal of Climate*, 14:2266–2280.

Ganachaud, A. and Wunsch, C. (2000). Improved estimates of global ocean circulation, heat transport and mixing from hydrographic data. *Nature*, 408:453–456.

Greatbatch, R. J., Fanning, A. F., Goulding, A. D., and Levitus, S. (1991). A Diagnosis of Interpentadal Circulation Changes in the North Atlantic. *Journal of Geophysical Research*, 96:22,009–22,023.

Gröger, M., Maier-Reimer, E., Mikolajewicz, U., Schurgers, G., Vizcaíno, M., and Winguth, A. (2007). Changes in the hydrological cycle, ocean circulation, and carbon/nutrient cycling during the last interglacial and glacial transition. *Paleoceanography*, 22:PA4205.

Häkkinen, S. and Rhines, P. B. (2004). Decline of subpolar North Atlantic circulation during the 1990s. *Science*, 304:555–559.

Hansen, B. and Østerhus, S. (2000). North Atlantic - Nordic Seas exchanges. *Progress in Oceanography*, 45:109–208.

Hansen, B., Østerhus, S., Quadfasel, D., and Turrell, W. (2004). Already the Day After Tomorrow? *Science*, 305:953–954.

Hátún, H., Sandø, A. B., Drange, H., Hansen, B., and Valdimarsson, H. (2005). Influence of the Atlantic Subpolar Gyre on the Thermohaline Circulation. *Science*, 309:1841–1844.

Hays, J. D., Imbrie, J., and Shackleton, N. J. (1976). Variations in the Earth's Orbit: Pacemaker of the Ice Ages. *Science*, 194 (4270):1121–1132.

Khodri, M., Leclainche, Y., Ramstein, G., Braconnot, P., Marti, O., and Cortijo, E. (2001). Simulating the amplification of orbital forcing by ocean feedbacks in the last glaciation. *Nature*, 410:570–574.

Khodri, M., Ramstein, G., Paillard, D., Duplessy, C., Kageyama, M., and Ganopolski, A. (2003). Modelling the climate evolution from the last interglacial to the start of the last glaciation: The role of Arctic Ocean freshwater budget. *Geophysical Research Letters*, 30(12):1606.

Kubatzki, C., Claussen, M., Calov, R., and Ganopolski, A. (2006). Sensitivity of the last glacial inception to initial and surface conditions. *Climate Dynamics*, 27:333–344.

Kuijpers, A., Malmgren, B. A., and Seidenkrantz, M.-S. (2009). Termination of the Medieval Warm Period: linking subpolar and tropical North Atlantic circulation changes to ENSO. *PAGES news*, 17(2):76–77.

Levermann, A. and Born, A. (2007). Bistability of the Atlantic subpolar gyre in a coarse-resolution model. *Geophysical Research Letters*, 34:L24605.

Li, C., Battisti, D. S., Schrag, D. P., and Tziperman, E. (2005). Abrupt climate shifts in Greenland due to displacements of the sea ice edge. *Geophysical Research Letters*, 32.

Lohmann, K., Drange, H., and Bentsen, M. (2009). Response of the North Atlantic subpolar gyre to persistent North Atlantic oscillation like forcing. *Climate Dynamics*, 32:273–285.

Lumpkin, R. and Speer, K. (2003). Large-scale vertical and horizontal circulation in the North Atlantic Ocean. *Journal of Physical Oceanography*, 33:1902–1920.

Lüthi, D., Floch, M. L., Bereiter, B., Blunier, T., Barnola, J.-M., Siegenthaler, U., Raynaud, D., Jouzel, J., Fischer, H., Kawamura, K., and Stocker, T. (2008). High-resolution carbon dioxide concentration record 650,000-800,000 years before present. *Nature*, 453:379–382.

McManus, J. F., Oppo, D. W., Keigwin, L. D., Cullen, J. L., and Bond, G. C. (2002). Thermohaline Circulation and Prolonged Interglacial Warmth in the North Atlantic. *Quaternary Research*, 58:17–21.

Meissner, K. J., Weaver, A. J., Matthews, H. D., and Cox, P. M. (2003). The role of land surface dynamics in glacial inception: a study with the UVic Earth System Model. *Climate Dynamics*, 21:515–537.

Mellor, G., Mechoso, C., and Keto, E. (1982). A diagnostic calculation of the general circulation of the Atlantic Ocean. *Deep-Sea Research*, 29:1171–1192.

Milankovitch, M. (1941). *Kanon der Erdbestrahlung und seine Anwendung auf das Eiszeitproblem*. (Royal Serbian Academy, Belgrade.

Monnin, E., Indermühle, A., Dällenbach, A., Flückiger, J., Stauffer, B., Stocker, T. F., Raynaud, D., and Barnola, J.-M. (2001). Atmospheric CO2 concentrations over the last glacial termination. *Science*, 291:112–114.

Muhs, D. R., Simmons, K. R., and Steinke, B. (2002). Timing and warmth of the last interglacial period: New U-series evidence from Hawaii and Bermuda and a new fossil compilation for North America. *Quaternary Science Reviews*, 21:1355–1383.

Myers, P. G., Fanning, A. F., and Weaver, A. J. (1996). JEBAR, Bottom Pressure Torque, and Gulf Stream Separation. *Journal of Physical Oceanography*, 26:671–683.

Otterå O. H. and Drange, H. (2004). Effects of solar irradiance forcing on the ocean circulation and sea-ice in the North Atlantic in an isopycnic coordinate ocean general circulation model. *Tellus*, 56A:154–166.

Otto-Bliesner, B. L., Marshall, S. J., Overpeck, J. T., Miller, G. H., Hu, A., and CAPE Last Interglacial Project members (2006). Simulating Arctic Climate Warmth and Icefield Retreat in the Last Interglaciation. *Science*, 311:1751–1753.

Overpeck, J. T., Otto-Bliesner, B. L., Miller, G. H., Muhs, D. R., Alley, R. B., and Kiehl, J. T. (2006). Paleoclimatic Evidence for Future Ice-Sheet Instability and Rapid Sea-Level Rise. *Science*, 311:1747–1750.

Penduff, T., Barnier, B., and de Verdière, A. C. (2000). Self-adapting open boundaries for a sigma coordinate model of the eastern North Atlantic. *Journal of Geophysical Research*, 105:11,279–11,298.

Petit, J. R., Jouzel, J., Raynaud, D., Barkov, N. I., Barnola, J.-M., Basile, I., Bender, M., Chappellaz, J., Davisk, M., Delaygue, G., Delmotte, M., Kotlyakov, V. M., Legrand, M., Lipenkov, V. Y., Lorius, C., pin, L. P., Ritz, C., Saltzmank, E., and Stievenard, M. (1999). Climate and atmospheric history of the past 420,000 years from the Vostok ice core, Antarctica. *Nature*, 399:429–436.

Rahmstorf, S. (2002). Ocean circulation and climate during the past 120,000 years. *Nature*, 419:207–214.

Ren, J., Jiang, H., Seidenkrantz, M.-S., and Kuijpers, A. (2009). A diatom-based reconstruction of Early Holocene hydrographic and climatic change in a southwest Greenland fjord. *Marine Micropaleontology*, 70:166–176.

Risebrobakken, B., Balbon, E., Dokken, T., Jansen, E., Labeyrie, C. K. L., Richter, T., and Senneset, L. (2006). The penultimate deglaciation: High-resolution paleoceanographic evidence from a north-south transect along the eastern Nordic Seas. *Earth and Planetary Science Letters*, 241:505–516.

Risebrobakken, B., Dokken, T., Otterå, O. H., Jansen, E., Gao, Y., and Drange, H. (2007). Inception of the Northern European ice sheet due to contrasting ocean and insolation forcing. *Quaternary Research*, 67:128–135.

Rostami, K., Peltier, W. R., and Mangini, A. (2000). Quaternary marine terraces, sea-level changes and uplift history of Patagonia, Argentina. Comparisons with predictions of ICE-4G (VM2) model of the global process of glacial isostatic adjustment. *Quaternary Science Reviews*, 19:1495–1525.

Ruddiman, W. F. and McIntyre, A. (1975). Warmth of the Subpolar North Atlantic Ocean During Northern Hemisphere Ice-Sheet Growth. *Science*, 204:173–175.

Scherer, R. P., Aldahan, A., Tulaczyk, S., Possnert, G., Engelhardt, H., and Kamb, B. (1998). Pleistocene collapse of the West Antarctic ice sheet. *Science*, 281:82–85.

Siegenthaler, U., Stocker, T. F., Monnin, E., Lüthi, D., Schwander, J., Stauffer, B., Raynaud, D., Barnola, J.-M., Fischer, H., Masson-Delmotte, V., and Jouzel, J. (2005). Stable Carbon Cycle-Climate Relationship During the Late Pleistocene. *Science*, 310:1313–1317.

Spall, M. A. (2004). Boundary Currents and Watermass Transformation in Marginal Seas. *Journal of Physical Oceanography*, 34:1197–1213.

Straneo, F. (2006). On the Connection between Dense Water Formation, Overturning, and Poleward Heat Transport in a Convective Basin. *Journal of Physical Oceanography*, 36:1822–1840.

Talley, L. D., Reid, J. L., and Robbins, P. E. (2003). Data-based meridional overturning streamfunctions for the global ocean. *Journal of Climate*, 16:3213–3226.

Thornalley, D. J. R., Elderfield, H., and McCave, I. N. (2009). Holocene oscillations in temperature and salinity of the surface North Atlantic. *Nature*, 457:711–714.

Treguier, A. M., Theetten, S., Chassignet, E. P., Penduff, T., Smith, R., Talley, L., Beismann, J. O., and Böning, C. (2005). The North Atlantic Subpolar Gyre in Four High-Resolution Models. *Journal of Physical Oceanography*, 35:757–774.

Vettoretti, G. and Peltier, W. R. (2003). Post-Eemian Glacial Inception. Part II: Elements of a Cryospheric Moisture Pump. *Journal of Climate*, 16:912–927.

Wunsch, C. and Heimbach, P. (2006). Estimated Decadal Changes in the North Atlantic Meridional Overturning Circulation and Heat Flux 1993-2004. *Journal of Physical Oceanography*, 36:2012–2024.

Yoshimori, M., Reader, M. C., Weaver, A. J., and McFarlane, N. A. (2002). On the causes of glacial inception 115 kaBP. *Climate Dynamics*, 18:383–402.

Zachos, J., Pagani, M., Sloan, L., and andKatharina Billups, E. T. (2001). Trends, Rhythms, and Aberrations in Global Climate 65 Ma to Present. *Science*, 292 (5517):686–693.

Zhang, R. (2008). Coherent surface-subsurface fingerprint of the Atlantic meridional overturning circulation. *Geophysical Research Letters*, 35:L20705.

Paper I

Sea ice induced changes in ocean circulation during the Eemian[1]

Born, A., K. H. Nisancioglu and P. Braconnot (2010)

Climate Dynamics, doi:10.1007/s00382-009-0709-2

[1]Reproduced with permission of the publisher

Clim Dyn
DOI 10.1007/s00382-009-0709-2

Sea ice induced changes in ocean circulation during the Eemian

Andreas Born · Kerim H. Nisancioglu · Pascale Braconnot

Received: 24 March 2009 / Accepted: 10 November 2009

Abstract We argue that Arctic sea ice played an important role during early stages of the last glacial inception. Two simulations of the Institut Pierre Simon Laplace coupled model 4 are analyzed, one for the time of maximum high latitude summer insolation during the last interglacial, the Eemian, and a second one for the subsequent summer insolation minimum, at the last glacial inception. During the inception, increased Arctic freshwater export by sea ice shuts down Labrador Sea convection and weakens overturning circulation and oceanic heat transport by 27 and 15%, respectively. A positive feedback of the Atlantic subpolar gyre enhances the initial freshening by sea ice. The reorganization of the subpolar surface circulation, however, makes the Atlantic inflow more saline and thereby maintains deep convection in the Nordic Seas. These results highlight the importance of an accurate representation of dynamic sea ice for the study of past and future climate changes.

Keywords Sea ice · Ocean circulation · Eemian · Glacial inception · Subpolar gyre · North Atlantic

A. Born (✉) · K. H. Nisancioglu
Bjerknes Centre for Climate Research,
Allegaten 55, 5007 Bergen, Norway
e-mail: andreas.born@bjerknes.uib.no

A. Born
Geophysical Institute, University of Bergen,
Allegaten 70, Bergen, Norway

P. Braconnot
IPSL/LSCE, Unité mixte CEA-CNRS-UVSQ,
Gif sur Yvette, France

1 Introduction

From paleoclimatic records, we know that warm interglacial periods, like the present Holocene (last 10,000 years) and the Eemian (129 to 113 thousand years before present), are relatively short-lived (Siegenthaler et al. 2005) and probably only stable during times of high northern latitude summer insolation. According to Milankovitch theory, an orbital configuration giving cold Northern Hemisphere summers allows snow to persist throughout the year resulting in the growth of large ice masses on land. Summer incoming shortwave radiation (insolation) at the top of the atmosphere at 65°N was at a local maximum 126,000 years before present (126 ka), followed by a minimum at 115 ka (Fig. 1) (Berger 1978). The growth of continental scale ice sheets and the transition into a full glacial, however, is generally assumed to require amplification by the internal dynamics of the climate system.

Previous model studies identified several potential feedback mechanisms amplifying the insolation signal. Retreating boreal forest over northern high latitude continents was found to lower albedo sufficiently to change local climate and favor ice growth (Calov et al. 2005; Meissner et al. 2003; de Noblet et al. 1996). Perennial snow cover is furthermore enhanced by an increased moisture convergence in the Arctic circle, result of less evaporation in a colder climate (Vettoretti and Peltier 2003). Several studies also recognize the important role of the ocean for glacial inception. Realistic snow accumulation over the Canadian Arctic is only obtained in an atmospheric model with 116 ka sea surface conditions, not present day (Yoshimori et al. 2002). Calov et al. (2005) report a subtle dependence of Scandinavian land ice growth on ocean circulation in the Nordic Seas. More intense deep

Published online: 01 December 2009

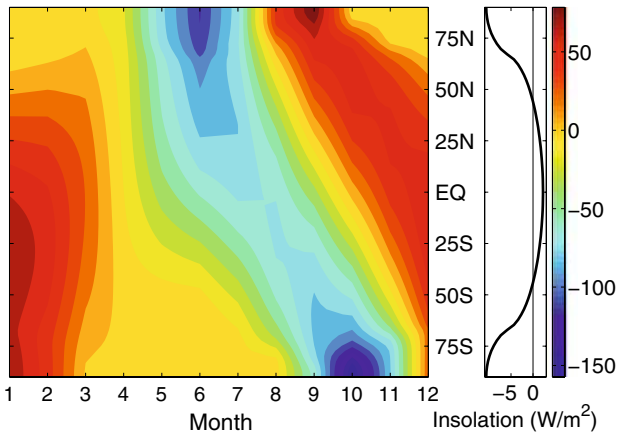

Fig. 1 Incoming short wave radiation difference at the top of the atmosphere, 115–126 ka, in W/m^2. *Left*: Seasonal variations, *right*: annual average. The seasonal cycle was reduced in high northern latitudes and the Earth received less annual mean radiation poleward of 45° at 115 ka than at 126 ka

convection results in warmer and more moist climate that increases snow accumulation.

In addition to these mechanisms, sea ice is likely to have played a major role during glacial inception. Due to its short life time, it responds quickly to changes in boundary conditions. Moreover, it provides strong feedbacks due to its high albedo in contrast to open water, its thermodynamic and mechanical decoupling of ocean and atmosphere, and due to its redistribution of freshwater in the Arctic and subarctic marine environment. Surface freshwater plays an important role for deep convection and the circulation of the deep ocean through the formation of deep water masses. A weaker deep circulation in turn implies less northward heat transport by the Atlantic meridional overturning circulation (AMOC), which can assist glacial inception. While the impact of sea ice changes on ocean circulation will be the main focus of this study, the modification of surface fluxes by sea ice also affects the growth of land ice. With more sea ice, a reduced ocean to atmosphere heat flux results in colder temperatures that favor ice growth. Concurrently, less evaporation reduces snowfall and counteracts the first process. The gross effect of a sea ice change on land ice volume thus depends on the background climate of the respective region.

Changes in the strength of deep water formation and the AMOC have often been regarded as potentially important feedback process. Gröger et al. (2007) report that in their model experiments lower sea surface temperatures result in a higher density in the North Atlantic deep water formation regions at 115 thousand years before present (115 ka) and thus a more intense AMOC than at 126 ka. Besides this direct effect of the low annual average insolation at high latitudes, the response of the ocean circulation to changes in freshwater forcing has been investigated. One such study concludes that decreased sea ice melting at 115 ka yields higher salinities in the Nordic Seas sinking regions and intensifies the AMOC compared to 126 ka (Otterå and Drange 2004). Similarly, less precipitation over the Arctic Ocean at 115 ka could have the same result (Khodri et al. 2003). On the other hand, Khodri et al. (2001) find that a weak AMOC during the last glacial inception is consistent with model results due to an increased poleward moisture transport.

A certain disagreement is evident between different models, indicating that climate interactions during the last glacial inception were highly complex and that the role of the AMOC is unclear. The present study analyzes two experiments with a state-of-the-art coupled climate model: one for the Eemian climate optimum at 126 ka and a second for the subsequent summer insolation minimum at 115 ka. The AMOC is found to be weaker at the last glacial inception (115 ka) due to enhanced advection of Arctic sea ice into the North Atlantic. The sea ice melts at the southern tip of Greenland and weakens convection in this region. Positive feedbacks due to changes in the subpolar gyre circulation enhance the freshening. These results are only expected in models explicitly including sea ice dynamics.

The climate model and the configuration of the two experiments are described in the following Sect. 2. The results are presented in Sects. 3–5, with a description of general changes in the Atlantic ocean circulation before focussing on the increase in Arctic sea ice export and the dynamic feedback related to the Atlantic subpolar gyre. The implications of the results and a discussion of the available proxy data are addressed in Sect. 6, followed by a short summary.

2 Model description and experiments

The simulations analyzed here have been carried out with the Institut Pierre Simon Laplace coupled model version 4 (IPSL CM4), comprising ocean, sea ice, atmosphere and land surface components (Marti et al. 2009). The dynamical core of the ocean model is based on the OPA system (Madec et al. 1997). The configuration used here (ORCA2) uses a horizontal resolution based on a 2 degree Mercator mesh, enhanced to 0.5 degree meridional resolution near the equator for a better representation of the equatorial wave channel and with two poles over the continents in the Northern Hemisphere in order to avoid a singularity in the Arctic Ocean. There are 31 unevenly spaced levels in the vertical. The horizontal grid resolution in northern high latitudes can be inferred from arrow spacing and the model coast line in Fig. 2. A free surface formulation is used for the upper boundary (Roullet and Madec 2000), and a diffusive boundary parametrization is used for the bottom (Beckmann 1998).

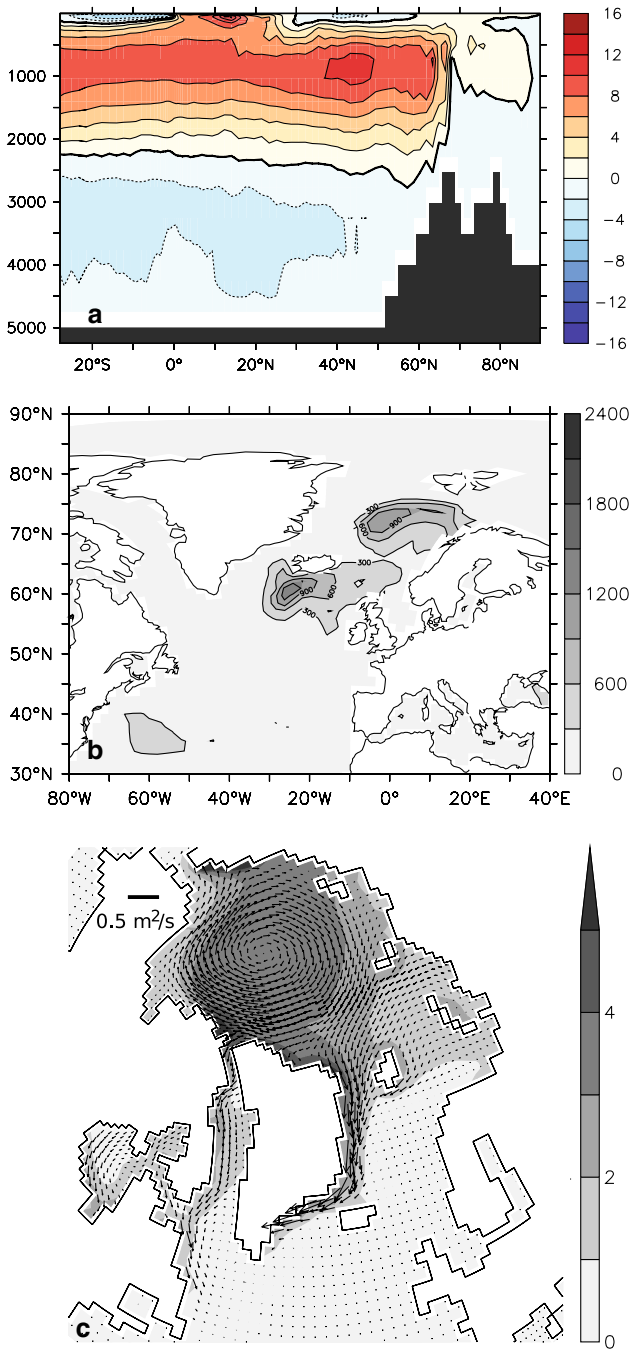

Fig. 2 Preindustrial control experiment. **a** Atlantic Meridional overturning stream function. Flow is *clockwise* around positive contour lines, in Sv. **b** Winter mixed layer depth, in m. **c** March sea ice thickness (*shading*, in m) and transport (*arrows*, scale as indicated)

The dynamic sea ice model (LIM2, Fichefet and Maqueda 1999, 1997) uses the horizontal ocean grid to compute ice rheology and advection. Thermodynamics are computed in three vertical layers, the uppermost for snow. Ice growth and melting are determined by an energy balance at both the snow-ice- and water boundary and in leads. Internal forces follow a viscous-plastic law (Hibler 1979). The model features parametrizations for the trapping of shortwave radiation by brine pockets, leads in the ice, as well as an implicit representation of subgrid variations in snow and ice thickness.

The atmosphere is simulated by a comprehensive general circulation model (LMDZ, Hourdin et al. 2006) with a resolution of 3.75 zonally and 2.5 meridionally on 19 vertical levels. Precipitation over land is returned to the ocean by means of a river routing scheme implemented in the land surface model (ORCHIDEE, Krinner et al. 2005).

This model has been used in several studies of past climate states (Braconnot et al. 2008; Zheng et al. 2008), present day climate sensitivity to anomalous freshwater forcing (Swingedouw et al. 2007b), and future projections (Swingedouw et al. 2007a; IPCC 2007).

After initializing the model with preindustrial boundary conditions, it exhibits a relatively weak AMOC of about 11 Sv (Fig. 2a). Deep convection is active in the Nordic Seas and the Irminger Basin south of Iceland (Fig. 2b). March sea ice thickness exceeds 3 m in large parts of the central Arctic Ocean (Fig. 2c). Sea ice is advected in a large anticyclonic gyre inside the Arctic Ocean and exported mainly through Fram Strait between Greenland and Spitsbergen, but also through the Canadian Archipelago and south of Spitsbergen. Although thin and not continuous, sea ice covers the entire Labrador Sea, probably preventing deep convection. The export of Arctic sea ice can only be reliably compared to modern observations by means of an area transport for which long time series exist from satellite data. A recent study estimates the maximum sea ice area export through Fram Strait between December and March to be 38,580 m^2/s (Smedsrud et al. 2008), while our preindustrial control experiment yields 46,038 m^2/s for the same time period. Overall, the model simulates thicker and more Arctic sea ice compared to present day observations, which is consistent with the lower atmospheric greenhouse gas concentration in the simulated preindustrial period. Historic records document a larger Arctic sea ice cover before the twentieth century (Divine and Dick 2006). A detailed discussion of the model's performance with present day boundary conditions and comparison with data can be found in Arzel et al. (2008).

For the present study, we analyzed two simulations forced with orbital parameters for the Eemian (126 ka) and the Last Glacial Inception (115 ka), using preindustrial greenhouse gas concentrations (Table 1) (Braconnot et al. 2008). Both experiments were initiated with an ocean at rest and preindustrial hydrography (Levitus 1982). This choice is motivated by the insufficient coverage of paleo data and relies on the assumption that the climate of the last interglacial was not fundamentally different from the present (Oppo and Lehman 1995; Müller and Kukla 2004). One potentially important difference is a significantly

Table 1 Boundary conditions for the experiments in this study. The orbital parameters were calculated following Berger (1978)

Experiment	Axial tilt (°)	Longitude of perihelion (°)	Eccentricity	CO_2 (ppm)
126 ka	23.92	112.03	0.0397	280
115 ka	22.40	291.72	0.0414	280
Preindustrial	23.46	280.84	0.0168	280

reduced height of the southern Greenland ice sheet at the last interglacial (de Vernal and Hillaire-Marcel 2008; Otto-Bliesner et al. 2006b), which is disregarded in our experiments and prescribed at its present day configuration. We believe that this simplification is not a problem for the study of the last glacial inception, which is a period of renewed ice growth.

The simulations for 126 ka and 115 ka were integrated for 300 and 800 years, respectively, and temperature drift in the lowest ocean level stabilizes at 0.06 and 0.005°C/100 years, respectively. Both sets of boundary conditions are relatively close to present day climate, and the surface ocean adjusts to the forcing in 50 years and the deep ocean in less than 150 years. The results presented are calculated from averages over the last 100 years of the simulations.

Disregarding changes in land ice, which presumably were small at the beginning of the last glacial, it is reasonable to assume that all other components of the climate system were close to equilibrium with the slowly varying insolation forcing.

3 Ocean response

Sea surface temperatures poleward of 43° latitude in the northern Pacific and Southern Ocean are lower at 115 ka, while tropical surface waters are generally warmer (Fig. 3). This can largely be attributed to a direct response to the changed orbital forcing. In the Atlantic Ocean, however, surface cooling extends further south and warming in low latitudes is more pronounced. This is the signature of a weaker oceanic heat transport Q (Fig. 4), which has been decomposed into an overturning and a horizontal component, the latter representing the large scale gyre circulation:

$$\begin{aligned} Q_{\text{total}} &= Q_{\text{overturning}} + Q_{\text{gyre}} \\ &= \rho_0 c_p \left\{ \int\int \mathrm{d}x\mathrm{d}z\overline{v}\cdot\overline{T} + \int\int \mathrm{d}x\mathrm{d}z v'\cdot T' \right\}, \end{aligned} \quad (1)$$

with reference density ρ_0, specific heat capacity of sea water c_p, the zonal averages of meridional velocity and potential temperature $(\overline{v}, \overline{T})$ and deviations thereof (v', T'). The integral spans over the entire basin width and depth (Bryden and Imawaki 2001).

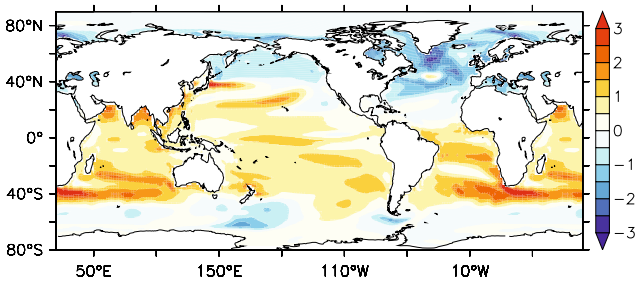

Fig. 3 Difference in annual average sea surface temperature, 115–126 ka, in °C. The zonal pattern with cold anomalies poleward of 43° latitude is a direct effect of the change in annual average insolation forcing (Fig. 1). The more southward extent of the cold anomaly in the North Atlantic, however, indicates a reorganization of the ocean dynamics

This decomposition shows that heat transport is reduced due to a reduction in overturning heat transport in most of the Atlantic, peaking at ~15°N with a reduction of 0.15 PW, or ~15%. While the overturning component increases between 40°N and 60°N, the gyre heat transport overcompensates this increase resulting in a decrease of the total heat transport. Heat transport into the Nordic Seas at 60°N is virtually unchanged. The change in Atlantic heat transport causes an asymmetric global pattern: the high latitude cooling in the Southern Hemisphere is weaker than in the Northern Hemisphere.

Consistent with the reduction in overturning heat transport, the AMOC is weaker and shallower at 115 ka with a maximum transport of 11 Sv (10^6 m^3/s) and North Atlantic Deep Water reaching down to 2,500 m depth, compared to 15 Sv and 2,900 m at 126 ka (Fig. 5). As can also be inferred from the zonally integrated stream function, the reduction in maximum transport is primarily due to a reduction in downwelling around 50°N. Waters that do not sink there carry heat further north which explains the local increase in overturning heat transport around this latitude.

Although not directly related, weaker downwelling around 50°N is accompanied by a reduction in convection in this region. At 126 ka, deep convection takes place in three different regions; the Nordic Seas, the Irminger Basin and the at the mouth of the Labrador Sea while the latter is absent at 115 ka (Fig. 6). Late winter (February and March) temperature and salinity profiles of the Labrador Sea convection region reveal that the buoyancy gain in the upper 100 m is due to freshening (Fig. 7). Below 100 m water depth, the salinity difference abates quickly while the temperature difference reverses, showing warmer subsurface waters at 115 ka, probably the result of reduced convection. The source of the surface freshening is the subject of the next section, followed by a discussion of the interaction with the gyre circulation.

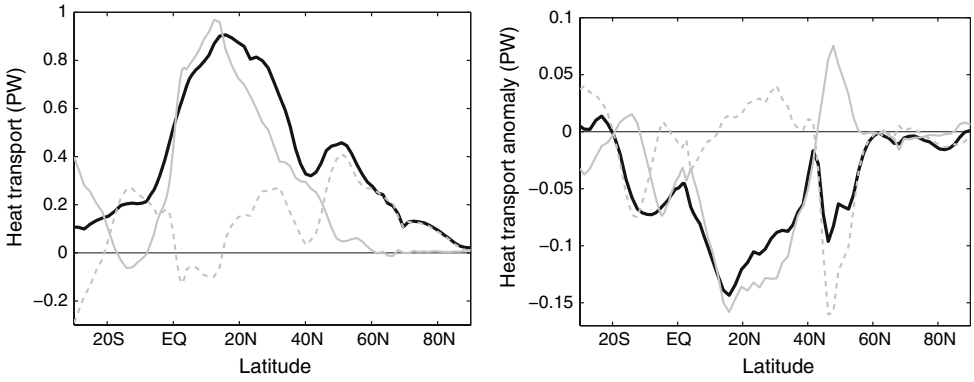

Fig. 4 Heat transport in the Atlantic Ocean (*black*), decomposed into overturning (*solid gray*) and gyre (*dashed gray*) components, *left*: 126 ka, *right*: difference 115–126 ka. The heat transport is weaker due to a weaker overturning. Around 50°N, a significantly weaker subpolar gyre reduces the heat transport

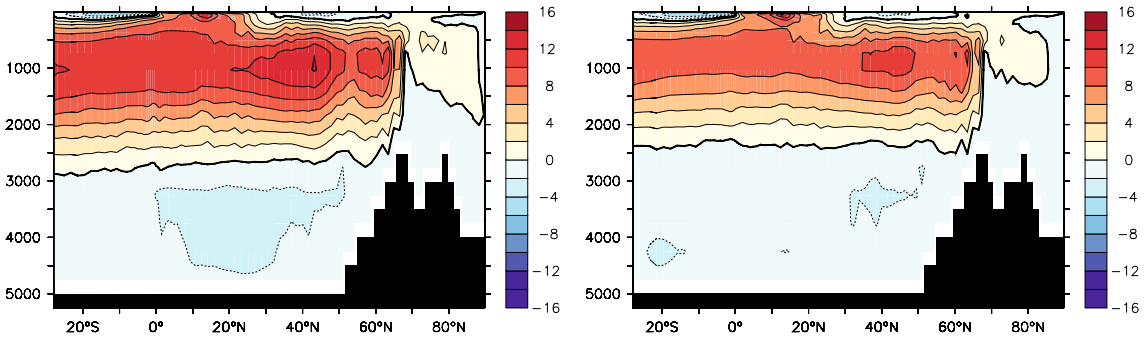

Fig. 5 Atlantic Meridional Overturning stream function. Flow is *clockwise* around positive contour lines, *left*: 126 ka, *right*: 115 ka, in Sv (10^6 m^3/s). The overturning is slightly weaker and shallower at 115 ka

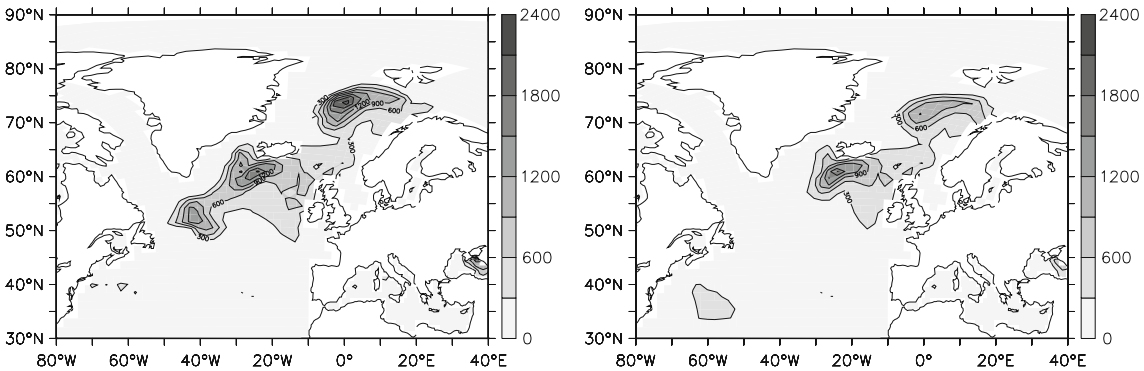

Fig. 6 Winter mixed layer depth, in m, *left*: 126 ka, *right*: 115 ka. Deep water formation occurs in three regions at 126 ka: the Nordic Seas, the Irminger Basin and off Labrador Sea. At 115 ka, Labrador Sea water formation is not active

4 Arctic sea ice export

Lower annual average insolation in high latitudes at 115 ka (Fig. 1), in particular the colder summer, gives less sea ice melting in the Arctic Ocean. Because sea ice can persist through the summer, the ice is thicker at 115 ka (Fig. 8). As a consequence, more sea ice is exported southward, almost doubling the volume transport through Fram Strait (Fig. 9). Changes in ice velocity are minor (not shown). The stronger sea ice export implies increased sea ice growth in the central Arctic which makes surface waters more saline. Thus, water exported from the Arctic in the East Greenland Current and through the Canadian Archipelago partly counteracts the freshening by sea ice. The equivalent freshwater fluxes in the upper 100 m of various sections (see Fig. 9) are calculated as follows:

$$F_t = \int_C \mathrm{d}x \int_{100\,\mathrm{m}}^{0\,\mathrm{m}} \mathrm{d}z v \frac{S - S_0}{S_0}, \tag{2}$$

where v is the northward velocity component and S the local salinity at the section. The reference salinity S_0 is taken as the average over the upper 100 m of the convection region (red box, Fig. 9) which is the depth interval of

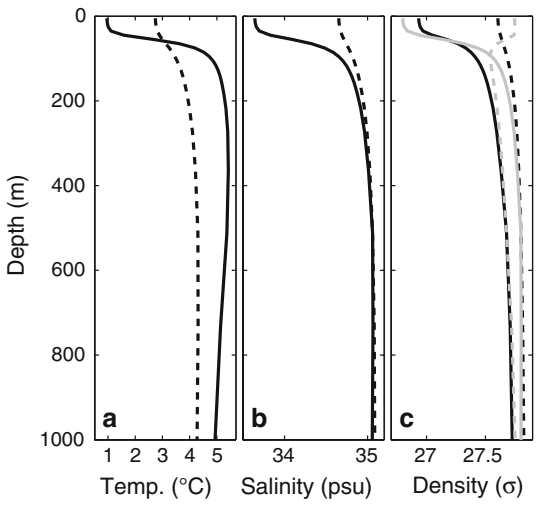

Fig. 7 Vertical profiles temporally averaged over the main convection season (February and March) and spatially over the center of the subpolar gyre (red box in Fig. 9), *solid black*: 115 ka, *dashed black*: 126 ka; *a* temperature; *b* salinity; *c* density. The *solid gray curve* in *panel c* shows the density change at 115 ka as compared to 126 ka due to salinity changes only, the *dashed gray curve* the same for temperature. Salinity changes dominate the density difference in the upper 100 m while the temperature difference plays a more important role below

most pronounced freshening (Fig. 7). In order to identify surface freshwater flux anomalies into this region, we integrate over the entire width C of the section and the upper 100 m. The zonal freshwater transport is computed likewise. Since our aim is to identify surface freshwater flux changes, sections are open at depth and the freshwater budget cannot be closed. Two sections are chosen according to the width of currents but the results do not depend critically on this choice. Freshwater transport in sea ice is based on Eq. 2 with a fixed sea ice salinity of 4 psu taken from the sea ice model. All variables are based on annual averages of the monthly model output, which itself is an average of the last 100 years of the simulations.

Only a small fraction of the Arctic freshwater export anomaly remains in the Nordic Seas. Most of the sea ice that enters the basin through Fram Strait, exits through Denmark Strait (Fig. 9). Sea ice melt produced along this pathway is largely advected through Denmark Strait by the prevailing currents. Taking into account the total freshwater transport, sea ice and liquid fraction, only 8 mSv of the total Arctic freshwater export remains in the Nordic Seas. This difference is compensated for by a stronger Atlantic inflow east of Iceland.

Ice export through Denmark Strait increases by 43 mSv at 115 ka representing a more than ninefold increase. The East Greenland Current transports 14 mSv less freshwater in 115 ka (33% less than at 126 ka) across Denmark Strait. West of Greenland, 35 mSv less freshwater is advected southward, passing through the Labrador Sea (−34%). Taken together, this results in a small salinification of the North Atlantic (−6 Sv). A decrease in evaporation and a slight increase in precipitation into the convection region yield a freshening of comparable amplitude (4 mSv, +25%).

The total freshwater transport by sea ice and ocean currents south of the Greenland Scotland Ridge is close to zero. Yet it has a strong effect on deep convection. This is due to two reasons. First, freshwater in sea ice is transported in a thin surface layer and primarily during late winter which is also the main convection season. It thus has a more concentrated effect on convection than the counteracting Arctic currents. Secondly, additional freshening is

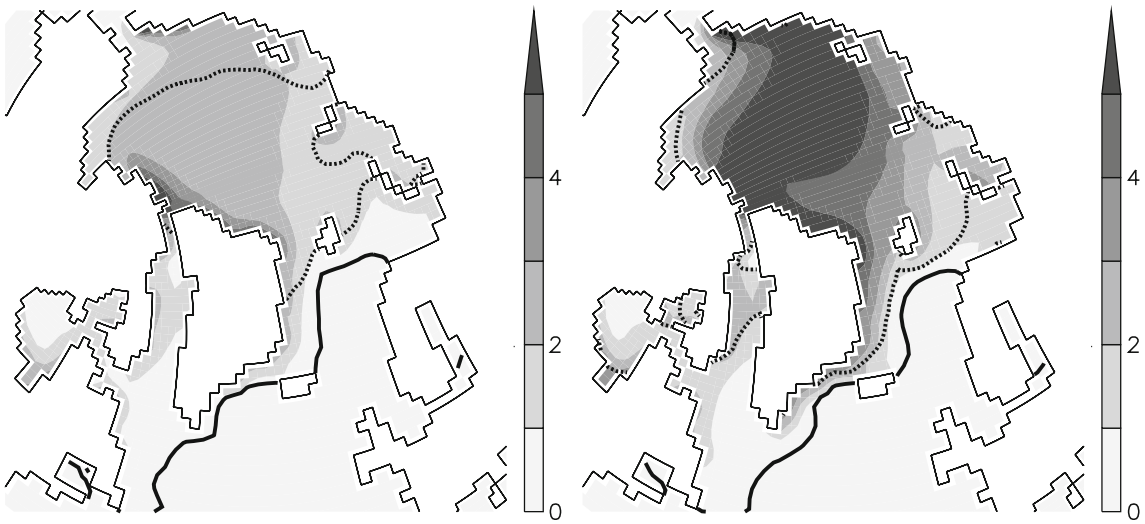

Fig. 8 Maximum winter sea ice thickness (*shading*, in m). *Lines mark* the sea ice extent defined as the area with at least 15% coverage, *solid* for winter maximum, *dashed* for summer minimum. *Left*: 126 ka, *right*: 115 ka. During summer, higher insolation melts most of the Arctic sea ice at 126 ka, resulting in thinner winter ice

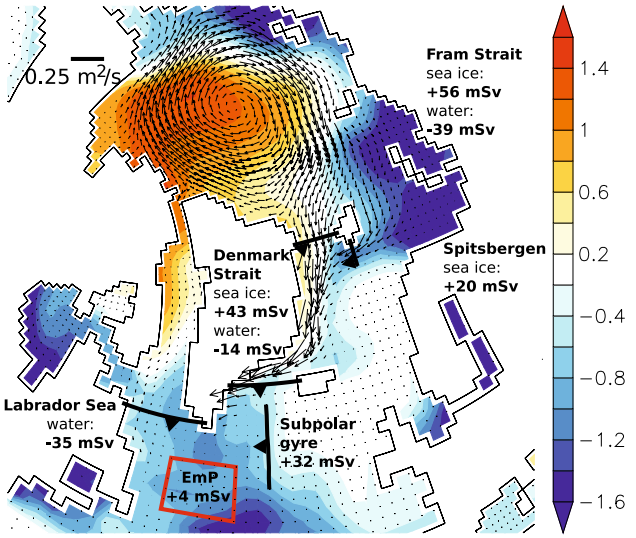

Fig. 9 Sea surface salinity (*colours*, in psu) and sea ice volume transport (*arrows*, scale as indicated) anomalies 115–126 ka. The *sections* show the corresponding freshwater transport anomalies by sea ice and ocean currents. Arctic sea ice export through Fram Strait is stronger at 115 ka, and a new path opens south of Spitsbergen. Melting of the sea ice results in fresher surface waters particularly south of Greenland. A weaker subpolar gyre advects less salt and thus contributes to the freshening of the region. *EmP*: evaporation minus precipitation

caused by a weakening of the Irminger Current. This northern branch of the subpolar gyre carries saline tropical water westward. Its weakening at 115 ka hence results in an implicit freshwater transport of 32 mSv, a fourfold increase from 126 ka.

Convection north of the Greenland Scotland Ridge is less sensitive to the increase in sea ice export. This is the result of sea ice and associated melt water in the Nordic Seas being concentrated mostly in the East Greenland Current (Fig. 9). Besides, the weaker salt transport into the western North Atlantic by the Irminger Current makes the Atlantic inflow into the Nordic Seas more saline, a mechanism that has been observed in present day climate (Hátún et al. 2005). This is seen here as an area with no salinity difference despite the general freshening trend (Fig. 9). Hence, relatively more salt is advected into the eastern Nordic Seas at 115 ka than at 126 ka, balancing the increased Arctic freshwater flux and stabilizing deep convection. Note that this reorganization of the subpolar gyre circulation and the subsequent redistribution of salt results in opposite signals for Labrador Sea and Nordic Seas convection.

5 Feedbacks of the subpolar North Atlantic

The reduction in volume transport in the Irminger Current, resulting in an implicit freshwater transport into the western North Atlantic, is a consequence of a weaker subpolar gyre, of which the Irminger Current is the northern branch. The gyre transport weakens from 26 Sv at 126 ka to 18 Sv at 115 ka (Fig. 10).

The physical reason for this circulation change is an altered density pattern in the North Atlantic. Transport changes due to wind are two orders of magnitude smaller and thus deemed negligible (Fig. 11). The subpolar gyre is at least partly controlled by the density contrast between its center and rim (Born et al. 2009; Häkkinen and Rhines 2004). A higher density in the center requires a deeper depression of the sea surface, if a level of no motion is assumed at depth where horizontal density gradients disappear. The strengthening of the gyre can thus be understood as the geostrophic response to the change in sea surface height.

To a good approximation, the changes in subpolar gyre strength seen here are the result of density changes in the upper 1,000 m in its center alone. Besides external forcing, the density in the gyre center is controlled by two positive feedbacks. The first concerns the freshening implied by a weaker gyre that reduces the density in its center and weakens the gyre even more—a positive salinity feedback (Fig. 7b). Secondly, reduced convection due to the more buoyant surface and less isopycnal diffusion as a result of

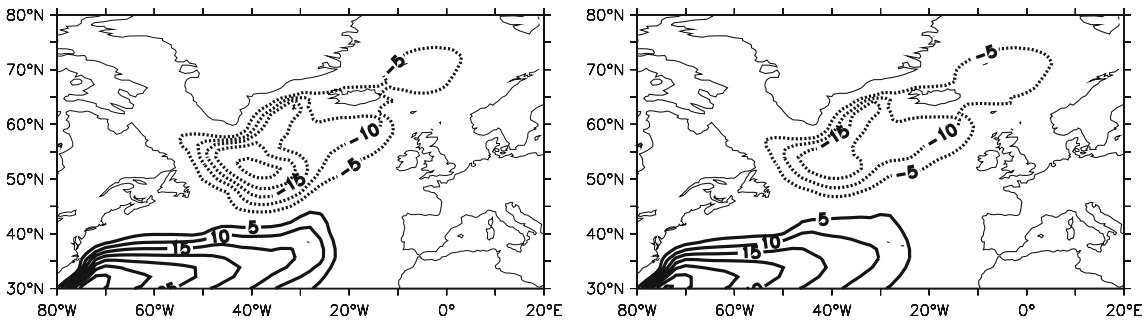

Fig. 10 Horizontal transport stream function (in Sv), negative contours denote cyclonic circulation, *left*: 126 ka, *right*: 115 ka. The subpolar gyre is approximately 30% weaker in 115 k, resulting in a weaker salt transport into the western North Atlantic by its northern branch, the Irminger Current

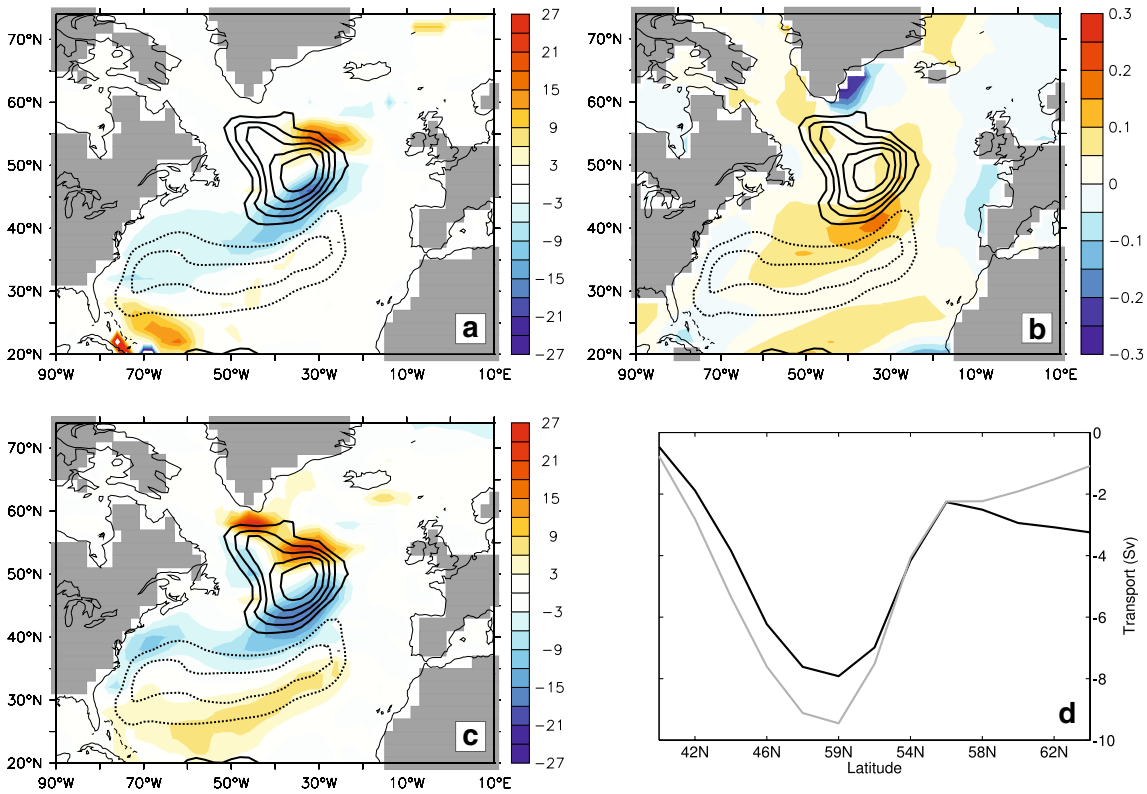

Fig. 11 Differences 115–126 ka in the vertically integrated, zonal transport are shown in *color*, *positive values* indicate eastward transport (m^2/s). Contours are the differences of the horizontal transport stream function (spacing 2 Sv) and demonstrate the spatial agreement of the changes with the subpolar gyre. The positive transport difference weakens the cyclonic subpolar gyre. **a** Vertically integrated zonal transport as computed from the density field. **b** Vertically integrated zonal transport due to changes in the wind stress. **c** Vertically integrated zonal transport as derived from the model's simulated velocities. Differences due to wind stress are small as compared to density and do not reproduce the gyre pattern. **d** Vertically integrated transport as shown in *left panels*, zonally averaged over the gyre center (40°W–20°W) and meridionally integrated in order to obtain a measure of the gyre strength difference. For details on the calculation, refer to Born et al. (2009). The *black curve* corresponds to the transport derived from the density field (**a**), the gray one to the simulated velocities (**b**). Differences in the density field generally agree with pattern and amplitude of the observed changes in the subpolar gyre

the already weaker isopycnal doming leads to a warming in subsurface waters (Fig. 7a). This again decreases the density—a positive temperature feedback (Levermann and Born 2007).

This qualitative understanding supports the interpretation that the weakening of the subpolar gyre is triggered by freshening due to Arctic sea ice export, subsequently amplified by positive feedbacks. The initial surface freshening by sea ice efficiently weakens convection in the center of the subpolar gyre. Thus, the density of the entire water column is reduced (Fig. 7c) which results in a weakening of the gyre and further freshening due to the positive feedbacks.

This allows for a better understanding of the large scale freshening in the subpolar North Atlantic. While the sea ice transport has a major impact on convection, its effect on the large scale freshening not obvious. More freshwater transported in sea ice inevitably coincides with more saline Arctic currents due to brine release. However, because sea ice triggers changes in the subpolar gyre and the associated freshwater transport, it indirectly accounts for the large scale freshening.

6 Discussion

The results presented show how changes in orbital parameters between 126 and 115 ka cause enhanced growth and export of Arctic sea ice, and how ocean circulation is reorganized in response to this redistribution of freshwater in the Arctic and subpolar North Atlantic. Most noteworthy is the shutdown of Labrador Sea Water formation and the consequent weakening of the AMOC, which has not been reported in previous studies of this time period.

Differences in complexity between climate models are the most likely reason for this discrepancy. Models previously used to simulate the last glacial inception simulated

only the thermodynamic effect of sea ice but neglected its dynamics (Khodri et al. 2001), or employed a highly simplified representation of sea ice on a zonally averaged ocean grid (Khodri et al. 2003). Both simplifications cannot accurately resolve the effect of Arctic sea ice export and the redistribution of freshwater described above. Our results also disagree with an ocean-sea ice model of higher complexity (Otterå and Drange 2004). The main difference here is that the ocean-sea ice model of this study does not simulate the atmosphere explicitly. Thus, it potentially does not capture the sensitivity of sea ice to changes in boundary conditions precisely. Moreover, the effect of changes in incoming shortwave radiation at the top of the atmosphere has to be communicated to the ocean and sea ice boundary by means of a parametrization, a source of additional uncertainties. A comparison of different models thus suggests that the representation of sea ice plays a major role in accurately simulating the last glacial inception. For lack of reliable sea ice paleo data of the last interglacial, we must assume the physically more detailed model used in the present study to capture sea ice dynamics more precisely than the examples given above.

The dynamic link between Labrador Sea convection and the subpolar gyre circulation provides a positive feedback that amplifies the surface buoyancy forcing by sea ice. A stronger gyre circulation associated with an increased density gradient between center and rim is supported by observations (Häkkinen and Rhines 2004), high resolution model studies (Spall 2004) as well as theoretical considerations (Straneo 2006).

The experiments for the present study have been carried out with present day ice sheet configuration, while observational evidence (de Vernal and Hillaire-Marcel 2008) as well as model simulations (Otto-Bliesner et al. 2006b) suggest that ice volume in southern Greenland was reduced during the Eemian. The removal of large land ice masses has two main impacts, a change in atmospheric wind patterns (Otto-Bliesner et al. 2006a) and freshwater forcing of the ocean due to increased meltwater runoff. The latter effect did probably not play a significant role during the last glacial inception since land ice masses were in a phase of regrowth. A change in wind pattern does potentially have an effect on the subpolar gyre circulation. However, we showed that changes in wind stress are negligible for our results as compared to ocean internal feedbacks (Fig. 11). The path of Arctic sea ice export in the East Greenland current is constrained by topography and hence robust to different winds.

From marine proxy data, namely dinoflagellate cysts and the oxygen isotope ratio (δ^{18}O) in foraminifera, it has been suggested that Labrador Sea convection was not active during the Eemian (Hillaire-Marcel et al. 2001). More recent data, based on the ratio of stable carbon isotopes (δ^{13}C) in foraminifera and foraminiferal assemblages, refine this view finding a convection similar to the Holocene but shifted further north in the Labrador Sea and probably starting relatively late during the last interglacial (Rasmussen et al. 2003). Silt deposits by the deep western boundary current suggest that the rate of Labrador Sea Water production was probably weaker in the Eemian than during the Holocene (Evans et al. 2007). One possible reason for a delayed onset of Labrador Sea convection is meltwater inflow from a continuously melting Greenland Ice Sheet during the early Eemian. This meltwater flux probably continued until a reorganization in deep water formation took place, dated in the Nordic Seas to approximately 125 ka (Fronval et al. 1998). Disregarding dating uncertainties in the observations, the proxy data suggests that the experiment presented for 126 ka is indeed a better analog for an ocean circulation which developed after 125 ka. This again is at least partly due to neglecting the meltwater input from a shrinking Greenland ice sheet.

Continued ventilation of the deep Atlantic and strong NADW at 115 ka finds support in several marine proxy records (Govin et al. 2009; Molyneux et al. 2007; Adkins et al. 1997). A significant reduction did probably not occur before 70 ka. However, there is evidence for a slight decrease between 126 and 115 ka (Cortijo et al. 1994; Oppo and Lehman 1995). Cortijo et al. (1994) find strong cooling and freshening in the northern Nordic Seas between 125 and 120 ka. In our simulations, this area is affected by enhanced sea ice export south of Spitsbergen. Little is known from proxy data about how the relative contributions of Nordic Seas and Labrador Sea deep waters evolved during the last glacial inception. The simulations presented here suggest that convection in the Labrador Sea is more vulnerable to changes in orbital forcing than in the Nordic Seas due to two reasons: First, sea ice is rapidly transported through the Nordic Seas in the East Greenland Current resulting in the bulk of the ice melting south of the Greenland Scotland Ridge; Secondly, a reorganization of the North Atlantic surface circulation, namely the subpolar gyre, advects less salt into the Labrador Sea and more into the Nordic Seas. The latter mechanism has previously been reported for present day climate (Hátún et al. 2005; Levermann and Born 2007).

The simulated freshening both north and south of the Greenland Scotland Ridge is relatively weak compared to present day variability (Curry and Mauritzen 2005). However, the differences presented here represent sustained changes calculated from centennial averages. Sea ice area transport decreased by almost 40% in recent years (Smedsrud et al. 2008). While incomplete data of ice thickness makes volume transport estimates difficult, the doubling of volume transport found here for the Eemian has likely not been matched in recent decades.

The Eemian interglacial has often been used as an example of a climate similar but warmer than present, and as an estimate of changes expected due to global warming by the end of this century. It must be noted that the cause of the Eemian warming was a change in insolation as compared to the future greenhouse world with a more uniform forcing over latitudes and seasons. However, model results estimate a change in sea ice export through Fram Strait of 61 mSv (Holland et al. 2006) and 70–100 mSv (Swingedouw et al. 2007a) in global warming scenarios which is comparable to the 56 mSv difference found between the Eemian and the inception. Thus, this aspect of the two different scenarios is comparable indeed although the temporal evolution is reverse. Reduced Arctic sea ice export as a result of global warming probably provides a negative feedback stabilizing Labrador Sea convection which previous studies have found to be vulnerable to warming (Vellinga and Wood 2002).

However, the stabilizing effect of reduced sea ice advection on Labrador Sea Water formation in simulations with increased levels of CO_2 is delayed with respect to local thermal buoyancy forcing. Hence, a future warming trend weakens Labrador Sea Water formation in IPSL CM4 (Swingedouw et al. 2007a) until the end of the twenty-first century, in agreement with other model studies (Holland et al. 2006; Wood et al. 1999). After this period, weaker sea ice transport balances the thermal forcing.

7 Summary

We analyzed the response of a coupled climate model to changes in insolation forcing between the last interglacial (126 ka) and the last glacial inception (115 ka). The main findings are:

- low Northern Hemisphere summer insolation allows for more sea ice growth and export of freshwater from the Arctic. More sea ice is transported south during the glacial inception than in the Eemian.
- melting of Arctic sea ice is concentrated in the Labrador Sea Water formation region and occurs mainly during late winter which is also the main convection season. It thus efficiently weakens deep water formation in the subpolar North Atlantic.
- the initial freshening by sea ice is amplified by positive feedbacks attributed to the subpolar gyre. This makes convection in the Labrador Sea more vulnerable than in the Nordic Seas.

Acknowledgments We gratefully acknowledge Oliver Marti for technical assistance as well as discussions with Tor Eldevik, Bjørg Risebrobakken, Tore Furevik and Uwe Mikolajewicz. We further thank two anonymous referees whose reviews improved our earlier manuscript. A. Born was funded by the Marie Curie Actions project NICE (MRTN-CT-2006-036127). Computer time was provided by the Centre National de la Recherche Scientifique (IDRIS computing center) and the Commissariat à l'Energie Atomique (CCRT computing center). This work is a contribution to the French ANR blanc "PICC". This is publication number A260 from the Bjerknes Centre for Climate Research.

References

Adkins JF, Boyle EA, Keigwin LD, Cortijo E (1997) Variability of the North Atlantic thermohaline circulation during the last interglacial period. Nature 390:154–156

Arzel O, Fichefet T, Goosse H, Dufresne J-L (2008) Causes and impacts of changes in the Arctic freshwater budget during the twentieth and twenty-first centuries in an AOGCM. Clim Dyn 30:37–58

Beckmann A (1998) The representation of bottom boundary layer processes in numerical ocean circulation models. In: Chassignet EP and Verron J (eds) Ocean modeling and parametrization. Kluwer, Dordrecht, pp 135–154

Berger A (1978) Long-term variations of caloric solar radiation resulting from the Earth's orbital elements. Quat Res 9:139–167

Born A, Levermann A, Mignot J (2009) Sensitivity of the Atlantic ocean circulation to a hydraulic overflow parameterisation in a coarse resolution model: response of the subpolar gyre. Ocean Model 27(3–4):130–142

Braconnot P, Marzin C, Grégoire L, Mosquet E, Marti O (2008) Monsoon response to changes in Earth's orbital parameters: comparisons between simulations of the Eemian and of the Holocene. Clim Past 4:281–294

Bryden HL, Imawaki S (2001). Ocean heat transport. In: Siedler G, Church J, Gould J (eds) Ocean circulation and climate: observing and modelling the global ocean. Acdemic Press, San Diego, pp 455–474

Calov R, Ganopolski A, Petoukhov V, Claussen M, Brovkin V, Kubatzki C (2005) Transient simulation of the last glacial inception. Part II: sensitivity and feedback analysis. Clim Dyn 24:563–576

Cortijo E, Duplessy JC, Labeyrie L, Leclaire H, Duprat J, van Weering TCE (1994) Eemian cooling in the Norwegian Sea and North Atlantic ocean preceding continental ice-sheet growth. Nature 372:446–449

Curry R, Mauritzen C (2005). Dilution of the northern North Atlantic ocean in recent decades. Science 308:1772–1774

de Noblet N, Prentice I, Joussaume S, Texier D, Botta A, Haxeltine A (1996) Possible role of atmosphere-biosphere interactions in triggering the last glaciation. Geophys Res Lett 23:3191–3194

de Vernal A, Hillaire-Marcel C (2008) Nature variability of greenland climate vegetation, and ice volume during the past million years. Science 320:1622–1625

Divine DV, Dick C (2006) Historic variability of sea ice edge position in the Nordic Seas. J Geophys Res 111:C01001

Evans HK, Hall IR, Bianchi GG, Oppo DW (2007) Intermediate water links to deep Western boundary current variability in the subtropical NW Atlantic during marine isotope stages 5 and 4. Paleoceanography 22:PA3209

Fichefet T, Maqueda MAM (1997) Sensitivity of a global sea ice model to the treatment of ice thermodynamics and dynamics. J Geophys Res 102:12609

Fichefet T, Maqueda MAM (1999) Modelling the influence of snow accumulation and snow-ice formation on the seasonal cycle of the Antarctic sea-ice cover. Clim Dyn 15:251–268

Fronval T, Jansen E, Haflidason H, Sejrup JP (1998) Variability in surface and deep water conditions in the Nordic seas during the last interglacial period. Quat Sci Rev 17:963–985

Govin A, Michel E, Labeyrie L, Waelbroeck C, Dewilde F, Jansen E (2009) Evidence for northward expansion of Antarctic Bottom Water mass in the Southern Ocean during the last glacial inception. Paleoceanography 24:PA1202. doi:10.1029/2008PA001603

Gröger M, Maier-Reimer E, Mikolajewicz U, Schurgers G, Vizcaíno M, Winguth A (2007) Changes in the hydrological cycle, ocean circulation, and carbon/nutrient cycling during the last interglacial and glacial transition. Paleoceanography 22:PA4205

Häkkinen S, Rhines PB (2004) Decline of subpolar North Atlantic circulation during the 1990s. Science 304:555–559

Hátún H, Sandø AB, Drange H, Hansen B, Valdimarsson H (2005) Influence of the atlantic subpolar gyre on the thermohaline circulation. Science 309:1841–1844

Hibler WD (1979) A dynamic thermodynamic sea ice model. J Phys Oceanogr 9:815–846

Hillaire-Marcel C, de Vernal A, Bilodeau A, Weaver AJ (2001) Absence of deep-water formation in the Labrador Sea during the last interglacial period. Nature 410:1073–1077

Holland MM, Finnis J, Serrenze MC (2006) Simulated Arctic Ocean freshwater budgets in the twentieth and twenty-first centuries. J Clim 19:6221–6242

Hourdin F, Musat I, Bony S, Braconnot P, Codron F, Dufresne J, Fairhead L, Filiberti M, Friedlingstein P, Grandpeix J, Krinner G, Levan P, Li Z, Lott F (2006) The LMDZ4 general circulation model: climate performance and sensitivity to parametrized physics with emphasis on tropical convection. Clim Dyn 27(7–8):787–813

IPCC (2007) Climate Change 2007: The Physical Science Basis. In: Solomon S, Qin D, Manning M, Chen Z, Marquis M, Averyt KB, Tignor M, Miller HL (eds) Contribution of Working Group I to the fourth assessment report of the intergovernmental panel on climate change. Cambridge University Press, Cambridge

Khodri M, Leclainche Y, Ramstein G, Braconnot P, Marti O, Cortijo E (2001) Simulating the amplification of orbital forcing by ocean feedbacks in the last glaciation. Nature 410:570–574

Khodri M, Ramstein G, Paillard D, Duplessy C, Kageyama M, Ganopolski A (2003) Modelling the climate evolution from the last interglacial to the start of the last glaciation: the role of arctic ocean freshwater budget. Geophys Res Lett 30(12):1606

Krinner G, Viovy N, de Noblet-Ducoudre N, Ogee J, Polcher J, Friedlingstein P, Ciais P, Sitch S, Prentice IC (2005) A dynamic global vegetation model for studies of the coupled atmosphere–biosphere system. Glob Biogeochem Cycles 19(1):GB1015

Levermann A, Born A (2007) Bistability of the Atlantic subpolar gyre in a coarse-resolution model. Geophys Res Lett 34:L24605

Levitus S (1982) Climatological atlas of the world ocean. NOAA Professional Paper, vol 13. US Department of Commerce, Washington, DC

Madec G, Delecluse P, Imbard M, Lévy C (1997) OPA version 8.1 Ocean General Circulation Model reference manual. Institut Pierre-Simon Laplace, Note du Pôle de modélisation no. 11

Marti O, Braconnot P, Dufresne J-L, Bellier J, Benshila R, Bony S, Brockmann P, Cadule P, Caubel A, Codron F, de Noblet N, Denvil S, Fairhead L, Fichefet T, Foujols M-A, Friedlingstein P, Goosse H, Grandpeix J-Y, Guilyardi E, Hourdin F, Idelkadi A, Kageyama M, Krinner G, Lévy C, Madec G, Mignot J, Musat I, Swingedouw D, Talandier C (2009) Key features of the IPSL ocean atmosphere model and its sensitivity to atmospheric resolution. Clim Dyn 34(1):1–26. doi:10.1007/s00382-009-0640-6

Meissner KJ, Weaver AJ, Matthews HD, Cox PM (2003) The role of land surface dynamics in glacial inception: a study with the UVic Earth system model. Clim Dyn 21:515–537

Molyneux EG, Hall IR, Zahn R, Diz P (2007) Deep water variability on the southern Agulhas Plateau: interhemispheric links over the past 170 ka. Paleoceanography 22:PA4209

Müller UC, Kukla GJ (2004) North Atlantic Current and European environments during the declining stage of the last interglacial. Geology 32:1009–1012

Oppo DW, Lehman SJ (1995) Suborbital timescale variability of North Atlantic deep water during the past 200,000 years. Paleoceanography 10(5):901–910

Otterå OH, Drange H (2004). Effects of solar irradiance forcing on the ocean circulation and sea-ice in the North Atlantic in an isopycnic coordinate ocean general circulation model. Tellus 56A:154–166

Otto-Bliesner BL, Brady E, Clauzet G, Tomas R, Levis S, Kothavala Z (2006a) Last glacial maximum and holocene climate in CCSM3. J Clim 19:2526–2544

Otto-Bliesner BL, Marshall SJ, Overpeck JT, Miller GH, Hu A, CAPE Last Interglacial Project members (2006b) Simulating arctic climate warmth and icefield retreat in the last interglaciation. Science 311:1751–1753

Rasmussen TL, Oppo DW, Lehman ETSJ (2003). Deep sea records from the southeast Labrador Sea: ocean circulation changes and ice-rafting events during the last 160,000 years. Paleoceanography 18(1):1018

Roullet G, Madec G (2000). Salt conservation, free surface, and varying levels: a new formulation for ocean general circulation models. J Geophys Res 105:23927–23942

Siegenthaler U, Stocker TF, Monnin E, Lüthi D, Schwander J, Stauffer B, Raynaud D, Barnola J-M, Fischer H, Masson-Delmotte V, Jouzel J (2005) Stable carbon cycle-climate relationship during the late Pleistocene. Science 310:1313–1317

Smedsrud LH, Sorteberg A, Kloster K (2008) Recent and future changes of the arctic sea-ice cover. Geophys Res Lett 35:L20503

Spall MA (2004) Boundary currents and watermass transformation in marginal seas. J Phys Oceanogr 34:1197–1213

Straneo F (2006) On the connection between dense water formation, overturning, and poleward heat transport in a convective basin. J Phys Oceanogr 36:1822–1840

Swingedouw D, Braconnot P, Delecluse P, Guilyardi E, Marti O (2007a) Quantifying the AMOC feedbacks during a 2 × CO_2 stabilization experiment with land-ice melting. Clim Dyn 29:521–534

Swingedouw D, Braconnot P, Delecluse P, Guilyardi E, Marti O (2007b) The impact of global freshwater forcing on the thermohaline circulation: adjustment of North Atlantic convection sites in a CGCM. Clim Dyn 28:291–305

Vellinga M, Wood RA (2002) Global climatic impacts of a collapse of the atlantic thermohaline circulation. Clim Change 54:251–267

Vettoretti G, Peltier WR (2003) Post-Eemian glacial inception. Part II: elements of a cryospheric moisture pump. J Clim 16:912–927

Wood RA, Keen AB, Mitchell JFB, Gregory JM (1999) Changing spatial structure of the thermohaline circulation in response to atmospheric CO_2 forcing in a climate model. Nature 399:572–575

Yoshimori M, Reader MC, Weaver AJ, McFarlane NA (2002) On the causes of glacial inception 115 kaBP. Clim Dyn 18:383–402

Zheng W, Braconnot P, Guilyardi E, Merkel U, Yu Y (2008) ENSO at 6ka and 21ka from ocean-atmosphere coupled model simulations. Clim Dyn 30(7–8):745–762

Paper II

Late Eemian warming in the Nordic Seas as seen in proxy data and climate models

Born, A., K. H. Nisancioglu and B. Risebrobakken (2010)

Paleoceanography, (in revision)

Late Eemian warming in the Nordic Seas as seen in proxy data and climate models

A. Born[1]**,**

Bjerknes Centre for Climate Research, Bergen, Norway

Geophysical Institute, University of Bergen, Bergen, Norway

Potsdam Institute for Climate Impact Research, Potsdam, Germany

K. H. Nisancioglu,

Bjerknes Centre for Climate Research, Bergen, Norway

UNI Research, Bergen, Norway

B. Risebrobakken

Bjerknes Centre for Climate Research, Bergen, Norway

UNI Research, Bergen, Norway

[1] Corresponding author: andreas.born@bjerknes.uib.no

Abstract

We analyze a transient simulation of the last glacial inception in a climate model of intermediate complexity, focusing on sea ice-ocean circulation dynamics in the North Atlantic and Nordic Seas. As northern high latitude summer insolation decreases towards the end of the Eemian interglacial, Arctic sea ice export to the North Atlantic increases. This surface fresh water transport weakens deep water formation in the North Atlantic and the near surface circulation of the subpolar gyre. As a consequence, the relative contribution of subpolar gyre waters to the Atlantic inflow into the Nordic Seas is reduced, giving way to more warm and saline subtropical waters from the North Atlantic Current. We thus find an episode of relatively high heat and salt transport into the Nordic Seas during the last glacial inception between 119,000 and 115,000 years before present. This stabilizes deep ocean convection in the region and warms Scandinavia during a phase of low insolation. These findings are in good agreement with proxy data from the Nordic Seas and North Atlantic. At the end of the warm interval, sea surface temperature drops by about 3°C, marking the onset of large scale glacier growth over Scandinavia.

1 Introduction

The last glacial inception about 115,000 years ago (115 ka) was a period of exceptionally low summer insolation in northern high latitudes. This facilitated the nucleation of continental scale ice sheets in the Northern Hemisphere and triggered feedback processes which eventually led to the end of the interglacial climate and a shift to a cold glacial climate (*de Noblet et al.*, 1996; *Khodri et al.*, 2001; *Calov et al.*, 2005).

There is, however, evidence that the cooling due to lower insolation was not homogeneous and that relatively high temperatures prevailed in the eastern North

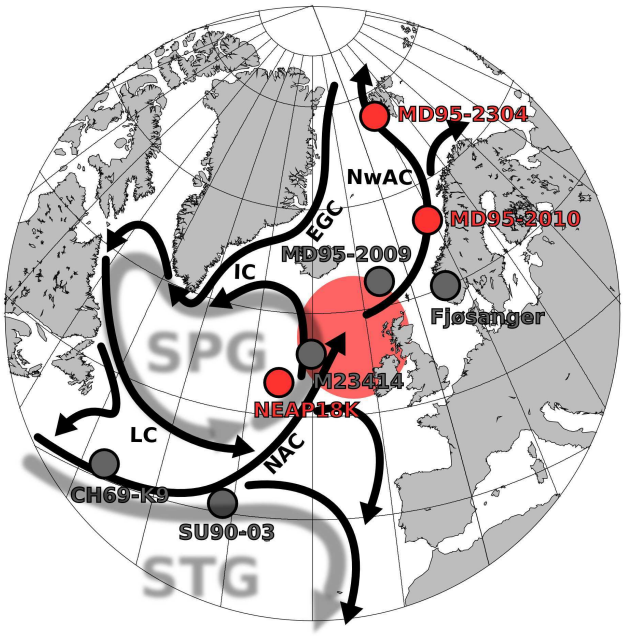

Figure 1: Map of the North Atlantic and Nordic Seas showing major ocean surface currents (arrows), marine sediment cores used in this study (red), and marine sediment cores and a terrestrial excavation site discussed in the text (gray). See Table 1 for references. Current systems of subpolar gyre (SPG) and subtropical gyre (STG) are illustrated in light gray. Source region of NwAC is highlighted in light red. Abbreviations: NAC, North Atlantic Current; NwAC, Norwegian Atlantic Current; EGC, East Greenland Current; LC, Labrador Current; IC, Irminger Current.

Atlantic (*Chapman and Shackleton*, 1999; *Bauch and Kandiano*, 2007) and the eastern and northern Nordic Seas (*Risebrobakken et al.*, 2007) throughout the insolation minimum. The warming is attributed to a strengthening of the Norwegian Atlantic Current (NwAC), carrying warm and saline water from the Atlantic Ocean through the Nordic Seas into the Barents Sea and Arctic Ocean (Fig. 1). It plays an important role in the formation of deep waters and changes in its strength likely impact the deep outflow from the Nordic Seas. A weakening of this deep current only after the insolation minimum also suggests that the NwAC continued to be active (*Rasmussen et al.*, 1999). Further south, in the central North Atlantic, a northward shift of the North Atlantic Current is reported coeval with the strengthening of the NwAC (*Cortijo et al.*, 1999). The combined evidence from proxy data thus indicates a reorganization of the large scale current system.

Previous modeling work identified the following chain of events in the coupled climate model IPSL CM4 (*Born et al.*, 2010): decreased summer insolation in northern high latitudes at 115 ka compared to 126 ka increases the Arctic sea ice volume. Thus, thicker sea ice is transported southward in the East Greenland Current, freshening the surface waters of the North Atlantic. Consequently, deep convection is shut down in this region and the altered density structure weakens the subpolar gyre. This in turn reduces the relative contribution of the subpolar gyre to a water mass formed in the Rockall region of the eastern North Atlantic, giving way to more warm and saline subtropical waters to enter the Nordic Seas (*Hátún et al.*, 2005). This mechanism counteracts decreasing insolation and the general freshening trend due to enhanced sea ice transport (Fig. 2). The weaker subpolar gyre also allows for a northward shift of the North Atlantic Current, observed as a warm anomaly and a salinity dipole off Newfoundland.

In the present study we expand this work with a transient simulation. The aim is to investigate if findings from proxy data can be reproduced in a physically consistent climate model and thus provide a detailed description of the regional climate evolution of the last glacial inception. The North Atlantic surface circulation is found to play an important role. Following a description of models in Section 2 and proxy data in Section 3, results of the two coupled climate models are analyzed in Section 4. Based on the model results, an interpretation and discussion of proxy data is given in Section 5. We summarize and conclude in Section 6.

2 Model Description and Experiments

This study combines simulations of a high resolution ocean atmosphere general circulation model, IPSL CM4 (*Marti et al.*, 2010), and a coupled climate model of intermediate complexity CLIM*BER*-3α (*Montoya et al.*, 2005). Time slice experiments have been carried out for 126 ka and 115 ka in both models, and integrated to quasi-equilibrium. In addition, a transient simulation with CLIM*BER*-3α was integrated from the end of the 126 ka equilibrium with variable orbital forcing through 110 ka. A series of sensitivity experiments with CLIM*BER*-3α is used to test the models response to anomalous freshwater flux at 126 ka.

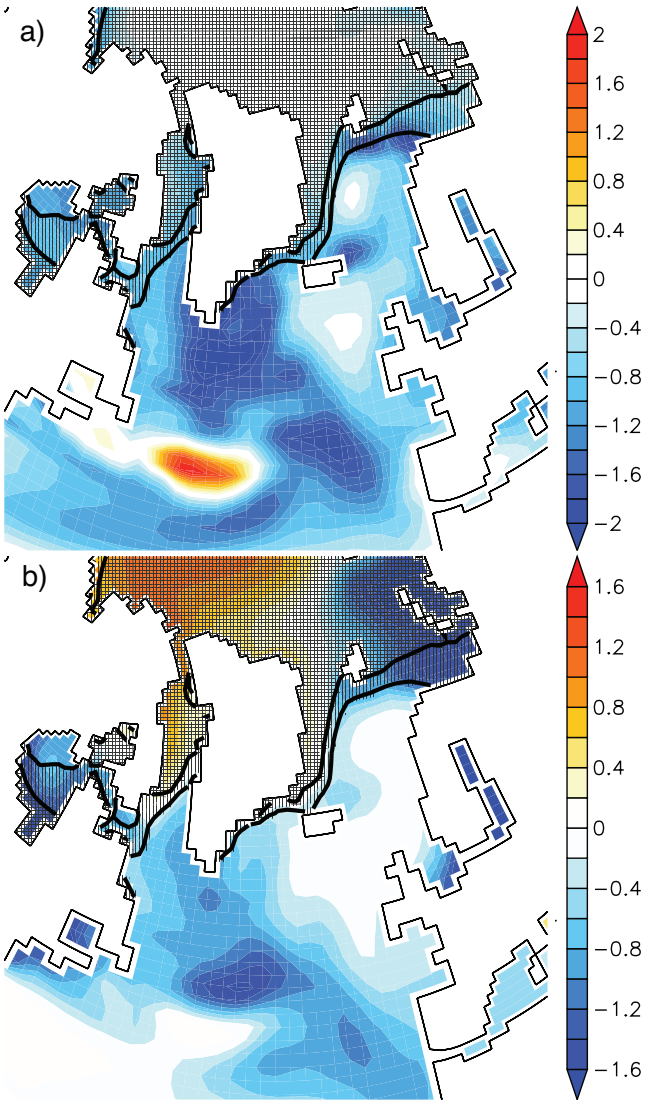

Figure 2: Differences 115k - 126k for IPSL CM4, averaged over the upper 50 m, **a)** temperature in °C, **b)** salinity in psu. Areas covered by more than 50 % sea ice annually averaged are hatched horizontally (126 ka) and vertically (115 ka) to mask regions directly affected by sea ice. Temperature and salinity show almost no change in the NwAC source region in the eastern North Atlantic and along the path of the Atlantic inflow into the Nordic Seas.

All experiments are forced by orbital insolation following *Berger* (1978) and fixed greenhouse gas concentrations at the preindustrial level (CO_2, 280 ppmv). The latter is a good approximation for the Eemian and the last glacial inception until about 112 ka (*Petit et al.*, 1999; *Lüthi et al.*, 2008). CO2 concentration started decreasing gradually at 112 ka, reaching 250 ppmv at 110 ka. This is not included in the simulations. However, this only concerns the very last part and not the main study interval. Details of the models and relevant references are given below.

2.1 IPSL

The Institut Pierre Simon Laplace coupled model version 4 (IPSL CM4) comprises ocean, sea ice, atmosphere and land surface components. The ocean model's dynamical core is based on the OPA system (*Madec et al.*, 1997). The configuration used here (ORCA2) uses a horizontal resolution based on a 2°Mercator mesh, enhanced to 0.5°meridional resolution near the equator for a better representation of the equatorial wave channel. Two poles are placed over continents in the Northern Hemisphere in order to avoid a singularity in the Arctic Ocean. There are 31 unevenly spaced levels in the vertical. A free surface formulation is used for the upper boundary (*Roullet and Madec*, 2000), and a diffusive boundary parametrization is used for the bottom (*Beckmann*, 1998).

The dynamic sea ice model (LIM2, *Fichefet and Maqueda* (1997, 1999)) uses the horizontal ocean grid to compute ice rheology and advection. Thermodynamics are computed in three vertical layers, the uppermost for snow. Ice growth and melting are determined by an energy balance at both the snow-ice and water-ice boundary and in leads. Internal forces follow a viscous-plastic law (*Hibler*, 1979). The model features parametrizations for the trapping of shortwave radiation by brine pockets, leads in the ice, as well as an implicit representation of subgrid variations in snow and ice thickness.

The atmosphere is modeled by a comprehensive general circulation model (LMDZ, *Hourdin et al.* (2006)) with a resolution of 3.75 zonally and 2.5 meridionally on 19 vertical levels. Precipitation over land is returned to the ocean by means of a river routing scheme implemented in the land surface model (ORCHIDEE, *Krinner et al.*

(2005)).

The simulations for 126 ka and 115 ka were initiated with an ocean at rest and preindustrial hydrography (*Levitus*, 1982) and integrated for 300 and 800 years, respectively. The results presented are calculated from averages over the last 100 years of the simulations. More information on the simulations can be found in *Braconnot et al.* (2008) and *Born et al.* (2010).

2.2 CLIM*BER*-3α

CLIM*BER*-3α consists of the statistical-dynamical atmospheric model POTSDAM-2 (*Petoukhov et al.*, 2000) coupled to a global, 24-layer ocean general circulation model based on the Geophysical Fluid Dynamics Laboratory (GFDL) Modular Ocean Model version 3 (MOM-3) code and to the dynamic and thermodynamic sea ice module of *Fichefet and Maqueda* (1997). The sea ice component is based on the same code-base as in IPSL CM4. The oceanic horizontal resolution is $3.75^\circ \times 3.75^\circ$. We apply a weak background vertical diffusivity of 0.2×10^{-4} m^2/s. For a discussion of the model's sensitivity to this parameter refer to *Mignot et al.* (2006). Sea ice albedo is increased by 5% compared to *Montoya et al.* (2005) in order to ensure a more realistic Arctic sea ice cover at 126 ka. This change is within uncertainties of observed ice albedo values.

The atmospheric model has a coarse spatial resolution (7.5° in latitude and 22.5° in longitude) and is based on the assumption of a universal vertical structure of temperature and humidity, which allows reducing the three-dimensional description to a set of two-dimensional prognostic equations. Heat and freshwater fluxes between the ocean and the atmosphere are computed on the oceanic grid and applied without flux adjustments. The wind stress is computed as the sum of the NCEP-NCAR reanalysis wind stress climatology (*Kalnay and coauthors*, 1996) and the wind stress anomaly calculated by the atmospheric model relative to a preindustrial control run.

This model has been used in several studies of past climates (*Montoya et al.*, 2010; *Born and Levermann*, 2010) and future projections (*Feulner and Rahmstorf*, 2010) as well as in model intercomparisons (*Gregory et al.*, 2005; *Stouffer et al.*, 2006; *Levermann et al.*, 2007).

Time slice experiments for 126 ka and 115 ka were initialized from the preindustrial control experiment and run to equilibrium for more than 2000 years. A transient simulation was started from the equilibrium of the 126 ka experiment and ran through 110 ka. Atmospheric chemical composition, land surface topography and albedo were fixed and thus neglect feedbacks of the progressing glacial inception. However, as discussed in Section 6, findings presented here do not depend critically on this simplification. A control experiment with forcing fixed at 126 ka was run in parallel for 4000 years. In order to test the model's sensitivity to increased sea ice export, a series of experiments was carried out with anomalous freshwater flux south of Denmark Strait. These experiments are based on the 126 ka equilibrium and run to equilibrium for 2000 years.

3 Marine sediment cores and proxy data

Marine proxy records from cores MD99-2304 (eastern Fram Strait), MD95-2010 (Vøring Plateau) and NEAP18K (Rockall Plateau) are presented (Fig. 1). The cores are located along the pathway of Atlantic water towards the Arctic. From MD99-2304 and MD95-2010 relative abundances of *Neogloboquadrina pachyderma* (sin) and *Neogloboquadrina pachyderma* (dex) are shown, as well as calculated sea surface temperatures. Planktic $\delta^{18}O$ of *Globigerina bulloides* and transfer function based sea surface temperatures are shown from NEAP18K. All records, except from the temperatures of MD99-2304 and MD95-2010, are previously published. Detailed information on methods and establishment of chronologies can be found in the original publications (Tab. 1). The chronology of NEAP18K is taken from *Chapman and Shackleton* (1999). The summer sea surface temperatures of MD99-2304 and MD95-2010 have been calculated based on the relative abundances of *N. pachyderma* (sin) ($T = -0.07 \cdot (\%N.\ pachyderma(sin)) + 12.5$) (*Johannessen*, 1987). This equation is restricted by an upper and lower temperature limit of 5.5°C and 12.4°C, respectively. The amplitude of our sea surface temperature estimates may be affected, most probably by providing too warm temperatures in the cold end.

Table 1: Locations of marine sediment cores used or discussed in the text. Original references to previously published proxy records are given.

Core name	Position	Depth (m)	References
MD95-2304	78°N, 10°E	1315	*Risebrobakken et al.* (2005, 2007)
MD95-2010	67°N, 5°E	1226	*Risebrobakken et al.* (2005, 2007)
MD95-2009	63°N, 4°W	1027	*Rasmussen et al.* (1999)
Fjøsanger	60°N, 5°E	0	*Mangerud et al.* (1981)
M23414	54°N, 20°W	2196	*Bauch and Kandiano* (2007)
NEAP18K	52°N, 30°W	3275	*Chapman and Shackleton* (1999), *Cortijo et al.* (1999)
CH69-K9	41°N, 47°W	4100	*Cortijo et al.* (1999)
SU90-03	40°N, 32°W	2475	*Cortijo et al.* (1999)

4 Model Results

4.1 Simulation of the last glacial inception

While resolution is significantly lower in CLIM*BER*-3α compared to IPSL CM4, the key elements determining the dynamical changes depend on large scale features of the climate system and are thus well reproduced (Fig. 3). At 126 ka, most of the Arctic winter sea ice is thinner than 3 m in IPSL CM4, and thinner than 2 m in CLIM*BER*-3α. Both models simulate a similar area of winter sea ice exceeding 5 m thickness at 115 ka. Sea ice volume transport through Denmark Strait increases in both models; by 53 mSv in IPSL CM4 and 23 mSv in CLIM*BER*-3α (1 Sv = 10^6 m^3/s). The subpolar gyre weakens from 26 Sv to 18 Sv between 126 ka and 115 ka in IPSL CM4 and from 29 Sv to 19 Sv in CLIM*BER*-3α.

Analysis of the transient experiment supports the following causal chain led by changes in summer insolation (Fig. 4). Arctic sea ice export through Denmark Strait increases as summer insolation decreases. The associated freshwater transport reduces the density in the subpolar gyre center (40°W - 30°W, 53°N - 57°N) and weakens the cyclonic circulation first gradually and after 119 ka in a rapid transition. Temperature changes in the subpolar gyre due to the changing insolation forcing are minor and cause only a small density signal. Changes in the freshwater exchange with the atmosphere are smaller than those due to import of freshwater by sea ice

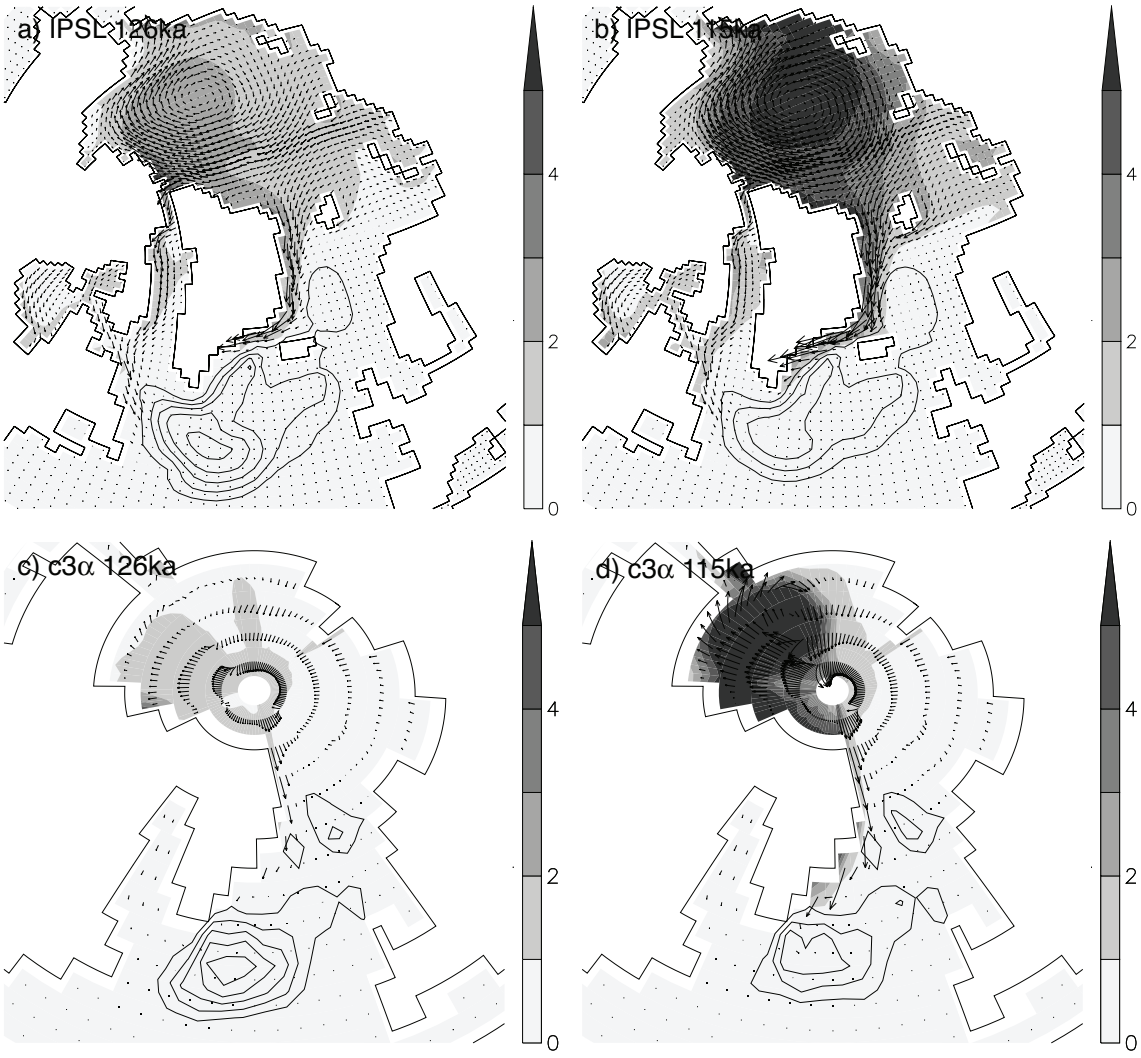

Figure 3: Arctic sea ice thickness (shading, in m), sea ice transport (arrows, in m^2/s) and depth integrated stream function (contours, spacing 2 Sv, cyclonic flow only); **upper row:** IPSL CM4; **lower row:** CLIM*BER*-3α; **left column:** 126 ka; **right column:** 115 ka. Both models agree well on sea ice thickening in the Arctic Ocean, more sea ice export in the East Greenland Current and the consequential weakening of the subpolar gyre circulation.

and are mostly due to changes in evaporation. Thus, they can be attributed to lower sea surface temperatures in the subpolar gyre center caused by the reorganization of the circulation (also seen in IPSL CM4, Fig. 2a). Consistent with this view, the air-sea freshwater balance changes rapidly coeval with the subpolar gyre index and is a response, rather than a cause of the observed changes. Concurrent with the change in circulation, northward heat transport by the NwAC increases by 16 % ($\sim 39 \cdot 10^{12}$ W). As summer insolation increases again the process is reversed with a second abrupt transition at 115 ka.

Due to its coarse resolution, the estuarine circulation of the Nordic Seas is not represented accurately in CLIM*BER*-3α. The consequences of higher heat transport into the Nordic Seas for sea surface temperatures can not be traced northward from the Greenland Scotland ridge. This does not affect the findings above that are based entirely on the circulation south of the Greenland Scotland ridge. Although not directly comparable, fluxes across the Greenland Scotland ridge in CLIM*BER*-3α are generally similar to present-day observations by *Hansen and Østerhus* (2000): about 7 Sv of Atlantic water and 0.25 PW of heat enter the Nordic Seas as a surface current between Iceland and Scotland. This is approximately the same section used for the model in figure 4e. Observed sinking in the Nordic Seas is about 6 Sv.

The increase in heat transport in CLIM*BER*-3α is in good agreement with the relative warming and salinification of the NwAC found in IPSL CM4 (Fig. 2b). Note that despite increased heat transport by the NwAC, no absolute warming of the Nordic Seas is expected at 115 ka because of the counteracting large insolation forcing (Fig. 4a). Similarly, enhanced salt transport counteracts the general freshening by sea ice locally but does not reverse it. However, this is enough to stabilize deep water formation in the Nordic Seas (Fig. 4f) (*Born et al.*, 2010).

Stabilization of Nordic Seas deep water formation is also seen in mixed layer depth (Fig. 5). Deep convection remains active in the Nordic Seas despite the general freshening and more extensive sea ice (Fig. 2b). Absolute values differ between the two models. IPSL CM4 simulates a shallower mixed layer than CLIM*BER*-3α. Besides slightly different definitions of the mixed layer complicating a direct comparison, it is possible that the high resolution IPSL CM4 model requires a longer integration time to equilibrate the deep ocean with possible impact on the formation

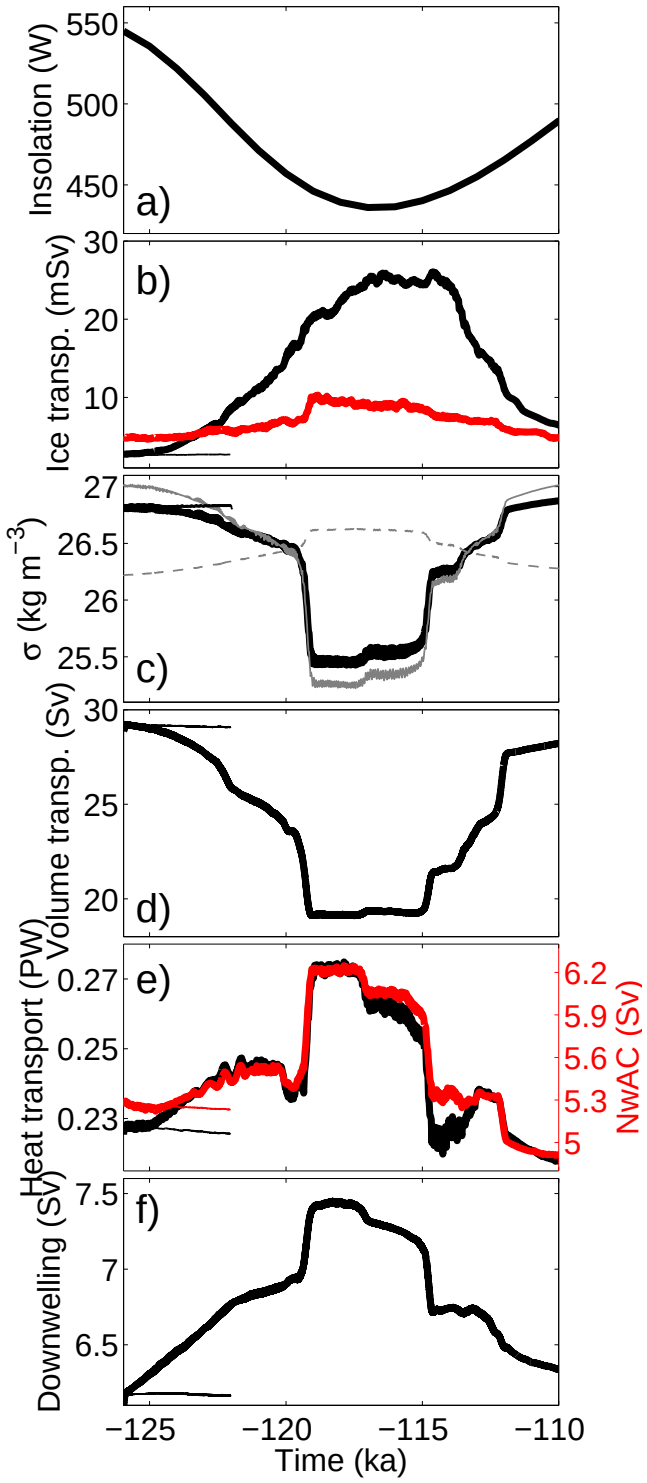

Figure 4: Key variables for climate evolution of the last glacial inception, averaged over 100 years, for CLIM*BER*-3α. Thin curves show results of a 126 ka control experiment: **(a)** June insolation at 65°N; **(b)** southward sea ice transport through Denmark Strait (black) and net air-sea freshwater flux in the subpolar gyre center (red, positive into ocean); **(c)** surface density in the subpolar gyre center (black), decomposed into salinity (gray solid) and temperature (gray dashed) contributions; **(d)** circulation strength of the subpolar gyre; **(e)** heat transport (black) and volume transport (red) in the NwAC across a zonal section at 64°N; **(f)** downwelling in the Nordic Seas.

of deep water. At the same time, a known deficiency of coarse resolution models is the imperfect representation of the southward outflow from the Nordic Seas over the deep and narrow sills of the Greenland Scotland ridge that also influences the mixed layer depth (*Roberts and Wood*, 1997; *Thorpe et al.*, 2004; *Born et al.*, 2009). As a result bottom waters leaving the Nordic Seas are less dense than observed and the reservoir of deep dense water in the Nordic Seas is not optimally represented in coarse resolution models which again impacts deep convection. The main conclusion, however, a stable deep circulation in the Nordic Seas at 115 ka, is consistent with both models. South of the Greenland Scotland ridge, IPSL CM4 shows two deep convection regions of which only one is active at 115 ka. CLIM*BER*-3α does not resolve two distinct regions but shows a weaker convection at 115 ka. This is a result of freshening in both models (Fig. 2b and 4c), caused by the enhanced sea ice transport into the region but partly also due to weaker salt advection in the subpolar gyre (*Levermann and Born*, 2007; *Born et al.*, 2010).

4.2 Sensitivity experiments

In order to test quantitatively how the increased Arctic sea ice export impacts the subpolar gyre, a series of experiments was carried out with CLIM*BER*-3α, simulating the redistribution of freshwater between the Arctic Ocean and a region south of Denmark Strait with anomalous fluxes of different strength, based on the 126 ka equilibrium experiment (Fig. 6). The freshwater forcing was applied continuously with no seasonal cycle. The experiments were run to equilibrium for 2100 years. Results shown are averages of the last 100 years. The subpolar gyre weakens rapidly to 19 Sv when an anomalous freshwater flux of 40 mSv is applied. This compares well to the reduction of the subpolar gyre to 19 Sv when the freshwater flux from sea ice equals 27 mSv in the transient experiment (Fig. 4), supporting the hypothesis that increased Arctic sea ice export is the primary cause for the weaker gyre.

There are several factors accounting for the weaker response of the subpolar gyre in the sensitivity experiments. The anomalous freshwater forcing was applied continuously while the freshwater transport by sea ice is stronger in winter and spring. The latter has a stronger impact on convection, which also occurs in late winter and plays an important role for the density structure of the deep water column and thus

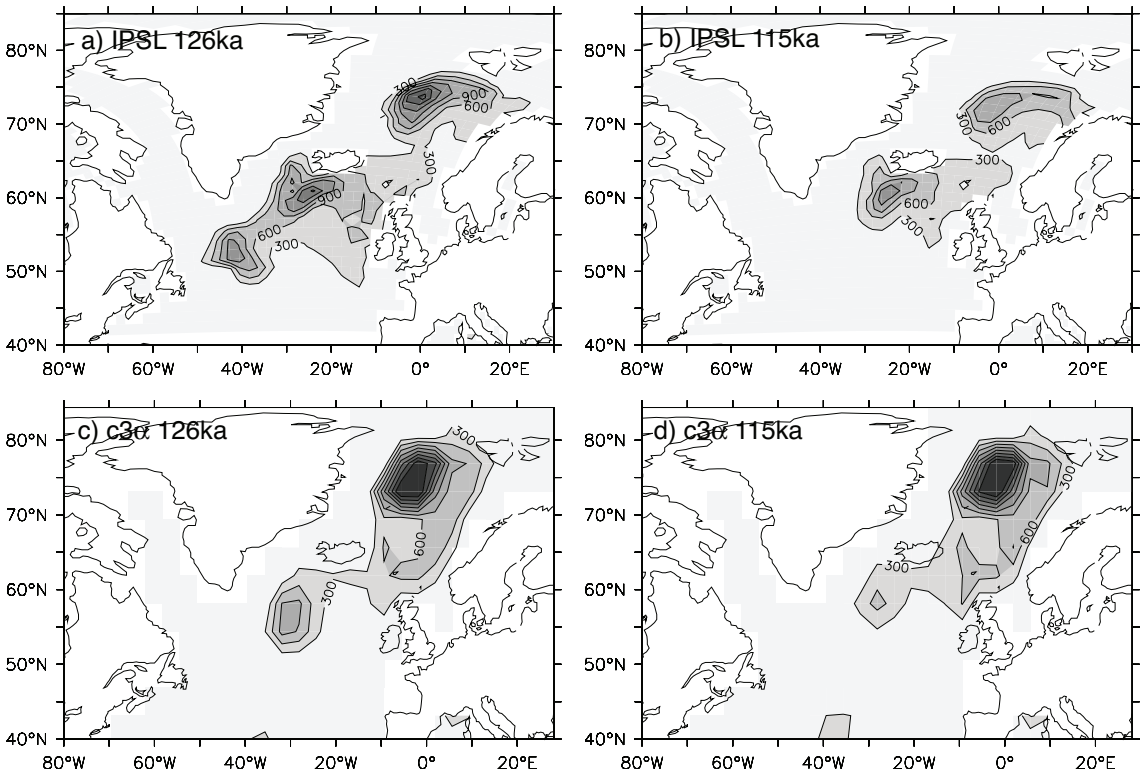

Figure 5: Mixed layer depth (in m); **upper row:** IPSL CM4; **lower row:** CLIM*BER*-3α; **left column:** 126 ka; **right column:** 115 ka. Deep convection in the Nordic Seas remains active at 115 ka in both models. South of the Greenland Scotland ridge, convection decreases leading to the shut-down of one convection region in IPSL CM4.

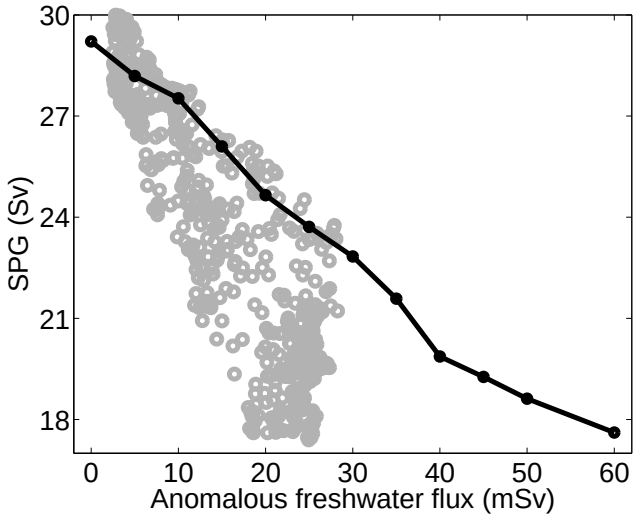

Figure 6: Equilibrium subpolar gyre strength at 126 ka as a function of anomalous freshwater flux south of Denmark Strait (black), for CLIM*BER*-3α, forcing region shown in figure. 7. Open gray circles show response of the subpolar gyre to sea ice transport through Denmark Strait in the transient experiment (see Fig. 4b,d)

the subpolar gyre. Contrary to sea ice melt, the anomalous freshwater flux was distributed evenly over the region south of Denmark Strait. The impact of the precise location and timing of freshwater forcing on the subpolar gyre is an interesting topic in itself and worthy of investigation, but beyond the scope of this study.

In addition to changes in buoyancy forcing, winds changed between 126 ka and 115 ka resulting in a stronger wind stress curl over the subpolar gyre (Fig. 7). The average anomaly over the subpolar gyre (45°W - 15°W, 45°N - 63°N) indicates a 1.3% strengthening of the atmospheric cyclonic circulation compared to the 34% weakening of the subpolar gyre circulation. Large differences are found around the sea ice edge. In addition to the analysis shown for IPSL CM4 in *Born et al.* (2010), this suggests that the buoyancy forcing dominates the weakening.

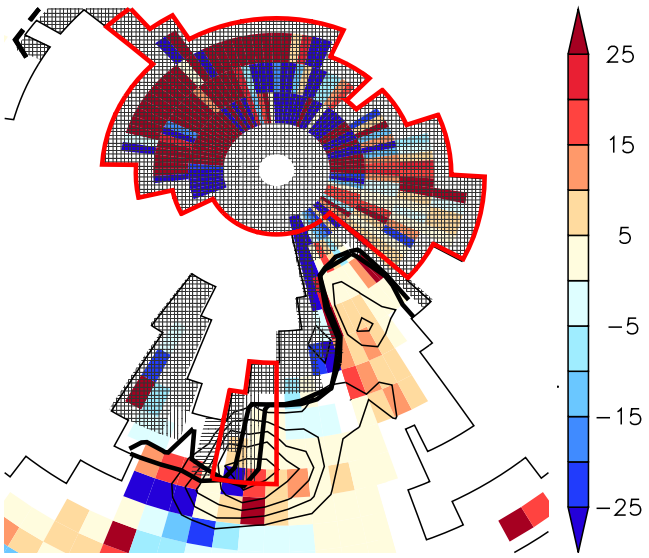

Figure 7: Relative changes in wind stress curl 115 ka minus 126 ka in Arctic Ocean, Nordic Seas and North Atlantic (colors, in %) and annual average 15% sea ice area hatched horizontally (126 ka) and vertically (115 ka), for CLIM*BER*-3α. The depth integrated stream function at 126 ka is given for orientation (contours, spacing 5 Sv, cyclonic flow only). Regions used for the anomalous freshwater forcing are shown in red. Changes in the subpolar gyre region indicate a 1.3% strengthening of the cyclonic circulation while the subpolar gyre actually weakens by 34%.

5 Evidence of strong Norwegian Atlantic Current from Proxy Data

Our model experiments compare well to a number of marine proxy records throughout the North Atlantic and Nordic Seas (Fig. 1 and Tab. 1). The simulation shows that maximum heat transport by the NwAC occurs around the time of minimum northern high latitude summer insolation, lasting from 119 ka until 115 ka, in good agreement with foraminiferal faunal data from the Vøring Plateau (MD95-2010, Fig. 8b) and the slope of western Spitsbergen (MD95-2304, Fig. 8a) (*Risebrobakken et al.*, 2007). Relatively high occurrence of the subpolar species *N. pachyderma* (dex) and *Turborotalita quinqueloba* (not shown) and low levels of the polar species *N. pachyderma* (sin) mark the peak of the interglacial warmth in both cores between approximately 126 ka and 120 ka. As insolation decreases, the relative abundance of *N. pachyderma* (sin) increases until 119 ka, when the trend reverses. The interval between 119 ka and 115 ka represents a partial recurrence of the subpolar species and thus interglacial conditions in both cores. By reconstructing surface temperature from the relative abundance of *N. pachyderma* (sin) (*Johannessen*, 1987), the temperature drop following the transient warm phase is estimated to about 3°C on the Vøring Plateau and 1.2°C off western Spitsbergen.

The late Eemian warming is also seen in many cores from the Norwegian Sea, and it has been argued for a late Eemian climatic optimum, with the most intense advection of Atlantic surface water 118.5 ka - 116 ka (*Bauch and Erlenkeuser*, 2008). Decreasing sea surface temperatures at 115 ka, probably due to a weaker inflow of Atlantic waters, are consistent with several marine records from the Nordic Seas (*Fronval et al.*, 1998; *Risebrobakken et al.*, 2005), and have been associated to the North Atlantic ocean cooling event C26 (*Müller and Kukla*, 2004).

A warm pulse is also found on the Rockall Plateau (NEAP18K) in the same time interval, both in transfer function sea surface temperature estimates based on foraminiferal assemblages and planktic $\delta^{18}O$ in the surface dwelling species *Globigerina bulloides* (Fig. 8c) (*Chapman and Shackleton*, 1999). These findings are supported by similar results seen in M23414 (*Bauch and Kandiano*, 2007). This North Atlantic warmth supports the hypothesis that the warm pulse in the Nordic

Seas originates in the North Atlantic and that it is related to increased meridional heat transport across the Greenland Scotland ridge.

Note that sea surface temperatures in the Nordic Seas can not be directly compared with the transient model simulation due to the coarse model resolution. They are consistent with the high resolution time slice simulations. However, temperature reconstructions from the relative abundance of *N. pachyderma* (dex) are based on the assumption that foraminifera are a water mass tracer. A relatively higher abundance of the warm-water subtype thus primarily indicates a stronger inflow of Atlantic water masses into the Nordic Seas, consistent with higher volume and heat transports. In this understanding, accounting for the original meaning of the proxy data, figure 8b and figure 4e represent a direct comparison.

The detailed time slice simulations with IPSL CM4 show surface warming off Newfoundland in the central North Atlantic (Fig. 2a). As explained above, this is the result of a weaker subpolar gyre and a subsequent northward shift of the North Atlantic Current, providing additional means to test the dynamical hypothesis of this study with proxy data. Warmer and more saline water is seen during the late interglacial in the central North Atlantic (Fig. 1, CH69-K9 and SU90-03), in reconstructions based on planktic $\delta^{18}O$ (*Cortijo et al.*, 1999). Generally, the prolonged warmth of the last interglacial, beyond the insolation minimum, is well documented for the eastern subpolar North Atlantic (*Ruddiman and McIntyre*, 1975; *McManus et al.*, 2002).

In addition to the surface proxy data, evidence exists for a stable deep outflow from the Nordic Seas until 115 ka (MD95-2009, (*Rasmussen et al.*, 1999)). This outflow is fed by downwelling water masses in the Nordic Seas and thus corroborates the model simulation of an active deep circulation in the Nordic Seas (Fig. 4f). A sharp decline in this supply to the densest part of North Atlantic Deep Water is also seen at the Bermuda rise at about the same time (*Lehman et al.*, 2002).

Warming towards the end of the Eemian interglacial can also be found in terrestrial data from southern Norway at Fjøsanger, indicated by the appearance of Ilex pollen (holly) (*Mangerud et al.*, 1981). Thus, there is consistence also between our marine data and terrestrial evidence. Glaciation started soon after this final warm peak. Although the data from Fjøsanger cannot be strictly correlated with the marine

cores, it suggests that a warming preceded imminent inception over Scandinavia and Spitsbergen. In an effort to correlate marine and terrestrial data of the last glacial inception on a common time scale, *Müller and Kukla* (2004) conclude that the cessation of the oceanic meridional heat transport into the Nordic Seas at 115 ka caused a substantial cooling of northern Europe and steeper vegetation and climate gradients over most of the continent.

6 Summary and Discussions

We present a physical mechanism for enhanced warmth in the eastern subpolar North Atlantic and along the path of the NwAC during times of minimum insolation forcing 115,000 years before present. Increased Arctic sea ice export in the East Greenland Current, as a direct result of the lower insolation, triggers nonlinear dynamical feedbacks of the subpolar gyre, and leads to a weaker circulation. This in turn increases the fraction of relatively warm and saline subtropical waters entering the Nordic Seas. The resulting increase in heat and salt transport into the Nordic Seas stabilizes ocean circulation and climate of the region. Comparison with marine sediment proxy data at the Fram Strait, Vøring Plateau and Rockall Plateau yields good agreement with model results.

In addition to a warm eastern North Atlantic and Nordic Seas, the weaker subpolar gyre results in a northward shift of the North Atlantic Current, creating a warm anomaly in the central North Atlantic which can also be found in proxy data. This distinctive warming pattern is the fingerprint of a weaker subpolar gyre circulation at the last glacial inception. The combination of independent proxy data thus supports the dynamical hypothesis presented here.

Intensification of the Atlantic meridional overturning circulation due to freshwater storage in growing ice sheets on land and decreased runnoff into the ocean was found to be the reason for large scale warming of the North Atlantic south of the Greenland Scotland ridge during the last glacial inception (*Ruddiman and McIntyre*, 1975; *Labeyrie et al.*, 1999; *McManus et al.*, 2002; *Meissner and Gerdes*, 2002). The North Atlantic remained warm for at least 5000 years after the Nordic Seas cooling *Müller and Kukla* (2004). The mechanism presented here does not address the

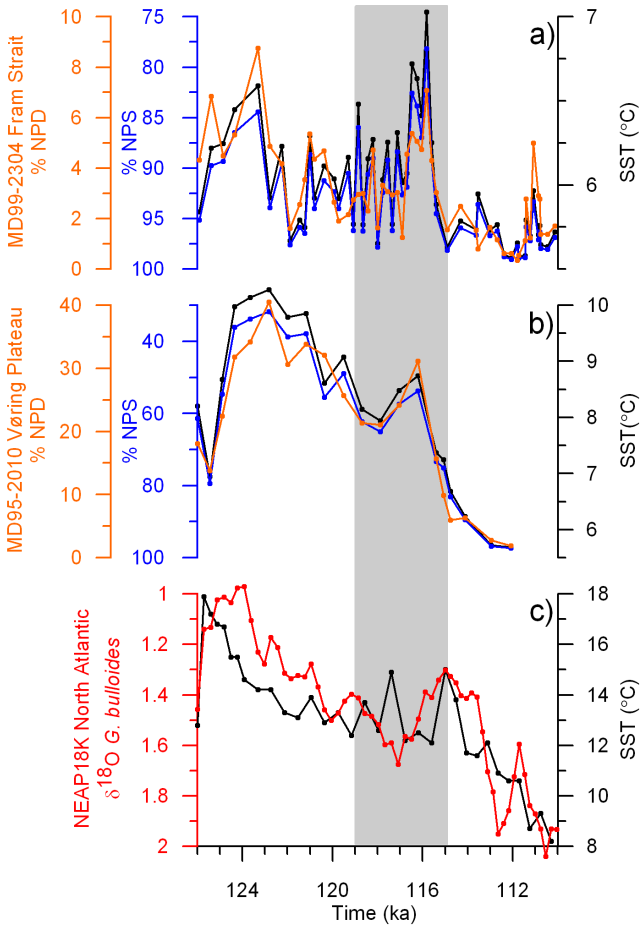

Figure 8: Proxy data reconstructions from the North Atlantic and Nordic Seas (see red dots in Fig. 1). Gray shading highlights period of maximum simulated heat transport in the NwAC (Fig. 4). **(a)** relative abundance of *N. pachyderma* (sin) (blue) and *N. pachyderma* (dex) (orange) at the western Spitsbergen slope (MD99-2304, *Risebrobakken et al.* (2007)). sea surface temperature estimate based on the relative abundance of *N. pachyderma* (sin) is shown in black (*Johannessen*, 1987); **(b)** Same as (a) but for the Vøring Plateau (MD95-2010); **(c)** *G. bulloides* $\delta^{18}O$ (red) (NEAP18K, *Chapman and Shackleton* (1999)) and sea surface temperature estimate based on modern analog technique (black) (*Cortijo et al.*, 1999). All NEAP18K data is presented on age model from (*Chapman and Shackleton*, 1999), age models of MD95-2010 and MD99-2304 follow *Risebrobakken et al.* (2005).

strengthening of the large scale deep ocean circulation, but specifically the inflow into the Nordic Seas and consequences for the northermost limb of the thermohaline circulation. The two different views are compatible.

It was suggested that Labrador Sea deep convection was not active during the last interglacial (*Hillaire-Marcel et al.*, 2001; *Cottet-Puinel et al.*, 2004). However, Labrador Sea water was produced throughout the Eemian, albeit probably at a weaker rate (*Evans et al.*, 2007) and associated to convection taking place further north in the Labrador Sea (*Rasmussen et al.*, 2003). This is consistent with the simulations presented here.

Atmospheric greenhouse gas concentrations, vegetation and ice sheet topography are kept constant at the preindustrial configuration in the experiments presented here. Recent reconstructions suggest that constant CO_2 concentration is a good approximation for the simulated period before 112 ka (*Petit et al.*, 1999; *Lüthi et al.*, 2008). It reached a value 30 ppm below the interglacial average at 110 ka, about one third of the full glacial-interglacial difference. The abrupt transition described here, however, occurred before the large changes in CO_2.

Several modeling studies identified the retreat of boreal forest and expansion of tundra with higher albedo as an important mechanism for glacier nucleation (*de Noblet et al.*, 1996; *Meissner et al.*, 2003; *Calov et al.*, 2005; *Kubatzki et al.*, 2006). However, a feedback to ocean circulation was not reported, and neglecting interactive vegetation dynamics are unlikely to change the mechanism described here.

The application of fixed present day ice sheet configuration probably introduces only negligible error to the simulation of the last glacial inception. The Eemian was very similar to present day with the Greenland ice sheet about 30 % smaller, equivalent to approximately 3 m sea level rise (*Otto-Bliesner et al.*, 2006; *de Vernal and Hillaire-Marcel*, 2008). Climate evolution was found to be insensitive to the exact choice of initial Greenland topography (*Kubatzki et al.*, 2006). Global eustatic sea level declined approximately 40 m between 120 ka and 110 ka, indicating significant ice growth on land (*Waelbroeck et al.*, 2002). However, the young ice sheets were probably relatively thin making their climatic effect little different from perennial snow fields which are included in the model used here.

Both marine and terrestrial proxy data indicate that large scale glacier growth started soon after the late Eemian warm phase (*Mangerud et al.*, 1981; *Baumann et al.*, 1995; *Risebrobakken et al.*, 2007), suggesting that the intrusion of Atlantic waters into the Nordic Seas played an important role for glacial inception over Scandinavia. Whether this warm water enhanced the air-sea temperature contrast, increased moisture transport, and accelerated ice growth, or rather delayed ice growth due to warming is unclear.

Acknowledgments

We kindly acknowledge Pascale Braconnot for access to IPSL CM4 model output as well as discussions with Jan Mangerud, John Inge Svendsen and Tore Furevik. A.B. was funded by the Marie Curie Actions project NICE (MRTN-CT-2006-036127) and the Research Council of Norway project TOPPNICE. Computer time was provided by the Research Council of Norway through the NOTUR project, Potsdam Institute for Climate Impact Research, Centre National de la Recherche Scientifique (IDRIS computing center) and the Commissariat à l'Energie Atomique (CCRT computing center). This is publication no. XXXX from the Bjerknes Centre for Climate Research.

References

Bauch, H. A., and H. Erlenkeuser (2008), A "critical" climatic evaluation of last interglacial (MIS 5e) records from the Norwegian Sea, *Polar Research*, *27*, 135–151.

Bauch, H. A., and E. S. Kandiano (2007), Evidence for early warming and cooling in North Atlantic surface waters during the last interglacial, *Paleoceanography*, *22*, PA1201.

Baumann, K.-H., K. S. Lackschewitz, J. Mangerud, R. F. Spielhagen, T. C. W. Wolf-Welling, R. Henrich, and H. Kassens (1995), Reflection of Scandinavia ice sheet

fluctuations in Norwegian Sea sediments during the last 150,000 years, *Quaternary Research*, *43*, 185–197.

Beckmann, A. (1998), *The representation of bottom boundary layer processes in numerical ocean circulation models. In: E.P. Chassignet and J. Verron, Editors: Ocean modeling and Parametrization*, pp. 135–154, Kluwer Academic Publishers, Dordrecht.

Berger, A. (1978), Long-Term Variations of Caloric Solar Radiation Resulting from the Earth's Orbital Elements, *Quaternary Research*, *9*, 139–167.

Born, A., and A. Levermann (2010), The 8.2 ka event: Abrupt transition of the subpolar gyre toward a modern North Atlantic circulation, *Geochemistry, Geophysics, Geosystems*, *11*, Q06,011, doi:10.1029/2009GC003024.

Born, A., A. Levermann, and J. Mignot (2009), Sensitivity of the Atlantic ocean circulation to a hydraulic overflow parameterisation in a coarse resolution model: Response of the subpolar gyre, *Ocean Modelling*, *27 (3-4)*, 130–142.

Born, A., K. H. Nisancioglu, and P. Braconnot (2010), Sea ice induced changes in ocean circulation during the Eemian, *Climate Dynamics*, *online*, doi: 10.1007/s00382-009-0709-2.

Braconnot, P., C. Marzin, L. Grégoire, E. Mosquet, and O. Marti (2008), Monsoon response to changes in Earth's orbital parameters: comparisons between simulations of the Eemian and of the Holocene, *Climate of the Past*, *4*, 281–294.

Calov, R., A. Ganopolski, V. Petoukhov, M. Claussen, V. Brovkin, and C. Kubatzki (2005), Transient simulation of the last glacial inception. Part II: sensitivity and feedback analysis, *Climate Dynamics*, *24*, 563–576.

Chapman, M. R., and N. J. Shackleton (1999), Global ice-volume fluctuations, North Atlantic ice-rafting events, and deep-ocean circulation changes between 130 and 70 ka, *Geology*, *27(9)*, 795–798.

Cortijo, E., S. Lehman, L. Keigwin, M. Chapman, D. Paillard, and L. Labeyrie (1999), Changes in meridional temperature and salinity gradients in the North Atlantic Ocean (30°N-72°N) in the last interglacial period, *Paleoceanography*, *14(1)*, 23–33.

Cottet-Puinel, M., A. J. Weaver, C. Hillaire-Marcel, A. de Vernal, P. U. Clark, and M. Eby (2004), Variation of Labrador Sea Water formation over the Last Glacial cycle in a climate model of intermediate complexity, *Quaternary Science Reviews*, *23*, 449–465.

de Noblet, N., I. Prentice, S. Joussaume, D. Texier, A. Botta, and A. Haxeltine (1996), Possible Role of Atmosphere-Biosphere Interactions in Triggering the Last Glaciation, *Geophysical Research Letters*, *23*, 3191–3194.

de Vernal, A., and C. Hillaire-Marcel (2008), Nature Variability of Greenland Climate Vegetation, and Ice Volume During the Past Million Years, *Science*, *320*, 1622–1625.

Evans, H. K., I. R. Hall, G. G. Bianchi, and D. W. Oppo (2007), Intermediate water links to Deep Western Boundary Current variability in the subtropical NW Atlantic during marine isotope stages 5 and 4, *Paleoceanography*, *22*, PA3209.

Feulner, G., and S. Rahmstorf (2010), On the effect of a new grand minimum of solar activity on the future climate on Earth, *Geophysical Research Letters*, *37*, L05,707.

Fichefet, T., and M. A. M. Maqueda (1997), Sensitivity of a global sea ice model to the treatment of ice thermodynamics and dynamics, *Journal of Geophysical Research*, *102*, 12,609.

Fichefet, T., and M. A. M. Maqueda (1999), Modelling the influence of snow accumulation and snow-ice formation on the seasonal cycle of the Antarctic sea-ice cover, *Climate Dynamics*, *15*, 251–268.

Fronval, T., E. Jansen, H. Haflidason, and J. P. Sejrup (1998), Variability in surface and deep water conditions in the Nordic seas during the last interglacial period, *Quaternary Science Reviews*, *17*, 963–985.

Gregory, J. M., et al. (2005), A model intercomparison of changes in the Atlantic thermohaline circulation in response to increasing atmospheric CO_2 concentration, *Geophysical Research Letters*, *32*, L12,703.

Hansen, B., and S. Østerhus (2000), North Atlantic - Nordic Seas exchanges, *Progress in Oceanography*, *45*, 109–208.

Hátún, H., A. B. Sandø, H. Drange, B. Hansen, and H. Valdimarsson (2005), Influence of the Atlantic Subpolar Gyre on the Thermohaline Circulation, *Science*, *309*, 1841–1844.

Hibler, W. D. (1979), A Dynamic Thermodynamic Sea Ice Model, *Journal of Physical Oceanography*, *9*, 815–846.

Hillaire-Marcel, C., A. de Vernal, A. Bilodeau, and A. J. Weaver (2001), Absence of deep-water formation in the Labrador Sea during the last interglacial period, *Nature*, *410*, 1073–1077.

Hourdin, F., et al. (2006), The LMDZ4 general circulation model: climate performance and sensitivity to parametrized physics with emphasis on tropical convection, *Climate Dynamics*, *27(7-8)*, 787–813.

Johannessen, T. (1987), Resente planktoniske foraminiferer fra Norskehavet, Islandhavet og Nordatlanteren: taksonomi, faunafordeling og stabilisotopsammensetning, Master's thesis, Universitetet i Bergen, (Hovedoppgave til cand. scient. eksamen i marin geologi).

Kalnay, E., and coauthors (1996), The NCEP/NCAR 40-year reanalysis project, *Bull. Amer. Meteor. Soc.*, *77*, 437–471.

Khodri, M., Y. Leclainche, G. Ramstein, P. Braconnot, O. Marti, and E. Cortijo (2001), Simulating the amplification of orbital forcing by ocean feedbacks in the last glaciation, *Nature*, *410*, 570–574.

Krinner, G., N. Viovy, N. de Noblet-Ducoudre, J. Ogee, J. Polcher, P. Friedlingstein, P. Ciais, S. Sitch, and I. C. Prentice (2005), A Dynamic Global Vegetation Model for Studies of the Coupled Atmosphere - Biosphere System, *Global Biogeochemical Cycles*, *19(1)*, GB1015.

Kubatzki, C., M. Claussen, R. Calov, and A. Ganopolski (2006), Sensitivity of the last glacial inception to initial and surface conditions, *Climate Dynamics*, *27*, 333–344.

Labeyrie, L., H. Leclaire, C. Waelbroeck, E. Cortijo, J. C. Duplessy, L. Vidal, M. Elliot, and B. L. Coat (1999), *Temporal variability of the surface and deep waters of the north west atlantic ocean at orbital and millenial scales. In: R. Webb, P. Clark, L. Keigwin (eds) Mechanisms of global climate change at millennial time scales*, AGU Geophysical Monograph Series no. 112, Washington DC.

Lehman, S., J. Sachs, A. Crotwell, L. Keigwin, and E. Boyle (2002), Relation of subtropical Atlantic temperature, high-latitude ice rafting, deep water formation, and European climate 130,000-60,000 years ago, *Quaternary Science Reviews*, *21*, 1917–1924.

Levermann, A., and A. Born (2007), Bistability of the Atlantic subpolar gyre in a coarse-resolution model, *Geophysical Research Letters*, *34*, L24,605.

Levermann, A., J. Mignot, S. Nawrath, and S. Rahmstorf (2007), The role of northern sea ice cover for the weakening of the thermohaline circulation under global warming, *Journal of Climate*, *20*, 4160–4171.

Levitus, S. (1982), *Climatological atlas of the world ocean. NOAA Professional Paper, vol 13*, 173 pp. pp., US Dept of Commerce, Washington DC.

Lüthi, D., et al. (2008), High-resolution carbon dioxide concentration record 650,000-800,000 years before present, *Nature*, *453*, 379–382.

Madec, G., P. Delecluse, M. Imbard, and C. Lévy (1997), *OPA version 8.1 Ocean General Circulation Model Reference Manual*, Institut Pierre-Simon Laplace, Note du Pôle de modélisation n^{o}11.

Mangerud, J., E. Sønstegaard, H.-P. Sejrup, and S. Haldorsen (1981), A continuous Eemian-Early Weichelian sequence containing pollen and marine fossils at Fjøsanger, western Norway, *Boreas*, *10*, 138–205.

Marti, O., et al. (2010), Key features of the IPSL ocean atmosphere model and its sensitivity to atmospheric resolution, *Climate Dynamics*, *34*, 1–26, doi: 10.1007/s00382-009-0640-6.

McManus, J. F., D. W. Oppo, L. D. Keigwin, J. L. Cullen, and G. C. Bond (2002), Thermohaline Circulation and Prolonged Interglacial Warmth in the North Atlantic, *Quaternary Research*, *58*, 17–21.

Meissner, K., and R. Gerdes (2002), Coupled climate modelling of ocean circulation changes during ice age inception, *Climate Dynamics*, *18*, 455–473.

Meissner, K. J., A. J. Weaver, H. D. Matthews, and P. M. Cox (2003), The role of land surface dynamics in glacial inception: a study with the UVic Earth System Model, *Climate Dynamics*, *21*, 515–537.

Mignot, J., A. Levermann, and A. Griesel (2006), A decomposition of the Atlantic meridional overturning circulation into physical components using its sensitivity to vertical diffusivity., *Journal of Physical Oceanography*, *36*, 636–650.

Montoya, M., A. Griesel, A. Levermann, J. Mignot, M. Hofmann, A. Ganopolski, and S. Rahmstorf (2005), The Earth System Model of Intermediate Complexity CLIM*BER*-3α. Part I: description and performance for present-day conditions, *Climate Dynamics*, *25*, 237–263.

Montoya, M., A. Born, and A. Levermann (2010), Reversed North Atlantic gyre dynamics in glacial climate, *Climate Dynamics*, *online*, doi:10.1007/s00382-009-0729-y.

Müller, U. C., and G. J. Kukla (2004), North Atlantic Current and European environments during the declining stage of the last interglacial, *Geology*, *32*, 1009–1012.

Otto-Bliesner, B. L., S. J. Marshall, J. T. Overpeck, G. H. Miller, A. Hu, and CAPE Last Interglacial Project members (2006), Simulating Arctic Climate Warmth and Icefield Retreat in the Last Interglaciation, *Science*, *311*, 1751–1753.

Petit, J. R., et al. (1999), Climate and atmospheric history of the past 420,000 years from the Vostok ice core, Antarctica, *Nature*, *399*, 429–436.

Petoukhov, V., A. Ganopolski, V. Brovkin, M. Claussen, A. Eliseev, C. Kubatzki, and S. Rahmstorf (2000), CLIM*BER*-2: a climate system model of intermediate complexity. Part I: model description and performance for present climate, *Climate Dynamics*, *16*, 1.

Rasmussen, T. L., E. Balbon, E. Thomsen, L. Labeyrie, and T. C. E. van Weering (1999), Climate records and changes in deep outflow from the Norwegian Sea 150-55 ka, *Terra Nova*, *11(2/3)*, 61–66.

Rasmussen, T. L., D. W. Oppo, E. Thomsen, and S. J. Lehman (2003), Deep sea records from the southeast Labrador Sea: Ocean circulation changes and ice-rafting events during the last 160,000 years, *Paleoceanography*, *18(1)*, 1018.

Risebrobakken, B., T. Dokken, and E. Jansen (2005), *The extent and variability of the Meridional Atlantic Circulation in the Nordic Seas during Marine Isotope Stage 5 and its influence on the inception of the last glacial. In: The Nordic Seas: An Integrated Perspective, edited by Drange, H., Dokken, T., Furevik, T., Gerdes, R., Berger, W. H.*, pp. 323–339, AGU Geophysical Monograph Series no. 158, Washington DC.

Risebrobakken, B., T. Dokken, O. H. Otterå, E. Jansen, Y. Gao, and H. Drange (2007), Inception of the Northern European ice sheet due to contrasting ocean and insolation forcing, *Quaternary Research*, *67*, 128–135.

Roberts, M. J., and R. A. Wood (1997), Topographic Sensitivity Studies with a Bryan Cox-Type Ocean Model, *Journal of Physical Oceanography*, *27*, 823–836.

Roullet, G., and G. Madec (2000), Salt conservation, free surface, and varying levels: A new formulation for ocean general circulation models, *Journal of Geophysical Research*, *105*, 23,927–23,942.

Ruddiman, W. F., and A. McIntyre (1975), Warmth of the Subpolar North Atlantic Ocean During Northern Hemisphere Ice-Sheet Growth, *Science*, *204*, 173–175.

Stouffer, R. J., et al. (2006), Investigating the Causes of the Response of the Thermohaline Circulation to Past and Future Climate Changes, *Journal of Climate*, *19*, 1365–1387.

Thorpe, R. B., R. A. Wood, and J. F. B. Mitchell (2004), Sensitivity of the modelled thermohaline circulation to the parameterisation of mixing across the Greenland-Scotland ridge, *Ocean Modelling*, *7*, 259–268.

Waelbroeck, C., L. Labeyrie, E. Michel, J. C. Duplessy, J. F. McManus, K. Lambeck, E. Balbon, and M. Labracherie (2002), Sea-level and deep water temperature changes derived from benthic foraminifera isotopic records, *Quaternary Science Reviews*, *21*, 295–305.

Paper III

Warm Nordic Seas delayed glacial inception in Scandinavia

Born, A., M. Kageyama and K. H. Nisancioglu (2010)

Climate of the Past Discussions **6**, 1503-1523

Warm Nordic Seas delayed glacial inception in Scandinavia

A. Born[1]**,**

Bjerknes Centre for Climate Research, Bergen, Norway

Geophysical Institute, University of Bergen, Bergen, Norway

M. Kageyama,

Laboratoire des Sciences du Climat et l'Environnement, Gif sur Yvette, France

K. H. Nisancioglu,

Bjerknes Centre for Climate Research, Bergen, Norway

July 7, 2010

[1] Corresponding author: andreas.born@bjerknes.uib.no

Abstract

We simulate the last glacial inception, 115,000 years ago, with a three dimensional thermomechanical ice sheet model of the Northern Hemisphere, forced by a comprehensive coupled climate model. High oceanic heat transport into the Nordic Seas prevents large scale ice growth over Scandinavia. Glacial inception in the region starts on the highest mountains in the south when sea surface temperatures in the Nordic Seas are reduced by at least 3°C. Ice growth in Northern Scandinavia requires a cooling by at least 4°C. This is in good agreement with marine proxy data from the Nordic Seas and North Atlantic as well as available terrestrial data. This study thus provides a physical understanding and revised timing of the first glacier advance over Scandinavia.

1 Introduction

During the past 800,000 years, climate has been relatively cold with ice sheets covering large parts of the Northern Hemisphere continents most of the time. At the last glacial maximum, 21,000 years before present, an ice sheet existed over North America with a volume equivalent to the present day Antarctic ice sheet, decreasing global sea level by 74 m (Peltier, 2004). Eurasia was covered with a ice volume equal to 2.5 times the Greenland ice sheet, or 17 m sea level equivalent. Additional 25-30 m of sea level equivalent accumulated on the Antarctic ice sheet (Lambeck and Chappell, 2001) for a total sea level decrease of 120 to 130 m relative to present (Waelbroeck et al., 2002).

While extensive work addresses the extent and volume of ice sheets at their maximum, the erosive effect of the ice masses themselves removed most of the sediments holding information about glacial inception. Thus, little is known about advancing glaciers at the end of the last interglacial, the epoch when climate for the last time was similar to present day. Geological data suggests that ice first grew over the Canadian Arctic islands, Labrador, northern continental Canada, continental west-

ern Siberia and Eurasian Arctic islands (Andrews and Barry, 1978; Mangerud and Svendsen, 1992; Clark et al., 1993; Svendsen et al., 2004; Lambeck et al., 2006).

The last glacial maximum Fennoscandian ice sheet is thought to be the result of ice masses spreading west and southward from mountain nucleation sites in western Siberia, the Eurasian Arctic islands, and probably on Svalbard. However, an independent glaciation over Scandinavia started soon after the first global sea level decrease (Mangerud et al., 1981). This first ice growth was apparently rapid and large because the glacio-isostatic depression in south-western Norway was as fast as the global sea level decrease due to ice growth elsewhere (Mangerud, 1991). The ice front reached the fjord within a few kilometers from an excavation site at Fjøsanger, close to Bergen, allowing the deposition of ice-rafted detritus in marine sediments off the coast (Baumann et al., 1995; Risebrobakken et al., 2005, 2007).

Despite these reconstructions, the history of early Scandinavian glaciation is inconclusive (Mangerud, 2004). Coastal ice limits are known for only four localities in southern Norway, and the earliest limit is based on a single record. Dating is problematic because the time period of interest is beyond the applicability of radiocarbon dating. Even in younger sediments only intervals between glacier advances contain enough organic material to be used for this method. Instead, the chronology is based on correlation with other regions that can be dated by other means. Evidence for early glacier advances and retreats in Southwestern Scandinavia is contrasted by speleothems from karst caves north of the Arctic circle that suggest ice-free conditions until approximately 95 ka (Lauritzen, 1984, 1986; Mangerud, 1991).

The last two decades brought only minor advances from new field observations. Numerical ice sheet modeling could improve the understanding of this period but most studies focus on the primary inception regions over North America and western Siberia (Marshall and Clarke, 1999; Zweck and Huybrechts, 2005; Calov et al., 2005a; Kubatzki et al., 2006; Charbit et al., 2007; Peyaud et al., 2007). This is probably due to the lack of constraints on timing and extent of ice from data, but also because the steep Scandinavian topography and variable climate are a challenge for the realistic representation of glaciers. The interaction of land based ice with floating ice shelves like in the Barents Sea remains an issue (Peyaud et al., 2007). Moreover, recent studies reveal a major reorganization of ocean currents in the region during

glacial inception (Risebrobakken et al., 2005, 2007; Born et al., 2010a,b), and ocean circulation is thought to have a crucial impact on glaciers in the maritime climate of Scandinavia. The importance of ocean circulation changes has been shown in the study by Calov et al. (2005b), where an artificially weakened Atlantic meridional overturning circulation facilitates ice sheet growth in southern Scandinavia due to lower temperatures, while less ice grows further north as a consequence of reduced precipitation.

Prolonged interglacial warmth in the North Atlantic, despite decreasing high latitude insolation and decreasing sea levels indicating progressing ice growth on land, is reported from a number of marine sediment cores (Ruddiman and McIntyre, 1975; McManus et al., 2002). Further north in the Nordic Seas, recent studies show that the gradual climate cooling due to decreasing insolation after the last interglacial was interrupted by a period of transient warmth (Risebrobakken et al., 2007; Born et al., 2010a,b). As a direct result of weaker summer insolation, Arctic sea ice grows thicker and ice export in the East Greenland Current intensifies. The freshwater transport by sea ice into the subpolar North Atlantic reduces deep convection in the northwest Atlantic and thereby effectively changes the density stucture of the region. This causes a nonlinear response of the subpolar gyre that amplifies freshening by sea ice. The weakening of the subpolar gyre results in a higher fraction of subtropical waters in the Atlantic inflow into the Nordic Seas and thus warming along the path of the Norwegian Atlantic Current.

As a result, ocean heat transport into the Nordic Seas increased between 119 ka and 115 ka. The anomalous warmth ends with rising insolation and an estimated temperature decrease of about 3°C as inferred from planktic foraminiferal data. Ice-rafted detritus indicates that ice growth over Scandinavia started at about the same time. However, dating of terrestrial sediments involves uncertainties of several millennia and the better-dated marine sediment records are ambiguous about the location of glacier advances. Furthermore, neither of these records provide information on whether the presence of a warm ocean favored glaciation due to enhanced moisture supply or if the relatively warm climate caused a delay in glacial inception.

In this study we suggest that a well documented transient strengthening of the Norwegian Atlantic Current delayed large scale glacier advance over Scandinavia

until after 115,000 years ago (115 ka), followed by a rapid accumulation of ice. The climate and ice sheet models used are described in section 2. Section 3 presents a simulation of land ice at 115 ka and investigates the impact of ocean heat transport variability on ice growth. Section 4 quantifies the reduction of sea surface temperature necessary to accumulate ice over Scandinavia. We discuss and conclude in sections 5 and 6.

2 Model description and experiments

The numerical ice sheet model used in this study is SICOPOLIS (SImulation COde for POLythermal Ice Sheets), a three dimensional thermomechanical ice sheet model (Greve, 1997). It simulates ice rheology and mass balance on a regular grid, using a stereographic projection centered on the North Pole (Fig. 1). The horizontal resolution is set to 40 km and there are 90 vertical layers: 80 equidistant layers in cold ice and 10 representing a layer of ice at the pressure melting point. The model employs the shallow ice approximation, neglecting longitudinal stress gradients. As a consequence of this simplification, floating ice shelves and ice streams cannot be accurately simulated. This introduces only a negligible error for the simulation of the Northern Hemispere at a time of relatively low ice volume.

Mass balance at the upper boundary of the model is computed on the basis of monthly surface temperature and total precipitation. The snow fraction of monthly precipitation is estimated as a linear function between -10 and 7 °C, with all precipitation falling as snow below that range and all as rain above. Only solid precipitation contributes to accumulation. Rain runs off immediately. Calculation of melt is based on a positive degree day model (Reeh, 1991) with parameters $\beta_s = 3\,mm\,K^{-1}$ for snow and $\beta_s = 12\,mm\,K^{-1}$ for ice. A constant geothermal heat flux of 55 mW/m^2 is assumed at the lower boundary.

Climate data is provided by the Institut Pierre Simon Laplace coupled model version 4 (IPSL CM4). This comprehensive climate model comprises ocean, sea ice, atmosphere and land surface components (Marti et al., 2010). It has previously been used to simulate the last glacial inception and was validated against the available proxy data to simulate the transient warmth in the Nordic Seas at 115 ka (Braconnot

et al., 2008; Born et al., 2010a,b). In addition to the coupled model experiments, we carried out a series of sensitivity experiments using only the atmosphere component of the model (LMDZ 3.3) with modified sea surface conditions taken from the coupled model equilibrium. In order to investigate the effect of weaker oceanic heat transport, sea surface temperatures in the Arctic Ocean, Nordic Seas and North Atlantic were decreased by fixed values of 1, 2, 3 and 4°C. Sea ice area was adjusted accordingly, increasing coverage linerarly from 0 % at 0 °C water temperature to 100 % at -1.8 °C. The simulations were ran into quasi-equilibrium for 20 years.

3 Glacial inception over Scandinavia and ocean heat transport

Forcing the ice sheet model with fixed 115 ka boundary conditions from the coupled climate model yields additional ice growth compared to a preindustrial control experiment (Fig. 1). Ice grows on northern continental Canada, Labrador, the Canadian Archipelago and western Siberia. Ice caps on Iceland and Baffin Island are larger than in the preindustrial control. However, the Scandinavian peninsula remains ice-free. Present-day ice caps in Scandinavia are below model resolution and thus not simulated.

Mass balance variability of extra-tropical glaciers is usually controlled by changes in ablation due to anomalous summer temperatures. Ice melting is a highly non linear function of temperature and easily exceeds accumulation once a threshold in temperature is reached. Typical variability in accumulation is smaller in all but the most marine climates, as has been shown for glaciers in southern Norway (Nesje and Dahl, 2000). In order to investigate further the robustness of an ice-free Scandinavia in a relatively cold 115 ka climate, the ice sheet model is forced by a composite climate based on the 40 years (10%) with coldest summers (April to September) over Scandinavia of the last 400 years of the coupled model experiment. Mass balance in the mountais of Scandinavia is close to positive under these conditions (Fig. 2). However, this is not sufficient to start ice accumulation.

Although the temperature criterion was defined over land (see red box in Fig. 3),

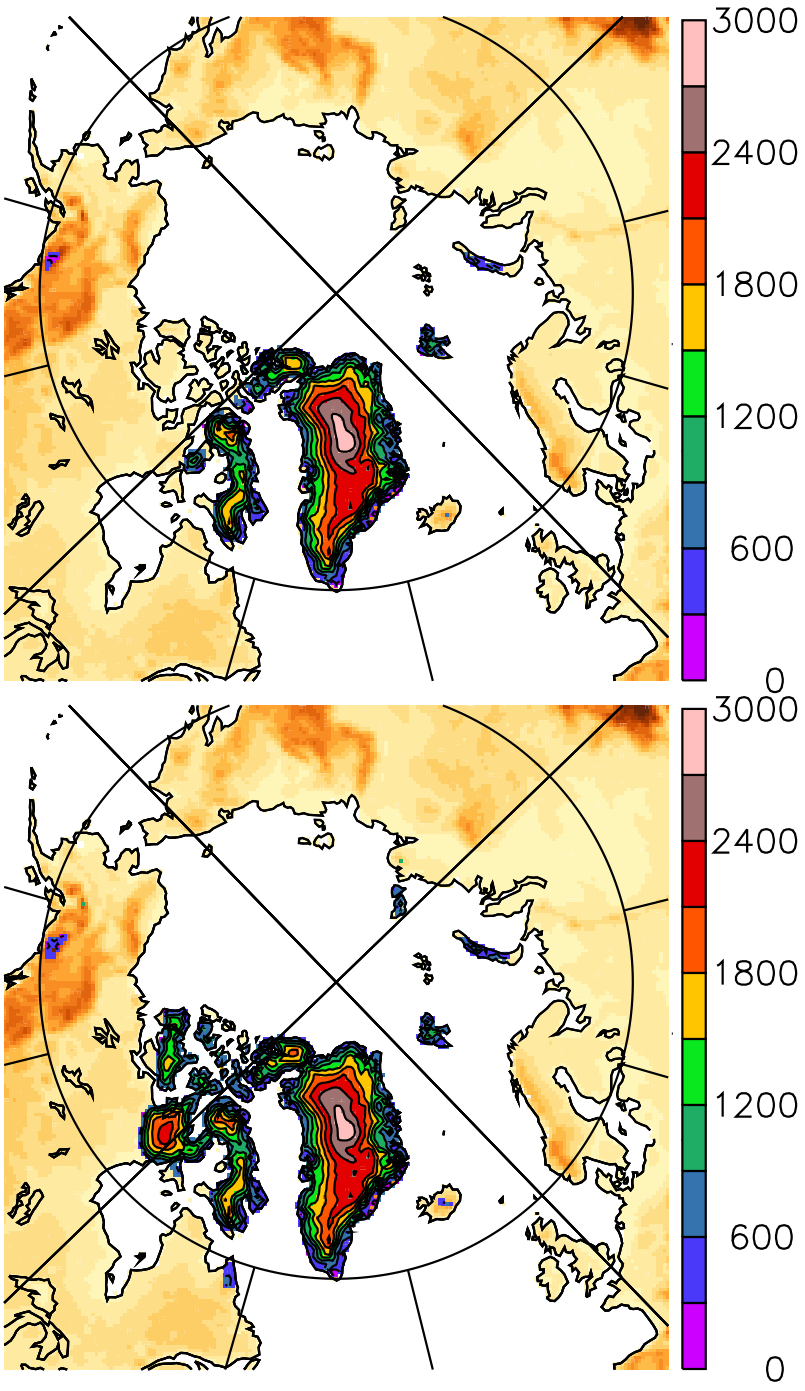

Figure 1: Modelled ice thickness (in m) for present day (upper) and 115 ka (lower). Preindustrial ice area and thickness are well reproduced. Besides the Greenland ice sheet, smaller ice caps are visible in the Canadian Arctic, Spitsbergen, Iceland, Novaya Zemlya, and south eastern Alaska. Most important differences with 115 ka forcing is additinal ice growth in northern continental Canada, Labrador, western Siberia and the Eurasian Arctic islands.

the temperature difference between the 40 years of warmest and coldest summers extends over the ocean tracing the sea ice edge. This suggests that sea ice and ocean heat transport into the Nordic Seas plays an important role for decadal variability over Scandinavia at 115 ka. Indeed, the correlation of air temperature over Scandinavia and ocean heat transport across the Greenland Scotland ridge is high with a coefficient r = 0.81 for ocean heat transport leading by 1 year (Fig. 4). The amplitude of surface air temperature variability over Scandinavia is about 1 K.

4 How much sea surface cooling is needed to start Scandinavian glaciation?

Despite low insolation levels at 115 ka and ice growth at similar latitudes over North America and Siberia, climate is too warm over Scandinavia to support ice growth (Fig. 1). This result is robust and no ice grows even in years with cold summers. Ocean heat transport, probably through its impact on the sea ice edge, plays an important role for surface air temperature and land ice growth over Scandinavia (Fig. 4).

A series of experiments with artificially lowered sea surface temperatures in the North Atlantic, Nordic Seas and Arctic Ocean was carried out. Sea ice area was extended according to the modified temperatures. At a reduction of 3°C relative to the 115 ka coupled model experiment, a permanent ice cap develops over southern Norway, approximately at the location of present-day Jostedalsbreen glacier (Fig. 5). For sea surface temperatures 4°C below the coupled model average for 115 ka, ice also grows over northern Norway. Ice caps grow also outside Scandinavia, most notably on the islands in the Barents and Kara Seas and in western and far-eastern continental Siberia.

These results show that sea surface temperatures have strong impact on the mass balance in Scandinavia. However, the fact that the mass balance is positive when sea surface temperatures are low is not trivial. In addition to more favorable conditions due to generally colder climate and weaker ablation, a cold sea surface also reduces moisture supply and accumulation. In the experiments presented here, the ablation

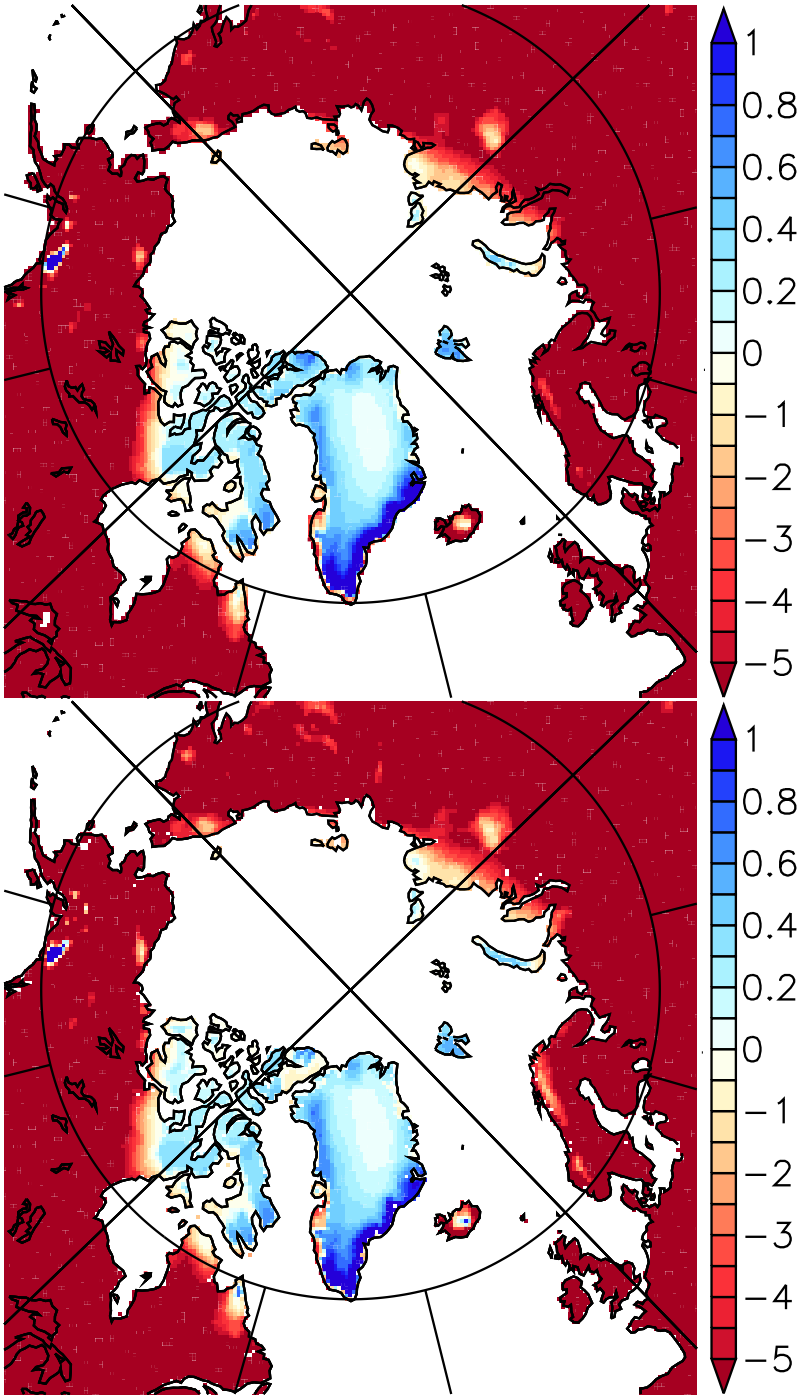

Figure 2: **Upper:** Mass balance of the 115 ka control experiment, forced by a 100 year average of the climate model. **Lower:** As above, but forced by an average of the 40 years of coldest summers over Scandinavia in the same model experiment (see Fig. 3).

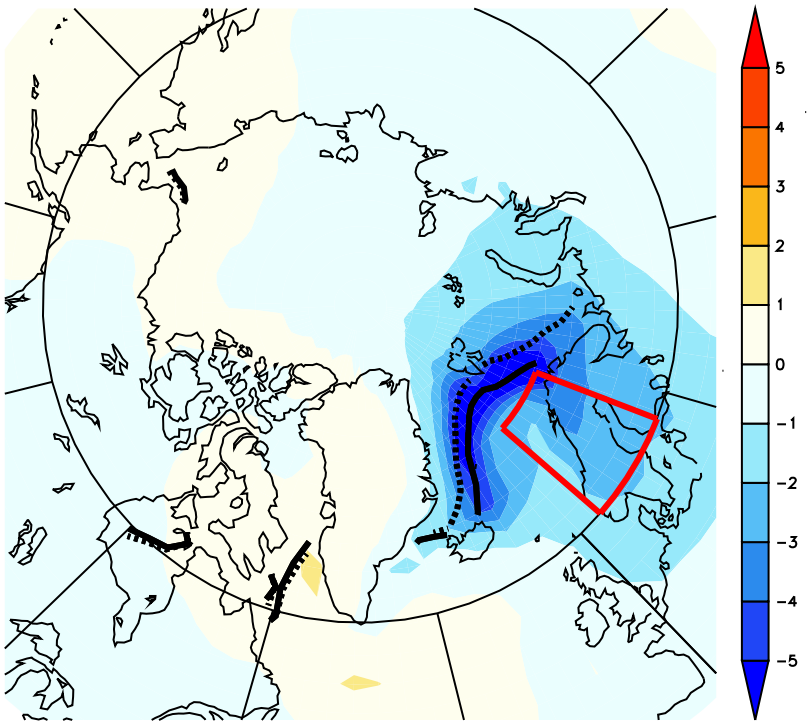

Figure 3: Difference in annual average surface air temperature, 40 years of coldest minus 40 years of warmest summers, in °C (colors). Contours show the annual average 50% sea ice edge for the years of coldest (solid) and warmest (dotted) summers. Red box shows region where summer surface air temperature over land is taken as selection criterion.

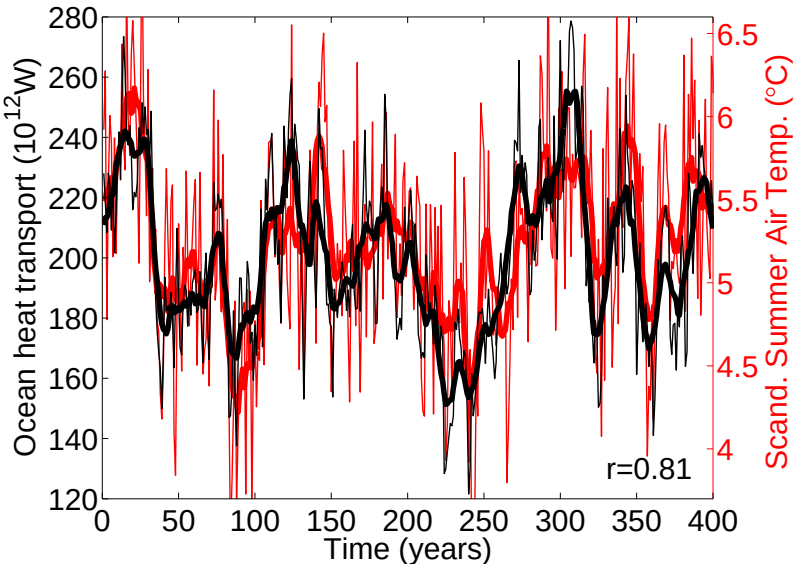

Figure 4: Time series of ocean heat transport into the Nordic Seas (black) and Scandinavian summer surface air temperature (red, see red box in Fig. 3), both filtered with a 11 years running average. Thin lines show unfiltered time series. Curves correlate with r=0.81 and ocean heat transport leads by one year.

effect dominates the mass balance change in most regions, especially over Southern Scandinavia and the Northern British Isles, where synoptic weather systems carry heat taken up from the Atlantic Ocean (Fig. 6). However, despite large changes, the mass balance remains negative in most regions.

The effect of the colder sea surface and larger sea ice area on accumulation is limited to coastal regions, most notably southeast Greenland and to some extent western Scandinavia (Fig. 6, lower). Changes in accumulation are about an order of magnitude weaker than changes in ablation and dominate exclusively in already glaciated areas of the unperturbed experiment (see Fig. 1). In these regions, summer temperatures are cold enough such that less snow melts in summer than accumulates in winter. Consequently, lower accumulation impacts the annual mass balance. In regions where summer melting exceeds accumulation, a small change in accumulation is unlikely to result in a positive mass balance because melting rates are usually much larger than accumulation.

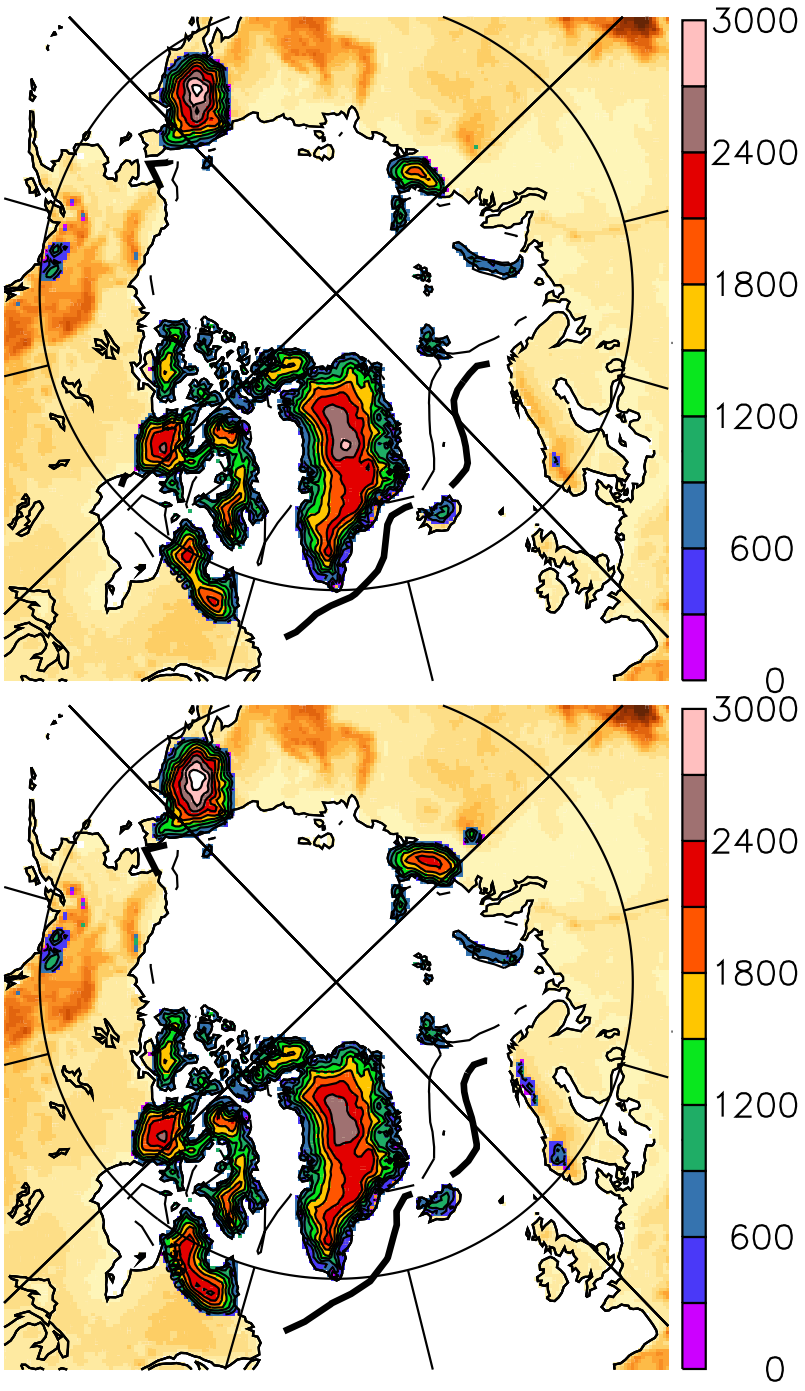

Figure 5: Ice thickness for experiments with sea surface temperatures reduced by 3°C (**upper**) and 4°C (**lower**) from the coupled model 115 ka average, in m. The 50% annual average sea ice extent is shown for the respective experiment (thick contour) and the unperturbed 115 ka experiment (thin contour). With 3°C colder sea surface, ice starts to grow in the region of present-day Jostedalsbreen in southern Norway. Cooling the sea surface by 4 K allows additional ice growth over northern Scandinavia.

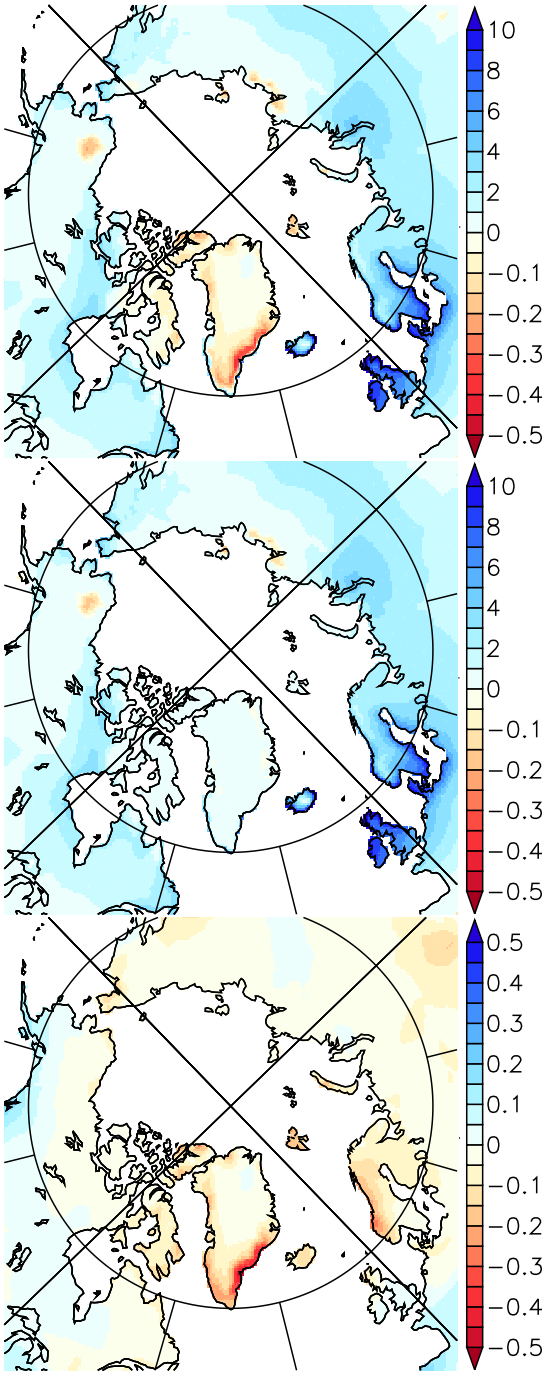

Figure 6: Mass balance difference (m/yr) between atmosphere only experiment with 3°C lower sea surface temperatures and the control run (upper), decomposed into melt (middle) and precipitation differences (lower). Lower sea surface temperatures strongly facilitate ice growth in most regions by decreasing melting. The negative effect of weaker moisture supply is limited and dominates over melt only in areas that are already glaciated in the unperturbed 115 ka experiment. Note the different scale in the lower panel.

5 Discussion

Combining results from a comprehensive coupled climate model and a three-dimensional land ice model, ice growth at the end of the last interglacial was investigated. Simulated ice nucleation regions at 115 ka include the Canadian Arctic, Labrador and Siberian islands, in good agreement with reconstructions (Clark et al., 1993; Svendsen et al., 2004). In particular, glacier advances from Siberian islands were found to be important for the build-up of the Kara Sea ice sheet (Möller et al., 2007).

No ice is found over Scandinavia with 115 ka climate forcing. Even when forcing the ice model only with years of particularly cold summers, ice did not accumulate. However, ice accumulation was found sensitive to ocean heat transport into the Nordic Seas (Fig. 4). This implies a relation between sea surface temperature and Scandinavian mass balance that can be used to help constrain the timing of the last glacial inception with high-resolution marine proxy data. Available terrestrial data for Scandinavia has much lower temporal resolution. Sea surface temperatures of the Nordic Seas need to cool by at least 3°C from the 115 ka average for inception over southern Scandinavia. A 4°C cooling induces ice growth over northern Scandinavia. Cooling also has a positive effect on other known nucleation sites like western Siberia, the Siberian islands and Beringia (Brigham-Grette, 2001; Brigham-Grette et al., 2001; Svendsen et al., 2004).

As shown by proxy data and models, strong ocean heat transport into the Nordic Seas between 119 ka and 115 ka was important for climate evolution of the last glacial inception (Risebrobakken et al., 2007; Born et al., 2010b). The climate model used in this study was validated against the available proxy data to simulate this feature (Born et al., 2010a). Layers of ice-rafted detritus, particles too big to be transported other than by icebergs detached from ice sheets, are found in marine sediments of the Nordic Seas following a period of relatively warm conditions and immediately after a 3°C drop in sea surface temperatures off the central Norwegian coast at 115 ka (Baumann et al., 1995; Risebrobakken et al., 2005, 2007), in good agreement with simulations presented here. This is also supported by terrestrial data from southwestern Scandinavia (Mangerud et al., 1981; Mangerud, 1991, 2004). However, the ice sheet model suggests that a larger temperature decrease is necessary to induce ice growth in northern Scandinavia. This is consistent with reconstructions

from speleothems in this region that suggest significant ice growth only after 95 ka (Lauritzen, 1984, 1986).

Numerous studies of the last glacial cycle show that the large ice sheets of the glacial maximum nucleated over North America and western Siberia (Marshall and Clarke, 1999; Siegert et al., 2001; Zweck and Huybrechts, 2005; Calov et al., 2005a; Kubatzki et al., 2006; Charbit et al., 2007; Peyaud et al., 2007). Glacier advance over Scandinavia early during the last glacial cycle is regarded as of secondary importance to the continental-scale glaciation. However, the mechanism presented here, a rapid glacier advance over Scandinavia at 115 ka, is consistent with this previous work. Decreasing heat transport into the Nordic Seas at 115 ka might also influence the primary nucleation sites around the Barents and Kara Seas and thereby the evolution of the Eurasian ice sheet later during the glacial.

While the climate model simulations have been discussed extensively in earlier publications (Braconnot et al., 2008; Born et al., 2010a,b), several aspects of the ice sheet model need clarification here. Relatively large glaciers are present in Scandinavia today, but are not shown in the control experiment (Fig. 1). This is because the model resolution of 40 km is too coarse to resolve these glaciers. Resolution can become critical for the representation of ice masses in areas of steep topography, because glacier nucleation often occurs on the highest peaks and propagates to lower elevations. It has been proposed to parameterize this effect by calculating the mass balance at the highest present day elevation within each grid cell if it is higher than the simulated ice sheet (Zweck and Huybrechts, 2005). While this approach preserves information that would otherwise be lost due to averaging the topography over the grid size, it neglects the effect of steep topographic gradients of sub-grid scale. Steep slopes typically accompany the occurrence of high peaks and limit the spatial extent of glaciers originating from high elevations. Ice is quickly transported to lower elevations and thus effectively removed. Accounting for the full sub-grid height distribution, including the presence of deep valleys and fjords, requires a more sophisticated approach and a parametrization of alpine glaciers (Marshall and Clarke, 1999). This, however, is beyond the scope of the present study. We acknowledge that the finite model resolution might impact the findings presented here quantitatively but not qualitatively.

The shallow ice approximation employed in our model inhibits the simulation of floating ice shelves that are believed to have played a significant role for the evolution of the Eurasian ice sheet as ice grew across the Barents and Kara Seas. However, the first glaciation of Scandinavia was the result of local accumulation of ice and the results presented here are thus not affected by the limitation to grounded ice. The offline coupling scheme used does not communicate elevation and albedo changes back to the climate model and thus neglects potentially important feedback mechanisms. However, simulated elevation changes are small due to limited ice accumulation. Albedo changes are minor because accumulation regions of the ice sheet model are already covered with snow in the climate model.

6 Conclusions

Our modeling results are in good agreement with proxy data and the main findings are:
a) Strong ocean heat transport into the Nordic Seas between 119 ka and 115 ka delayed large scale ice growth over Scandinavia.
b) Scandinavian gacial inception requires a 3°C drop in sea surface temperatures, in good agreement with marine and terrestrial proxy data.
c) The positive effect of strong oceanic heat transport on ablation dominates the positive effect of enhanced evaporation from the warm ocean surface.
d) At inception, ice first started growing in the high mountains of Southern Scandinavia.

Acknowledgments

We kindly acknowledge Pascale Braconnot for access to IPSL CM4 model output as well as Jan Mangerud and John-Inge Svendsen for insightful discussions. A. B. was funded by the Marie Curie Actions project NICE (MRTN-CT-2006-036127) and the Research Council of Norway project TOPPNICE. M. K. is supported by INSU-CNRS. Computer time was provided by the University of Bergen and CEA-CCRT.

This is publication no. XXXX from the Bjerknes Centre for Climate Research.

References

Andrews, J. T. and Barry, R. G. (1978). GLACIAL INCEPTION AND DISINTEGRATION DURING LAST GLACIATION. *Annual Review of Earth and Planetary Sciences*, 6:205–228.

Baumann, K.-H., Lackschewitz, K. S., Mangerud, J., Spielhagen, R. F., Wolf-Welling, T. C. W., Henrich, R., and Kassens, H. (1995). Reflection of Scandinavia ice sheet fluctuations in Norwegian Sea sediments during the last 150,000 years. *Quaternary Research*, 43:185–197.

Born, A., Nisancioglu, K. H., and Braconnot, P. (2010a). Sea ice induced changes in ocean circulation during the Eemian. *Climate Dynamics*, online.

Born, A., Nisancioglu, K. H., Risebrobakken, B., and Levermann, A. (2010b). Late Eemian warming in the Nordic Seas as seen in proxy data and climate models. *Paleoceanography*, in revision.

Braconnot, P., Marzin, C., Grégoire, L., Mosquet, E., and Marti, O. (2008). Monsoon response to changes in Earth's orbital parameters: comparisons between simulations of the Eemian and of the Holocene. *Climate of the Past*, 4:281–294.

Brigham-Grette, J. (2001). New perspectives on Beringian Quaternary paleogeography, stratigraphy, and glacial history. *Quaternary Science Reviews*, 20:15–24.

Brigham-Grette, J., Hopkins, D. M., Benson, S. L., Heiser, P., Ivanov, V. F., Basilyan, A., and Pushkar, V. (2001). Last Interglacial (isotope stage 5) glacial and sea-level history of coastal Chukotka Peninsula and St. Lawrence Island, Western Beringia. *Quaternary Science Reviews*, 20:419–436.

Calov, R., Ganopolski, A., Claussen, M., Petoukhov, V., and Greve, R. (2005a). Transient simulation of the last glacial inception. Part I: glacial inception as a bifurcation in the climate system. *Climate Dynamics*, 24:545–561.

Calov, R., Ganopolski, A., Petoukhov, V., Claussen, M., Brovkin, V., and Kubatzki, C. (2005b). Transient simulation of the last glacial inception. Part II: sensitivity and feedback analysis. *Climate Dynamics*, 24:563–576.

Charbit, S., Ritz, C., Philippon, G., Peyaud, V., and Kageyama, M. (2007). Numerical reconstructions of the Northern Hemisphere ice sheets through the last glacial-interglacial cycle. *Climate of the Past*, 3:15–37.

Clark, P. U., Clague, J. J., Curry, B. B., Dreimanis, A., Hicock, S. R., Miller, G. H., Berger, G. W., Eyles, N., Lamothe, M., Miller, B. B., Mott, R. J., Oldale, R. N., Stea, R. R., Szabo, J. P., Thorleifson, L. H., and Vincent, J.-S. (1993). Initiation and development of the Laurentide and Cordilleran Ice Sheets following the last interglaciation. *Quaternary Science Reviews*, 12:79–114.

Greve, R. (1997). A continuum-mechanical formulation for shallow polythermal ice sheets. *Philos Trans R Soc Lond A*, 355:921–974.

Kubatzki, C., Claussen, M., Calov, R., and Ganopolski, A. (2006). Sensitivity of the last glacial inception to initial and surface conditions. *Climate Dynamics*, 27:333–344.

Lambeck, K. and Chappell, J. (2001). Sea Level Change Through the Last Glacial Cycle. *Science*, 292:679–686.

Lambeck, K., Purcell, A., Funder, S., Kjær, K. H., Larsen, E., and Möller, P. (2006). Constraints on the Late Saalian to early Middle Weichselian ice sheet of Eurasia from field data and rebound modelling. *Boreas*, 35:539–575.

Lauritzen, S. E. (1984). Speleothem dating in Norway: An interglacial chronology. *Norsk geografisk tidsskrift*, 38:198.

Lauritzen, S. E. (1986). Karstformer i Nordland. Technical report, Direktoratet for Naturforvaltning, Oslo.

Mangerud, J. (1991). The Scandinavian Ice Sheet through the last interglacial/glacial cycle. In B. Frenzel (ed.): Klimageschichtliche Probleme der letzten 130 000 Jahre. *Päleoklimaforschung*, 1:307–330.

Mangerud, J. (2004). *Ice sheet limits on Norway and the Norwegian continental shelf. in Ehlers, J. and Gibbard, P. (eds.): Quaternary Glaciations - Extent and Chronology; Vol. 1 Europe*, pages 271–294. Elsevier, Amsterdam.

Mangerud, J., Sønstegaard, E., Sejrup, H.-P., and Haldorsen, S. (1981). A continuous Eemian-Early Weichelian sequence containing pollen and marine fossils at Fjøsanger, western Norway. *Boreas*, 10:138–205.

Mangerud, J. and Svendsen, J.-I. (1992). THE LAST INTERGLACIAL-GLACIAL PERIOD ON SPITSBERGEN, SVALBARD. *Quaternary Science Reviews*, 11:633–664.

Marshall, S. J. and Clarke, G. K. C. (1999). Ice sheet inception: subgrid hypsometric parameterization of mass balance in an ice sheet model. *Climate Dynamics*, 15:533–550.

Marti, O., Braconnot, P., Dufresne, J.-L., Bellier, J., Benshila, R., Bony, S., Brockmann, P., Cadule, P., Caubel, A., Codron, F., de Noblet, N., Denvil, S., Fairhead, L., Fichefet, T., Foujols, M.-A., Friedlingstein, P., Goosse, H., Grandpeix, J.-Y., Guilyardi, E., Hourdin, F., Idelkadi, A., Kageyama, M., Krinner, G., Lévy, C., Madec, G., Mignot, J., Musat, I., Swingedouw, D., and Talandier, C. (2010). Key features of the IPSL ocean atmosphere model and its sensitivity to atmospheric resolution. *Climate Dynamics*, 34:1–26.

McManus, J. F., Oppo, D. W., Keigwin, L. D., Cullen, J. L., and Bond, G. C. (2002). Thermohaline Circulation and Prolonged Interglacial Warmth in the North Atlantic. *Quaternary Research*, 58:17–21.

Möller, P., Lubinski, D., Ingólfsson, O., Forman, S. L., Siedenkrantz, M.-S., Bolshiyanov, D. Y., Lokrantz, H., Antonov, O., Pavlov, M., Ljung, K., Zeeberg, J. J., and Andreev, A. (2007). Erratum to: Severnaya Zemlya, Arctic Russia: a nucleation area for Kara Sea ice sheets during the Middle to Late Quaternary: [Quaternary Science Reviews 25(21-22) (2006) 2894-2936]. *Quaternary Science Reviews*, 26:1149–1191.

Nesje, A. and Dahl, S. O. (2000). *Glaciers and Environmental Change*. Arnold, London.

Peltier, W. (2004). GLOBAL GLACIAL ISOSTASY AND THE SURFACE OF THE ICE-AGE EARTH: The ICE-5G (VM2) Model and GRACE. *Annual Review of Earth and Planetary Sciences*, 32(1):111–149.

Peyaud, V., Ritz, C., and Krinner, G. (2007). Modelling the Early Weichselian Eurasian Ice Sheets: role of ice shelves and influence of ice-dammed lakes. *Climate of the Past*, 3:375–386.

Reeh, N. (1991). Parameterization of melt rate and surface temperature on the Greenland Ice Sheet. *Polarforschung*, 59:113–128.

Risebrobakken, B., Dokken, T., and Jansen, E. (2005). *The extent and variability of the Meridional Atlantic Circulation in the Nordic Seas during Marine Isotope Stage 5 and its influence on the inception of the last glacial. In: The Nordic Seas: An Integrated Perspective, edited by Drange, H., Dokken, T., Furevik, T., Gerdes, R., Berger, W. H.*, pages 323–339. AGU Geophysical Monograph Series no. 158, Washington DC.

Risebrobakken, B., Dokken, T., Otterå, O. H., Jansen, E., Gao, Y., and Drange, H. (2007). Inception of the Northern European ice sheet due to contrasting ocean and insolation forcing. *Quaternary Research*, 67:128–135.

Ruddiman, W. F. and McIntyre, A. (1975). Warmth of the Subpolar North Atlantic Ocean During Northern Hemisphere Ice-Sheet Growth. *Science*, 204:173–175.

Siegert, M. J., Dowdeswell, J. A., Hald, M., and Svendsen, J.-I. (2001). Modelling the Eurasian Ice Sheet through a full (Weichselian) glacial cycle. *Global and Planetary Change*, 31:367–385.

Svendsen, J. I., Alexanderson, H., Astakhov, V. I., Demidov, I., Dowdeswell, J. A., Funder, S., Gataullin, V., Henriksen, M., Hjort, C., Houmark-Nielsen, M., Hubberten, H. W., Ingolfsson, O., Jakobsson, M., Kjaer, K. H., Larsen, E., Lokrantz, H., Lunkka, J. P., Lysa, A., Mangerud, J., Matiouchkov, A., Murray, A., Moller, P., Niessen, F., Nikolskaya, O., Polyak, L., Saarnisto, M., Siegert, C., Siegert, M. J., Spielhagen, R. F., and Stein, R. (2004). Late quaternary ice sheet history of northern Eurasia. *Quaternary Science Reviews*, 23(11-13):1229–1271.

Waelbroeck, C., Labeyrie, L., Michel, E., Duplessy, J. C., McManus, J. F., Lambeck, K., Balbon, E., and Labracherie, M. (2002). Sea-level and deep water temperature changes derived from benthic foraminifera isotopic records. *Quaternary Science Reviews*, 21:295–305.

Zweck, C. and Huybrechts, P. (2005). Modeling of the northern hemisphere ice sheets during the last glacial cycle and glaciological sensitivity. *Journal of Geophysical Research*, 110:D07103.

Paper IV

The 8.2 ka event: abrupt transition of the subpolar gyre toward a modern North Atlantic circulation[1]

Born, A. and A. Levermann (2010)

Geochemistry, Geophysics, Geosystems **11**, Q06011

Geochemistry Geophysics Geosystems G3

Article
Volume 11, Number 6
25 June 2010
Q06011, doi:10.1029/2009GC003024
ISSN: 1525-2027

Published by AGU and the Geochemical Society

The 8.2 ka event: Abrupt transition of the subpolar gyre toward a modern North Atlantic circulation

A. Born

Bjerknes Centre for Climate Research, Allégaten 55, N-5007 Bergen, Norway (andreas.born@bjerknes.uib.no)

Also at Geophysical Institute, University of Bergen, N-5007 Bergen, Norway

A. Levermann

Potsdam Institute for Climate Impact Research, D-14412 Potsdam, Germany

Also at Institute of Physics, Potsdam University, D-14469 Potsdam, Germany

[1] Climate model simulations of the 8.2 ka event show an abrupt strengthening of the Atlantic subpolar gyre that allows us to connect two major but apparently contradictory climate events of the early Holocene: the freshwater outburst from proglacial lakes and the onset of Labrador Sea water formation. The 8.2 ka event is the largest climatic signal of our present interglacial with a widespread cooling in the North Atlantic region about 8200 years before present. It coincides with a meltwater outburst from North American proglacial lakes that is believed to have weakened the Atlantic meridional overturning circulation and northward heat transport, followed by a recovery of the deep ocean circulation and rising temperatures after a few centuries. Marine proxy data, however, date the onset of deep water formation in Labrador Sea to the same time. The subsequent strengthening of the slope current system created a regional signal recorded as an abrupt and persistent surface temperature decrease. Although similarities in timing are compelling, a mechanism to reconcile these apparently contradictory events was missing. Our simulations show that an abrupt and persistent strengthening of the Atlantic subpolar gyre provides a plausible explanation. The intense freshwater pulse triggered a transition of the gyre circulation into a different mode of operation, stabilized by internal feedbacks and persistent after the cessation of the perturbation. As a direct consequence, deep water formation around its center intensifies. This corresponds to the modern flow regime and stabilizes the meridional overturning circulation, possibly contributing to the Holocene's climatic stability.

Components: 5100 words, 5 figures.

Keywords: 8.2 ka event; Holocene; North Atlantic; climate model; subpolar gyre.

Index Terms: 4901 Paleoceanography: Abrupt/rapid climate change (1605); 0473 Biogeosciences: Paleoclimatology and paleoceanography (3344); 4936 Paleoceanography: Interglacial.

Received 4 January 2010; **Revised** 10 May 2010; **Accepted** 17 May 2010; **Published** 25 June 2010.

Born, A., and A. Levermann (2010), The 8.2 ka event: Abrupt transition of the subpolar gyre toward a modern North Atlantic circulation, *Geochem. Geophys. Geosyst.*, *11*, Q06011, doi:10.1029/2009GC003024.

1. Introduction

[2] During the relatively stable conditions of our present interglacial, the 8.2 ka event is the largest climatic signal with a widespread cooling in the North Atlantic region about 8200 years before present. It coincides with a meltwater outburst from North American proglacial lakes [*Alley et al.*, 1997; *Alley and Ágústsdóttir*, 2005, and references therein]. In current understanding, this caused a weakening of the Atlantic meridional overturning circulation (AMOC) and a subsequent reduction in northward heat transport, followed by a recovery of the deep ocean circulation and rising temperatures after a few centuries [*Bauer et al.*, 2004; *Hall et al.*, 2004; *Ellison et al.*, 2006; *Wiersma et al.*, 2006; *Kleiven et al.*, 2008].

[3] This two-dimensional explanation, however, is not able to explain a number of marine paleorecords that clearly call for a three-dimensional mechanism. An abrupt but persistent surface temperature decrease was reported from the western North Atlantic at the time of the 8.2 ka event (Figure 1) [*Solignac et al.*, 2004; *de Vernal and Hillaire-Marcel*, 2006; *Sachs*, 2007]. It has been suggested to be associated with the onset of deep water formation in Labrador Sea and a subsequent strengthening of the slope current system, the western branch of the subpolar gyre (SPG) [*Hillaire-Marcel et al.*, 2001; *Sachs*, 2007]. Proxy data from Reykjanes Ridge shows a similarly abrupt and persistent warming which provides evidence for an enhanced Irminger Current (Figure 1) [*Andersen et al.*, 2004; *Came et al.*, 2007]. This is the northeastern branch of the SPG and thus corroborates the hypothesis of a stronger gyre and enhanced convection in its center.

[4] The concurrence of these two events raises the question of how convection can increase at the time of the most severe freshwater flood of the past 10,000 years. We argue, based on coupled climate model experiments, that this is no contradiction but that a causal relationship connects the two events. A change in the density structure is found to provide positive feedbacks leading to a permanent strengthening of the SPG and convection. The impact of baroclinic adjustments on the SPG strength is well documented [*Eden and Willebrand*, 2001; *Häkkinen and Rhines*, 2004; *Hátún et al.*, 2005; *Treguier et al.*, 2005; *Levermann and Born*, 2007; *Born et al.*, 2009; *Lohmann et al.*, 2009; *Born et al.*, 2010; *Montoya et al.*, 2010] and this study aims to apply this physical understanding to data from the geological record.

2. Model Description

[5] To investigate the role of the SPG during the 8.2 ka event we make use of the coupled climate model CLIMBER-3α, which comprises atmosphere and sea ice components and the oceanic general circulation model MOM-3 (*Montoya et al.* [2005] and auxiliary material).[1] The oceanic horizontal resolution is 3.75° × 3.75° with 24 unevenly spaced vertical layers. Simplified atmosphere dynamics are solved on a coarse numerical grid (7.5° in latitude and 22.5° in longitude).

[6] Due to the coarse resolution of the model, the SPG and deep water formation in its center are shifted eastward and simulated boundary currents are relatively broad (Figure 2). A second deep water formation region is found in the Nordic seas. Despite shortcomings, the interaction between gyre advection, convection in its center and eddy transport in between, as well as the communication of deep water masses across the deepest passages of the Greenland-Scotland ridge, compares well to higher-resolution models [*Spall*, 2005; A. Born et al., Late Eemian warming in the Nordic seas as seen in proxy data and climate models, submitted to *Paleoceanography*, 2010]. For additional information we refer to sensitivity studies with glacial [*Montoya et al.*, 2010] and present-day boundary conditions [*Mignot et al.*, 2006] as well as under global warming [*Levermann et al.*, 2007].

[7] For the present study, the model was initialized with climatological hydrography [*Levitus*, 1982] and orbital parameters for 8,200 years before present [*Berger*, 1978]. Atmospheric CO_2 concentration was set to 260 ppm [*Raynaud et al.*, 2000]. The continental watershed over North America was shifted to the west and south in order to take into account changes in surface gradient due to the isostatic depression of glacial ice sheets. After the model was run into equilibrium over 2700 years, the simulated SPG exhibits a stable but weak volume transport of 19.5 Sv (1 Sv = 10^6 m^3 s^{-1}). In order to simulate the lake drainage, $160 \cdot 10^{12}$ m^3 of freshwater were added to the surface of the Labrador Sea coast during a period of two years, west of the deep convection region. This value is equivalent to a 2 year volume

[1] Auxiliary materials are available in the HTML. doi:10.1029/2009GC003024.

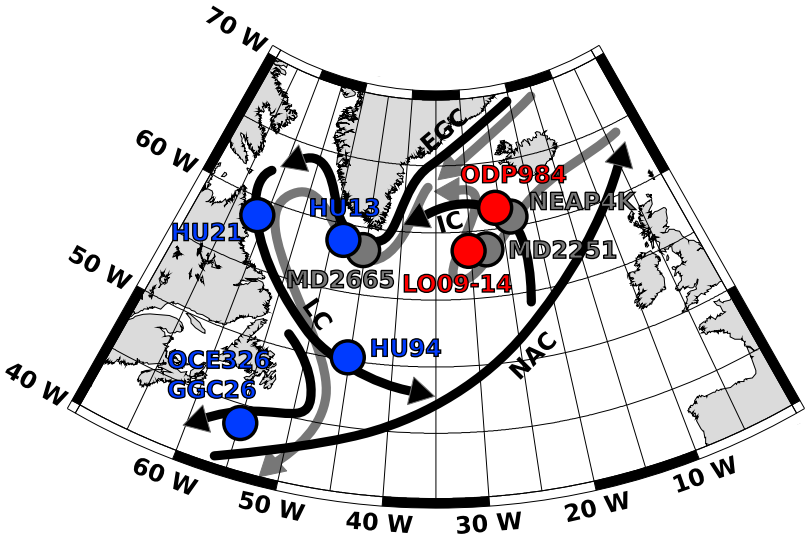

Figure 1. Map of the subpolar North Atlantic showing the location of core sites and of major ocean currents mentioned in the text. Blue dots denote cores that show an abrupt and persistent cooling after 8 ka before present; warming is reported from the Reykjanes Ridge and marked red. Grey dots show where the 8.2 ka event is evident as a temporal reduction in deep current flow speed. Black arrows illustrate the surface currents (IC, Irminger Current; EGC, East Greenland Current; LC, Labrador Current; NAC, North Atlantic Current); grey arrows illustrate the Deep Western Boundary Current. For a list of full core names and references, please refer to Table S1 in Text S1.

flux of 2.6 Sv, based on a recent estimate of the lake volume [*Leverington et al.*, 2002], and has been used in previous model studies [*Bauer et al.*, 2004; *LeGrande et al.*, 2006; *Wiersma et al.*, 2006]. For diagnostic purposes, a passive tracer was released simultaneously with the freshwater flux at the same location in order to track advection of the perturbation. This tracer does not influence the circulation. We define the strength of the subpolar gyre as the local minimum of the depth integrated stream function. For the cyclonic circulation of the SPG, this stream function is negative (Figure 2).

3. Model Results and Interpretation of Proxy Data

[8] In response to the meltwater release, the SPG switches into a significantly stronger mode with 29 Sv volume transport (Figures 2 and 3a). This represents a strengthening of about 50% and the stronger circulation is within the uncertainty of present-day observations [*Bacon*, 1997; *Read*, 2001]. Further integration shows that this stronger state is stable and not only a temporary response to the freshwater pulse.

[9] The abrupt transition is due to two positive feedbacks inherent to the SPG [*Levermann and Born*, 2007]. First, a stronger SPG transports less tropical saline water into the Nordic seas but accumulates these in the subpolar North Atlantic, making upper water masses in the center of the SPG more saline (Figures S7–S9 in Text S1). This is consistent with previous conclusions which are based on simulations with a high-resolution ocean general circulation model and confirmed by observations [*Hátún et al.*, 2005; *Lohmann et al.*, 2009]. Increased surface salinity enhances deep convection, cooling the deep water column. Besides, a stronger SPG results in enhanced outcropping of isopycnals

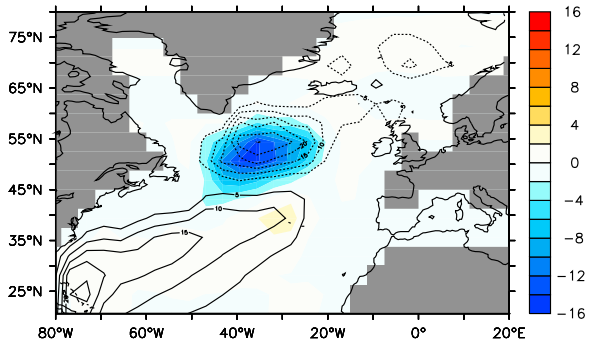

Figure 2. Colors indicate anomaly of the vertically integrated stream function, last 50 years of the perturbed simulation minus last 50 years before the meltwater pulse. Contours indicate vertically integrated stream function for the last 50 years of the simulation. For the cyclonic circulation of the SPG, the negative anomaly represents a strengthening. Outside the subpolar North Atlantic, currents are virtually unchanged.

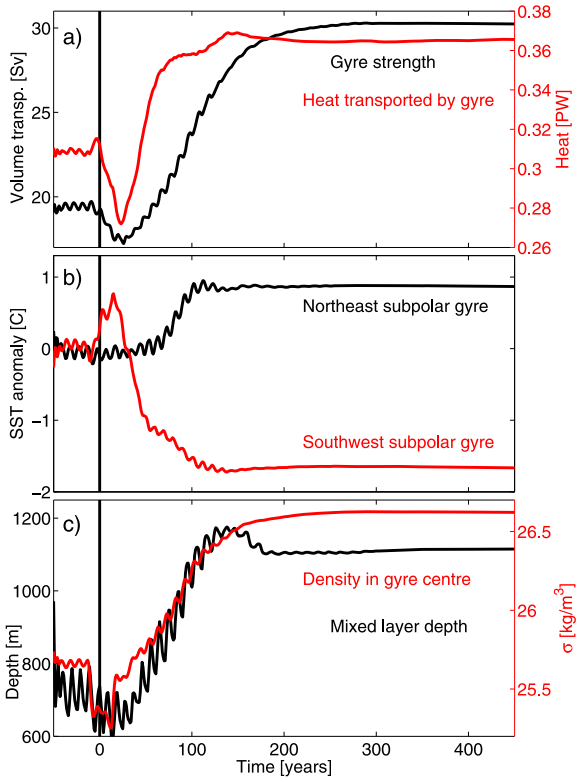

Figure 3. Temporal evolution of key quantities of the transition toward a stronger SPG during the 8.2 ka event. The vertical line indicates the timing of the lake Agassiz drainage; data are filtered with a 25 year running mean. (a) Volume and heat transport of the SPG, (b) sea surface temperature in the northeastern (black) and southwestern (red) subpolar region, and (c) maximum winter mixed layer depth in the center of the SPG and surface density in the center of the SPG (see Figure S7 in Text S1). The stronger heat transport leads to a warming of the northeastern gyre region while the southwestern part cools rapidly. Surface density and mixed layer depth increase simultaneously.

and hence a more efficient removal of heat from the gyre's center by isopycnal mixing. Both effects, salt accumulation and removal of heat, increase the core density of the gyre compared to the relatively light exterior, sea surface drops and the corresponding geostrophic response strengthens the cyclonic SPG circulation.

[10] In addition to these self-sustaining internal feedbacks, there exists an interaction with the flow over the Greenland-Scotland ridge. The meltwater perturbation reduces sinking in the Nordic seas and therewith the supply of dense overflow waters to the northern rim of the SPG. Consequently, the outer rim of the gyre gets lighter and the gyre slightly intensifies. This triggers the two internal feedbacks mentioned above and yields the stronger SPG state (Figure S1 in Text S1). Elsewhere, we have shown that a short reduction of dense deep outflow from the Nordic seas is sufficient to trigger the transition (≥25 years [*Levermann and Born*, 2007]) and that the described internal feedbacks dominate the dynamics. Changes in wind stress are small and do not show a consistent pattern (Figure S6 in Text S1). This is plausible because the freshwater flood does not impact wind patterns directly. Moreover, the coarse resolution of the atmosphere component might underestimate regional variations. Thus, the changes in wind stress seen after the transition are likely due to local changes in sea ice as suggested also by the irregular pattern. The mechanism of transition is robust to prescribed wind forcing and with respect to model setup and experimental design (see auxiliary material).

[11] Considering this change in surface circulation allows us to combine a number of proxy records into a consistent picture of the 8.2 ka event. Recent work found strong evidence for a reduction of dense water supply from the Nordic seas due to the lake Agassiz drainage [*Hall et al.*, 2004; *Ellison et al.*, 2006; *Kleiven et al.*, 2008]. However, proxy data suggests that the meltwater signal did not reach the convection region at the center of the Labrador Sea but was exported along the shelf in the Labrador Current [*Keigwin et al.*, 2005; *Hillaire-Marcel et al.*, 2007]. From there a large portion moved northeastward and was diluted by mixing with water of the North Atlantic Current before reaching the Nordic seas and causing a moderate reduction in convection there. Our model reproduces this path qualitatively. 30 years after the lake drainage, highest concentrations of meltwater are found in the Nordic seas where 25% of the meltwater pulse has been advected to (Figure 4).

[12] After the transition, the stronger SPG circulation intensifies oceanic heat transport (Figure 3a). More warm tropical water reaches the northern SPG while more cold water is advected toward the west and south. This results in a sea surface temperature (SST) dipole (Figure S7 in Text S1). The southwestern SPG region cools abruptly (Figure 3b, red) while rapid warming is seen in the northeastern SPG region (Figure 3b, black).

[13] An abrupt and persistent SST decrease coeval with the lake drainage has indeed been reported from dinoflagellate cysts and alkenones for many locations throughout Labrador Sea and downstream Labrador Current south of Newfoundland [*Solignac et al.*, 2004; *de Vernal and Hillaire-Marcel*, 2006; *Sachs*, 2007]. Consistent with our simulations this

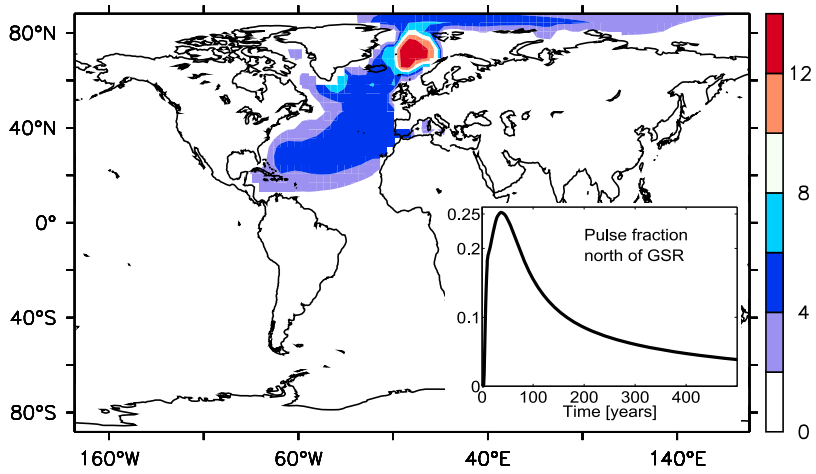

Figure 4. Distribution of the meltwater pulse 30 years after its release into the Labrador Sea, integrated over depth (in m). Highest concentrations are found in the Nordic seas. Inset shows the fraction of the pulse in the Nordic seas and the Arctic Ocean. After approximately 30 years, 25% of the meltwater is advected north of the Greenland-Scotland ridge, followed by a decline as it is diluted globally.

data indicates a drastic reorganization of the slope current system. No persistent cooling is seen in foraminiferal data from Eirik Drift in the northern Labrador Sea, probably because of its location too far offshore to record changes in the coastal current [*Kleiven et al.*, 2008]. The warming signal on the eastern side of the gyre is not easily detected in proxy records because the strengthening of the surface circulation also changed the position of frontal systems. Thus, the strengthening of the SPG is recorded as a subsurface cooling inferred from foraminifera at a relatively eastern location [*Thornalley et al.*, 2009]. However, approximately 400 km further west on Reykjanes Ridge, where currents are more constrained by topography, an increase and stabilization of surface temperatures reconstructed using diatoms, foraminiferal $\delta^{18}O$ and Mg/Ca data has been associated with an intensification of the Irminger Current, the northern limb of the SPG (Figure 1) [*Andersen et al.*, 2004; *Came et al.*, 2007].

[14] Further support for a transition toward a stronger SPG following the 8.2 ka event comes from increased sea surface salinities throughout the subpolar region that started similarly abrupt as the temperature changes and were equally persistent, both in our model experiments (Figures S7–S9 in Text S1) and proxy data [*Solignac et al.*, 2004; *de Vernal and Hillaire-Marcel*, 2006; *Hillaire-Marcel et al.*, 2007; *Came et al.*, 2007]. The cooling of western slope waters can thus not be attributed to more intense transport of cold and fresh Arctic waters through the East Greenland Current. Their upstream source must be the relatively saline Irminger Current which suggests a SPG intensification. A sudden increase in advection of Atlantic water into Labrador Sea has also been concluded from diatoms, fossil shell data and foraminiferal assemblages at several locations along the Greenland west coast [*Donner and Jungner*, 1975; *Lloyd et al.*, 2005; *Ren et al.*, 2009]. The intensification of westward salt transport and the eastward movement of the subpolar front with a stronger SPG results in a freshening of inflow into the Nordic seas (Figure S7 in Text S1), consistent with paleo-observations [*Thornalley et al.*, 2009] and present-day instrumental records [*Hátún et al.*, 2005]. Salt accumulation in the center of a anomalously strong SPG has been shown in a higher-resolution model [*Lohmann et al.*, 2009].

[15] Proxy data of Labrador Sea convection furthermore supports a significant reorganization of the surface circulation. In our simulations, enhanced surface salinity together with subsurface cooling in the center of the SPG results in a density increase and a subsequent intensification of convection south of the Greenland-Scotland ridge (Figure 3c). These results match well with existing data of the geological record. Little or no Labrador Sea Water was produced in the early Holocene and formation intensified not long after the meltwater outburst [*Hillaire-Marcel et al.*, 2001, 2007]. Isotopic changes in Labrador Sea sediments show a persistent reorganization of the deep current system after 8,000 years before present [*Fagel et al.*, 2004] with deeper Labrador Sea Water found in Pa/Th data [*Gherardi et al.*, 2009] and a permanent reduction of deep water formed in the Nordic seas

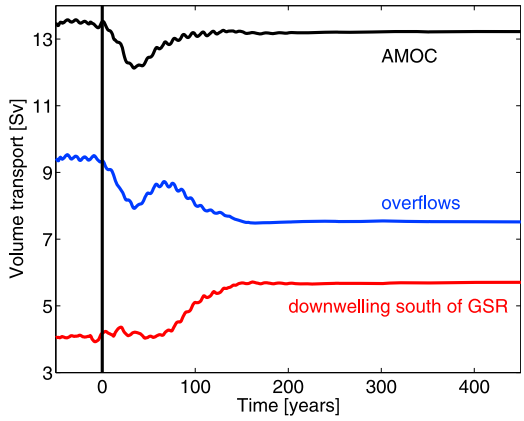

Figure 5. The Atlantic Meridional Overturning Circulation (AMOC), decomposed into deep water contributions from sinking in the Nordic seas (blue) and south of the Greenland-Scotland ridge (red). The vertical line indicates the timing of the lake Agassiz drainage, and a 25 year running mean filter is applied. The AMOC weakens abruptly in response to the freshwater event and recovers gradually over approximately 100 years. While the initial weakening is caused by the reduction of deep water supply from the Nordic seas, the recovery is due to a delayed intensification of Labrador Sea deep water formation. Both Nordic seas and Labrador Sea downwelling change significantly and persistently.

recorded in benthic δ^{13}C data [*Evans et al.*, 2007]. This points toward a persistent reorganization of both the horizontal surface and the deep meridional circulation, as simulated here.

[16] In contrast to significant changes in SPG strength (47%), the AMOC weakens by just 1.5 Sv (11%) in response to the meltwater pulse, significantly less than the 30%–50% reduction reported from previous model studies [*Bauer et al.*, 2004; *Wiersma et al.*, 2006; *LeGrande et al.*, 2006] (Figure 5). The strong response in earlier simulations might be due to the application of the meltwater pulse directly on the Labrador Sea convection region with dramatic consequences for SPG and AMOC. Such a freshwater perturbation leads to a reduction of convection in the Labrador Sea contradicting the paleorecord that shows the intensification of convection in this region. Moreover, this scenario removes a significant fraction of the freshwater pulse from the surface, inconsistent with proxy data indicating its advection in the Labrador Current. Hence, a smaller fraction is advected into the Nordic seas which is crucial to initiate the mechanism amplifying the SPG as discussed above (see auxiliary material for further discussion). The initial AMOC weakening in our simulation is followed by a rapid recovery over approximately 100 years and then a more gradual increase. The decomposition into deep water formation regions shows that the initial weakening is due to reduced sinking in the Nordic seas, reaching its minimum after 150 years. The recovery and weak overall reduction is due to an increase in deep water formation south of the Greenland-Scotland ridge with a time lag of approximately 50 years (Figures 5 and 3c).

[17] A distinctive reduction in deep current flow speeds, probably delayed by at least several decades, is reported from the Greenland-Scotland ridge overflows and off the southern tip of Greenland (Figure 1) [*Hall et al.*, 2004; *Ellison et al.*, 2006; *Kleiven et al.*, 2008]. This is upstream from where Labrador Sea Water joins the Deep Western Boundary Current, the southward flowing branch of the AMOC. Further south in the North Atlantic, the reduction of northern source deep waters is minor for the 8.2 ka event if recorded at all [*Keigwin and Boyle*, 2000; *Oppo et al.*, 2003; *Keigwin et al.*, 2005]. The onset of Labrador Sea Water formation following the meltwater pulse might explain this discrepancy.

4. Summary and Conclusions

[18] Expanding previous studies that focused on the AMOC response, i.e., changes in the meridional circulation, to the lake Agassiz drainage, we propose that many observed but hitherto unexplained abrupt changes and discrepancies require taking into account a reorganization of the horizontal circulation. The most striking result is the persistent strengthening of the SPG in response to the short freshwater pulse. The transition between the two circulation patterns is triggered by an external positive feedback and stabilized by two positive feedback mechanisms within the SPG.

[19] While our results do not contradict an abrupt and considerable AMOC reduction in response to the lake Agassiz drainage, it might have been relatively short lived and weaker than suggested by previous simulations for two reasons: (1) The freshwater flood had the biggest impact not in the Labrador Sea but primarily affected deep water formation in the Nordic seas after mixing in the North Atlantic Current (Figure 4) and (2) this deep water reduction was partly compensated by enhanced sinking in the Labrador Sea (Figures 3c and 5). The latter mechanism has already been observed in models and data on time scales of several millennia [*Renssen et al.*, 2005; *Solignac et al.*, 2004].

[20] In our model the reorganization of the SPG surface circulation and subsequent changes in heat and salt advection provide the precondition for a more intense Labrador Sea convection and stabilize it. It has been suggested that this circulation mode is a unique feature of the Holocene, with Labrador Sea Water probably missing in the warmer climate of the last interglacial [*Hillaire-Marcel et al.*, 2001] and implications for the stability of the AMOC by the end of this century. Our results might provide the base for a future investigations of these hypotheses.

Acknowledgments

[21] We gratefully acknowledge useful discussions with Ulysses S. Ninnemann, Kerim H. Nisancioglu, and Trond Dokken. An earlier version of this manuscript greatly benefited from comments of three anonymous reviewers. A.B. was funded by the Marie Curie Actions project NICE (MRTN-CT-2006-036127). This is publication A290 from the Bjerknes Centre for Climate Research.

References

Alley, R. B., and A. M. Ágústsdóttir (2005), The 8k event: Cause and consequences of a major Holocene abrupt climate change, *Quat. Sci. Rev.*, *24*, 1123–1149.

Alley, R. B., P. A. Mayewski, T. Sowers, M. Stuiver, K. C. Taylor, and P. U. Clark (1997), Holocene climatic instability: A prominent, widespread event 8200 years ago, *Geology*, *25*, 483–486.

Andersen, C., N. Koc, and M. Moros (2004), A highly unstable Holocene climate in the subpolar North Atlantic: Evidence from diatoms, *Quat. Sci. Rev.*, *23*, 2155–2166.

Bacon, S. (1997), Circulation and fluxes in the North Atlantic between Greenland and Ireland, *J. Phys. Oceanogr.*, *27*, 1420–1435.

Bauer, E., A. Ganopolski, and M. Montoya (2004), Simulation of the cold climate event 8200 years ago by meltwater outburst from Lake Agassiz, *Paleoceanography*, *19*, PA3014, doi:10.1029/2004PA001030.

Berger, A. (1978), Long-term variations of caloric solar radiation resulting from the Earth's orbital elements, *Quat. Res.*, *9*, 139–167.

Born, A., A. Levermann, and J. Mignot (2009), Sensitivity of the Atlantic Ocean circulation to a hydraulic overflow parameterisation in a coarse resolution model: Response of the subpolar gyre, *Ocean Modell.*, *27*(3–4), 130–142.

Born, A., K. H. Nisancioglu, and P. Braconnot (2010), Sea ice induced changes in ocean circulation during the Eemian, *Clim. Dyn.*, doi:10.1007/s00382-009-0709-2, in press.

Came, R. E., D. W. Oppo, and J. F. McManus (2007), Amplitude and timing of temperature and salinity variability in the subpolar North Atlantic over the past 10 k.y., *Geology*, *35*, 315–318.

de Vernal, A., and C. Hillaire-Marcel (2006), Provincialism in trends and high frequency changes in the northwest North Atlantic during the Holocene, *Global Planet. Change*, *54*, 263–290.

Donner, J., and H. Jungner (1975), Radiocarbon dating of shells from marine deposits in the Disko Bugt, West Greenland, *Boreas*, *4*, 25–45.

Eden, C., and J. Willebrand (2001), Mechanism of interannual to decadal variability of the North Atlantic Circulation, *J. Clim.*, *14*, 2266–2280.

Ellison, C. R. W., M. R. Chapman, and I. R. Hall (2006), Surface and deep ocean interactions during the cold climate event 8200 years ago, *Science*, *312*, 1929–1932.

Evans, H. K., I. R. Hall, G. G. Bianchi, and D. W. Oppo (2007), Intermediate water links to Deep Western Boundary Current variability in the subtropical NW Atlantic during marine isotope stages 5 and 4, *Paleoceanography*, *22*, PA3209, doi:10.1029/2006PA001409.

Fagel, N., C. Hillaire-Marcel, M. Humblet, R. Brasseur, D. Weis, and R. Stevenson (2004), Nd and Pb isotope signatures of the clay-size fraction of Labrador Sea sediments during the Holocene: Implications for the inception of the modern deep circulation pattern, *Paleoceanography*, *19*, PA3002, doi:10.1029/2003PA000993.

Gherardi, J.-M., L. Labeyrie, S. Nave, R. Francois, J. F. McManus, and E. Cortijo (2009), Glacial-interglacial circulation changes inferred from $^{231}Pa/^{230}Th$ sedimentary record in the North Atlantic region, *Paleoceanography*, *24*, PA2204, doi:10.1029/2008PA001696.

Häkkinen, S., and P. B. Rhines (2004), Decline of subpolar North Atlantic circulation during the 1990s, *Science*, *304*, 555–559.

Hall, I. R., G. Bianchi, and J. R. Evans (2004), Centennial to millenial scale Holocene climate-deep water linkage in the North Atlantic, *Quat. Sci. Rev.*, *23*, 1529–1536.

Hátún, H., A. B. Sandø, H. Drange, B. Hansen, and H. Valdimarsson (2005), Influence of the Atlantic Subpolar Gyre on the thermohaline circulation, *Science*, *309*, 1841–1844.

Hillaire-Marcel, C., A. de Vernal, A. Bilodeau, and A. J. Weaver (2001), Absence of deep-water formation in the Labrador Sea during the last interglacial period, *Nature*, *410*, 1073–1077.

Hillaire-Marcel, C., A. de Vernal, and D. J. W. Piper (2007), Lake Agassiz Final drainage event in the northwest North Atlantic, *Geophys. Res. Lett.*, *34*, L15601, doi:10.1029/2007GL030396.

Keigwin, L. D., and E. A. Boyle (2000), Detecting Holocene changes in thermohaline circulation, *Proc. Natl. Acad. Sci. U. S. A.*, *97*, 1343–1346.

Keigwin, L. D., J. P. Sachs, Y. Rosenthal, and E. A. Boyle (2005), The 8200 year B.P. event in the slope water system, western subpolar North Atlantic, *Paleoceanography*, *20*, PA2003, doi:10.1029/2004PA001074.

Kleiven, H. F., C. Kissel, C. Laj, U. S. Ninnemann, T. O. Richter, and E. Cortijo (2008), Reduced North Atlantic Deep Water coeval with the glacial Lake Agassiz fresh water outburst, *Science*, *319*, 60–64.

LeGrande, A. N., G. A. Schmidt, D. T. Shindell, C. V. Field, R. L. Miller, D. M. Koch, G. Faluvegi, and G. Hoffmann (2006), Consistent simulations of multiple proxy responses to an abrupt climate change event, *Proc. Natl. Acad. Sci. U. S. A.*, *103*, 837–842.

Leverington, D., H. D. Mann, and J. T. Teller (2002), Changes in bathymetry and volume of glacial Lake Agassiz between 9200 and 7700 14C yr BP, *Quat. Res.*, *57*, 244–252.

Levermann, A., and A. Born (2007), Bistability of the Atlantic subpolar gyre in a coarse-resolution climate model, *Geophys. Res. Lett.*, *34*, L24605, doi:10.1029/2007GL031732.

Levermann, A., J. Mignot, S. Nawrath, and S. Rahmstorf (2007), The role of northern sea ice cover for the weakening of the thermohaline circulation under global warming, *J. Clim.*, *20*, 4160–4171.

Levitus, S. (1982), Climatological atlas of the world ocean, *NOAA Prof. Pap.*, *13*, 173 pp.

Lloyd, J., L. Park, A. Kuijpers, and M. Moros (2005), Early Holocene palaeoceanography and deglacial chronology of Disko Bugt, West Greenland, *Quat. Sci. Rev.*, *24*, 1741–1755.

Lohmann, K., H. Drange, and M. Bentsen (2009), Response of the North Atlantic subpolar gyre to persistent North Atlantic oscillation like forcing, *Clim. Dyn.*, *32*, 273–285.

Mignot, J., A. Levermann, and A. Griesel (2006), A decomposition of the Atlantic meridional overturning circulation into physical components using its sensitivity to vertical diffusivity, *J. Phys. Oceanogr.*, *36*, 636–650.

Montoya, M., A. Griesel, A. Levermann, J. Mignot, M. Hofmann, A. Ganopolski, and S. Rahmstorf (2005), The Earth system model of intermediate complexity CLIMBER-3α. Part I: Description and performance for present-day conditions, *Clim. Dyn.*, *25*, 237–263.

Montoya, M., A. Born, and A. Levermann (2010), Reversed North Atlantic gyre dynamics in present and glacial climates, *Clim. Dyn.*, doi:10.1007/s00382-009-0729-y, in press.

Oppo, D. W., J. F. McManus, and J. L. Cullen (2003), Deepwater variability in the Holocene epoch, *Nature*, *422*, 277–278.

Raynaud, D., J.-M. Barnola, J. Chappellaz, T. Blunier, A. Indermühle, and B. Stauffer (2000), The ice record of greenhouse gases: A view in the context of future changes, *Quat. Sci. Rev.*, *19*, 9–17.

Read, J. (2001), Water masses and circulation of the northeast Atlantic subpolar gyre, *Prog. Oceanogr.*, *48*, 461–510.

Ren, J., H. Jiang, M.-S. Seidenkrantz, and A. Kuijpers (2009), A diatom-based reconstruction of Early Holocene hydrographic and climatic change in a southwest Greenland fjord, *Mar. Micropaleontol.*, *70*, 166–176.

Renssen, H., H. Goosse, and T. Fichefet (2005), Contrasting trends in North Atlantic deep-water formation in the Labrador Sea and Nordic seas during the Holocene, *Geophys. Res. Lett.*, *32*, L08711, doi:10.1029/2005GL022462.

Sachs, J. P. (2007), Cooling of Northwest Atlantic slope waters during the Holocene, *Geophys. Res. Lett.*, *34*, L03609, doi:10.1029/2006GL028495.

Solignac, S., A. de Vernal, and C. Hillaire-Marcel (2004), Holocene sea-surface conditions in the North Atlantic—Contrasted trends and regimes in the western and eastern sectors (Labrador Sea vs. Iceland Basin), *Quat. Sci. Rev.*, *23*, 319–334.

Spall, M. A. (2005), Buoyancy-forced circulations in shallow marginal seas, *J. Mar. Res.*, *63*, 729–752.

Thornalley, D. J. R., H. Elderfield, and I. N. McCave (2009), Holocene oscillations in temperature and salinity of the surface North Atlantic, *Nature*, *457*, 711–714.

Treguier, A. M., S. Theetten, E. P. Chassignet, T. Penduff, R. Smith, L. Talley, J. O. Beismann, and C. Böning (2005), The North Atlantic Subpolar Gyre in four high-resolution models, *J. Phys. Oceanogr.*, *35*, 757–774.

Wiersma, A. P., H. Renssen, H. Goosse, and T. Fichefet (2006), Evaluation of different freshwater forcing scenarios for the 8.2 ka BP event in a coupled climate model, *Clim. Dyn.*, *27*, 831–849.

Supplementary Information for

The 8.2k event: abrupt transition of the subpolar gyre towards a modern North Atlantic circulation

Andreas Born[1]

Bjerknes Centre for Climate Research, Bergen, Norway

Geophysical Institute, University of Bergen, Bergen, Norway

Anders Levermann

Potsdam Institute for Climate Impact Research, Potsdam, Germany

Institute of Physics, Potsdam University, Potsdam, Germany

This Supplement is organized as follows: The climate model is described in detail in section 1. Section 2 discusses the robustness of multiple subpolar gyre (SPG) modes by presenting findings from several climate models. Section 3 continues this discussion summarizing work on the sensitivity of the SPG primarily in CLIM*BER*-3α. This is followed by figures supporting conclusions in the main text and a table referencing the marine sediment cores discussed in the main text in section 4.

[1] Corresponding author: andreas.born@bjerknes.uib.no

1 The climate model CLIM*BER*-3α and experimental design

CLIM*BER*-3α consists of the statistical-dynamical atmosphere model POTSDAM-2 (*Petoukhov et al.*, 2000) coupled to a global ocean general circulation model based on the Geophysical Fluid Dynamics Laboratory (GFDL) Modular Ocean Model (MOM-3) code and to the dynamic and thermodynamic sea ice module of *Fichefet and Maqueda* (1997). The oceanic horizontal resolution is 3.75° × 3.75° with 24 unevenly spaced vertical layers. We apply a weak background vertical diffusivity of $0.2 \times 10^{-4} m^2 s^{-1}$. For a discussion on the model's sensitivity to this parameter refer to *Mignot et al.* (2006). The implemented second-order moment tracer advection scheme (*Prather*, 1986) minimizes numerical diffusion (*Hofmann and Maqueda*, 2006). The model makes use of a parametrization of boundary enhanced mixing depending both on near-bottom stratification and roughness of topography (*Ledwell et al.*, 2000), following *Hasumi and Suginohara* (1999). This leads locally to vertical diffusion coefficients of up to $10^{-4} m^2 s^{-1}$ for example over rough topography.

The atmosphere model has a coarse spatial resolution (7.5° in latitude and 22.5° in longitude) and is based on the assumption of a universal vertical structure of temperature and humidity, which allows reducing the three-dimensional description to a set of two-dimensional prognostic equations. Description of atmospheric dynamics is based on a quasi-geostrophic approach and a parametrization of the zonally averaged meridional atmospheric circulation. Synoptic processes are parametrized as diffusion terms with a turbulent diffusivity computed from atmospheric stability and horizontal temperature gradients. Heat and freshwater fluxes between ocean and atmosphere are computed on the oceanic grid and applied without any flux adjustments. The wind stress is computed as the sum of the NCEP-NCAR reanalysis wind stress climatology (*Kalnay and coauthors*, 1996) and the wind stress anomaly calculated by the atmospheric model relative to the control run. CLIM*BER*-3α has been validated against data both for Holocene (*Montoya et al.*, 2005) and glacial boundary conditions (*Montoya and Levermann*, 2008).

Deep water formation takes place in two regions, north of the Greenland Scotland ridge and in the SPG center. Deep water masses are communicated by overflows

through the deepest passages of the ridge. This deep outflow from the Nordic Seas facilitates a surface inflow in our model. Although only crudely represented, the exchange shows the dynamical behavior expected from Holocene paleo data (*Solignac et al.*, 2004) and model studies (*Renssen et al.*, 2005).

2 Evidence for multiple subpolar gyre modes in other models

The positive feedbacks that give rise to the SPG bistability are based exclusively on large scale dynamics. Thus, they are likely to be found in most ocean models even though the existence of multiple stable SPG modes circulation might be masked by other processes. While there are good indications from proxy data that a transition between two SPG modes took place indeed and was not masked by such secondary processes, here we shortly present some fundamental considerations regarding the existence of positive SPG feedbacks and discuss indications for these feedbacks in a number of different ocean models.

Convection in the SPG center is intimately linked to its strength (*Eden and Willebrand*, 2001; *Häkkinen and Rhines*, 2004; *Treguier et al.*, 2005; *Born et al.*, 2010a), because it increases density in the gyre's center around which water circulates baroclinically (*Born et al.*, 2009). Thus the bistability of the SPG circulation can also be understood in the framework of convection, with stronger convection entailing a stronger gyre. In addition, a stronger SPG advects more saline water into the western North Atlantic facilitating convection, a positive feedback that destabilizes the system (*Levermann and Born*, 2007).

Different modes of Labrador Sea deep convection are found in many ocean models. In HadCM3, *Kleinen et al.* (2009) discuss a 70 % weakening of the SPG coeval with a reduction of Labrador Sea convection in response to continuous freshwater forcing of the North Atlantic. Experiments with anomalous heat transports over Labrador Sea by *Wu and Wood* (2008) exhibit an abrupt strengthening of the SPG for higher heat loss and convection. A weaker SPG circulation in response to weaker convection in its center has also been confirmed for the Institut Pierre Simon Laplace Coupled

Model 4 (IPSL CM4) (*Born et al.*, 2010a). The positive feedback related to a weaker salt transport by the SPG was also quantified in this study.

In addition to *Levermann and Born* (2007), some further studies directly report on spontaneous transitions between active and inactive Labrador Sea convection modes. These suggest the presence of destabilizing positive feedbacks. *Jongma et al.* (2007) discuss a bistability of convection and overturning circulation. Their model (ECBilt-Clio) alternates between two meta-stable states with active and inactive convection. Along with an externally applied constant freshwater perturbation over Labrador Sea, the residence time in the inactive convection state gradually increases. *LeGrande et al.* (2006) and *LeGrande and Schmidt* (2008) also find a spontaneous transition to active Labrador Sea convection in their preindustrial control run with the Goddard Institute for Space Studies ModelE-R atmosphere ocean general circulation model. Two states of SPG circulation have also been observed in the Bergen Climate Model, an AOGCM (H. Drange, personal communication, 2009).

While models over a wide range of complexity suggest the existence of multiple SPG modes, earlier model simulations of the 8.2k event did not report persistent changes in the SPG circulation. Without the coeval intensification of deepwater formation south of the Greenland Scotland ridge, these models usually report a strong reduction of the Atlantic Meridional Overturning Circulation (AMOC), an apparent contradiction of our results. This is possibly due to the direct application of the meltwater pulse on the Labrador Sea convection region. As pointed out above, convection in the gyre's center has strong control on its strength, which will be discussed in more detail in the following section. *Bauer et al.* (2004) employ a zonally averaged, two-dimensional, ocean model. Hence, the freshwater anomaly is distributed over the entire basin width and inevitably affects convection south of the Greenland Scotland ridge directly. Moreover, gyre dynamics cannot be adequately included in zonally averaged models. *LeGrande et al.* (2006) and *LeGrande and Schmidt* (2008) simulate the 8.2k event in a three-dimensional ocean model using two different initial states. One result is that the state more realistic for the early Holocene, with weak Labrador Sea convection, simulates a significantly weaker AMOC reduction (30 %) than the strong initial state (50 %). This supports our findings that it is important not to apply the meltwater pulse directly on the convection region. *Wiersma et al.*

(2006) also report a weaker AMOC reduction when applying the meltwater pulse on a weak Labrador Sea convection state. However, in this study the meltwater pulse is applied in the center of the Labrador Sea and directly on the convection region, which is still active in the weak state. This forcing scenario favors a strong AMOC response but disagrees with paleo data (*Hillaire-Marcel et al.*, 2007; *Keigwin et al.*, 2005) and a high resolution model study (*Winsor et al.*, 2006). Another consequence of applying the meltwater pulse directly onto the Labrador Sea convection region is that it removes a significant fraction of the meltwater pulse from the surface. Hence, a smaller fraction is advected into the Nordic Seas. This, however, is crucial to initiate the mechanism amplifying the SPG as has been shown in the main text.

3 Model sensitivity of the subpolar gyre circulation to changes in external forcing

The strength of the SPG depends at least partially on the density gradient between its center and rim. The water column in the center is relatively denser, causing a depression in sea surface height around which water circulates cyclonically in geostrophic balance. Increasing this density gradient results in a deeper depression and a stronger gyre. This understanding differentiates two classes of mechanisms controlling the SPG strength, by modifying the density of the water column in its center or the rim (Fig. S1).

3.1 Sensitivity to the representation of Greenland Scotland ridge overflow and anomalous freshwater forcing

Density at the northern rim of the SPG is partially controlled by dense waters overflowing the Greenland Scotland ridge. Because the representation of these small scale currents is essential for the formation of North Atlantic Deep Water but problematic in ocean general circulation models, it is often enhanced by means of numerical techniques. A study of two different approaches, namely artificial deepending of the ridge and a hydraulic overflow parametrization, found that both simulate the large

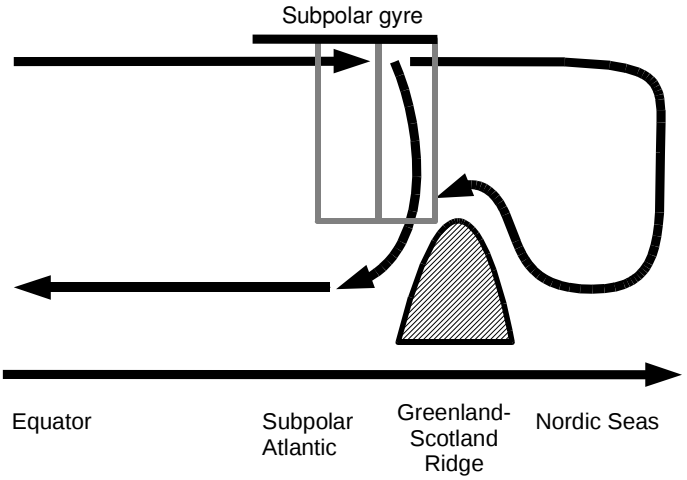

Figure S1: Schematic of the Atlantic Meridional Overturning Circulation (AMOC) and the subpolar gyre. Grey boxes show the center and exterior regions of the gyre referred to in the main text. Density changes in the center region are the result of positive feedbacks inherent to the subpolar gyre. The density on its rim is determined by two water masses mixing at intermediate depth, the denser one reaching the mixing region after sinking in the Nordic Seas and overflowing the Greenland-Scotland ridge and a second produced by sinking south of the ridge.

scale deep ocean circulation similarly well. However, the density of the resulting water mass south of the Greenland Scotland ridge, thus at the SPG rim, is lower in one case resulting in a significantly stronger SPG (*Born et al.*, 2009).

Besides continuous changes in the overflow transport, we also investigated the sensitivity of the SPG to a transient reduction in overflow strength in response to anomalous freshwater flux into the Nordic Seas (*Levermann and Born*, 2007). Two main conclusions can be drawn from this study. First, the increase in SPG strength persists even after the freshwater pulse. This illustrates the relative importance of reduced overflows and density in the SPG rim on one side to positive feedbacks of the SPG that increase the density in the gyre's center on the other, while both mechanisms strengthen the circulation. Once the SPG reaches a critical strength due to the overflows reduction, the SPG feedbacks increase the density in the SPG center and stabilize the strong circulation mode. Secondly, a freshwater pulse of 0.05 Sv over 25 years is sufficient to trigger a notable increase in SPG strength (Fig. S2). This is about a fourth of the lake Agassiz drainage volume and a good

approximation to the fraction of the drainage that is advected into the Nordic Seas over a similar period of time ($\sim$ 30 years, Fig. 4 in the main text). This earlier sensitivity study strongly supports the simulation presented here for the 8.2k event.

The dilution of the lake drainage before reaching the main impact region, the Nordic Seas, the multi-decadal delay due to advection and the fact that a fraction of the original freshwater volume is enough to trigger the transition helps to assess the importance of a possible multipulse event of two smaller volume discharges as proposed from observations (*Ellison et al.*, 2006).

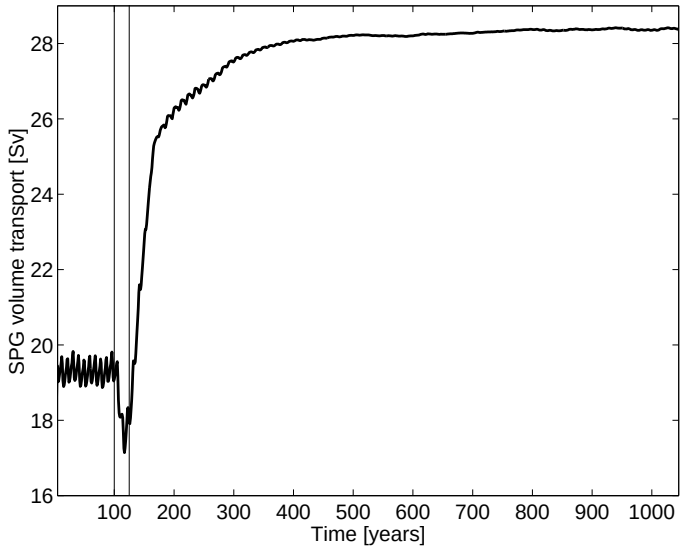

Figure S2: Temporal evolution of the SPG strength in response to freshwater forcing in the Nordic Seas. The vertical lines indicates the forcing period (25 years).

3.2 Sensitivity to wind stress

The transition of the SPG is robust to fixed surface wind stress (Fig. S3). In our model, the applied surface wind stress is generally based on anomalies from the atmospheric model added to climatological averages. We repeated the experiment presented in *Levermann and Born* (2007) with surface wind stress prescribed to climatology in order to test the sensitivity of the SPG transition to this technique.

In addition, the sensitivity to scalar multiples of the climatological wind stress

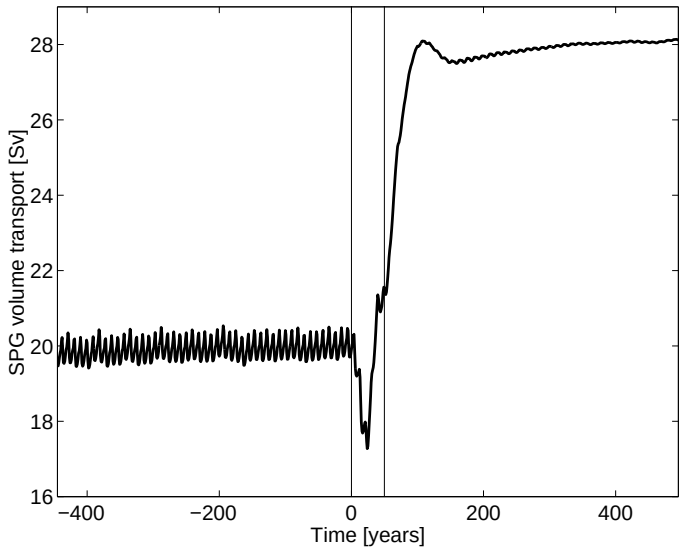

Figure S3: Temporal evolution of the SPG strength for an experiment with winds stress prescribed to present day climatology.

ranging over $\alpha \in [0.25, 2]$ has been investigated in preindustrial and Last Glacial Maximum (LGM) climate (*Montoya et al.*, 2010). The SPG strength is found to be considerably stronger in preindustrial than in LGM experiments, showing a qualitatively different sensitivity to surface wind stress. Under preindustrial boundary conditions, it decreases with increasing wind stress. Under LGM boundary conditions, it generally increases linearly with wind stress extrapolating to zero for zero wind stress. However, beyond a certain threshold for the wind stress the SPG sensitivity is reversed in the LGM and decreases with wind stress as well. This threshold is associated with the initiation of deep water formation in the Nordic Seas and the accompanying intensification of the Greenland Scotland ridge overflows.

Hence, even for changes in surface wind stress, the primary means of communicating this perturbation to the SPG is the overflow transport. This result from a fundamentally different set of experiments underlines the pivotal role of deep ocean baroclinicity for the sensitivity of the SPG and supports the findings of the present study.

3.3 Sensitivity to vertical mixing

The bistability of the SPG is robust to changes in vertical diffusivity. Global background diffusivity in our model is $\kappa = 0.2 \times 10^{-4} m^2 s^{-1}$. However, experiments with $\kappa = 0.5 \times 10^{-4} m^2 s^{-1}$ also show two stable SPG modes and with even larger contrast in strength (Fig. S4).

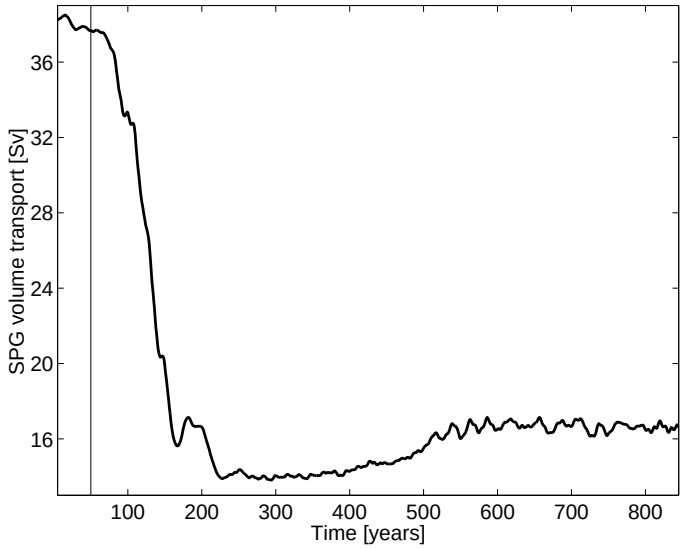

Figure S4: Temporal evolution of the SPG strength in a model version with higher vertical diffusivity. Starting from the strong circulation mode, a negative freshwater pulse of 0.1 Sv is applied over the first 50 years.

Multiple SPG equilibria are also found in a more fundamentally altered model set up. *Marzeion et al.* (2010) implemented a stratification-dependent mixing scheme and forced the model with an 1%-per-year increase scenario of atmospheric CO_2. Warming and enhanced freshwater influx reduce the surface density of the North Atlantic as the CO_2 concentration increases. This results in stronger stratification, thus weaker vertical mixing and a density increase in subsurface water masses that feed the Greenland Scotland ridge. If the sensitivity of the mixing to stratification is raised above a certain critical level, the weakening of the SPG is enhanced by the positive feedbacks described by *Levermann and Born* (2007).

3.4 Sensitivity to orbital parameters changes

The simulation of lake Agassiz drainage with preindustrial boundary conditions, i.e. with lower northern hemisphere summer insolation levels, gives a similar result (Fig. S5). This demonstrates the strength and robustness of the feedbacks involved.

However, with an even bigger change in orbital geometry one or the other circulation mode is preferred in CLIM*BER*-3α and IPSL CM4 (*Born et al.*, 2010a,b). A decrease in northern hemisphere summer insolation between 126,000 and 115,000 years before present is most pronounced in high northern latitudes. It thus favors Arctic sea ice growth causing an increase in sea ice export and a freshening south of Greenland. As a consequence, convection in the center of the SPG shuts down, density in the SPG center decreases and the gyre weakens. The analysis of the underlying dynamics confirm that the reorganization of the subpolar surface circulation is due to the same mechanism in both models indeed. However, changes in Arctic sea ice are much smaller for the simulated freshwater flood in this study and probably do not play a role for the stabilization of the circulation.

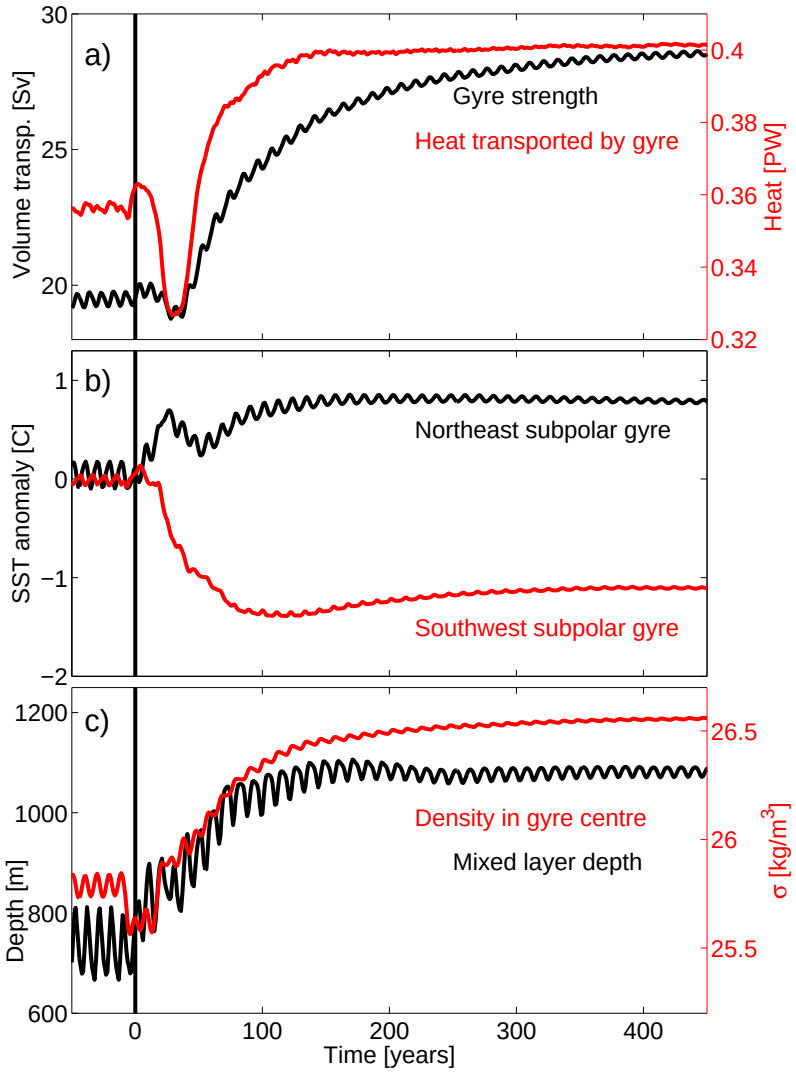

Figure S5: Simulation of the lake drainage in preindustrial climate, similar to figure 3 of the main text. The vertical line indicates the timing of the freshwater perturbation, data is filtered with a 25-year running mean. **a)** Volume and heat transport of the SPG; **b)** sea surface temperature in the north-eastern (black) and south-western (red) subpolar region; **c)** maximum winter mixed layer depth in the center of the SPG and surface density in the center of the SPG (see Fig. S7). The transition of the SPG and the underlying feedbacks are robust to a change in orbital geometry.

4 Supplemental figures and list of sediment cores

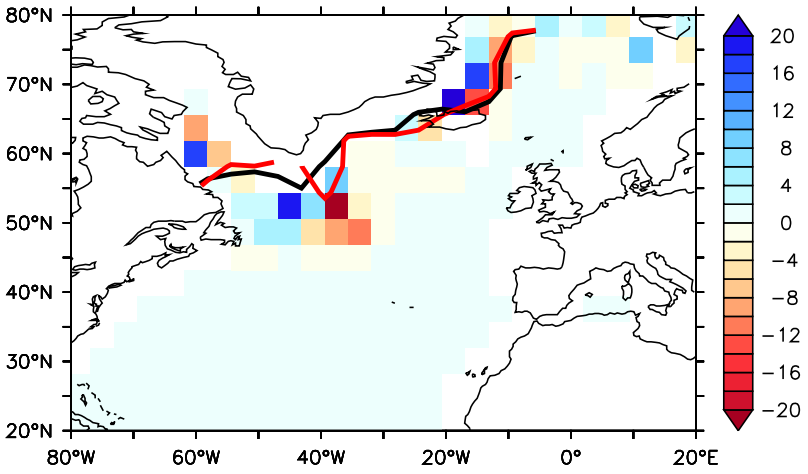

Figure S6: Colors: percental change in wind stress curl 'after' minus 'before' meltwater pulse; Contours: 15% sea ice concentration January to March average after (black) and before (red) transition. Wind stress curl changes are small, below 20% compared to the 47% strengthening of the SPG, and do not show a consistent pattern. Potential upwind changes in elevation, albedo or heat capacity due to the lake drainage are neglected in the model. Thus, the shown wind stress curl anomalies are likely due to local changes in sea ice as suggested also by the irregular pattern.

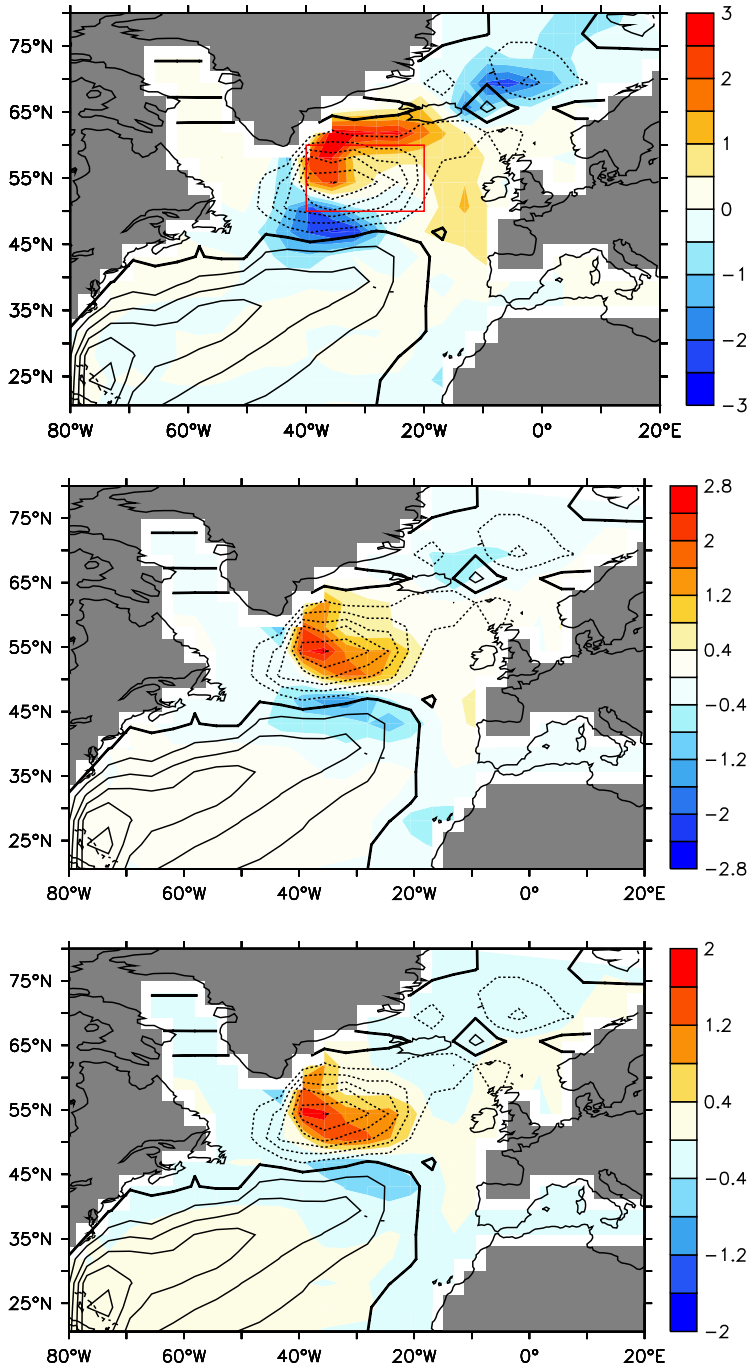

Figure S7: Difference 'after' minus 'before' meltwater pulse, averaged annually and over the upper 75m: temperature (in °C, upper), salinity (in psu, middle), and density (in kg m^{-3}, lower). Steamlines indicate the location of the subpolar gyre after the transition. The region used for averages in figures 3 of the main text and S8 is shown in red.

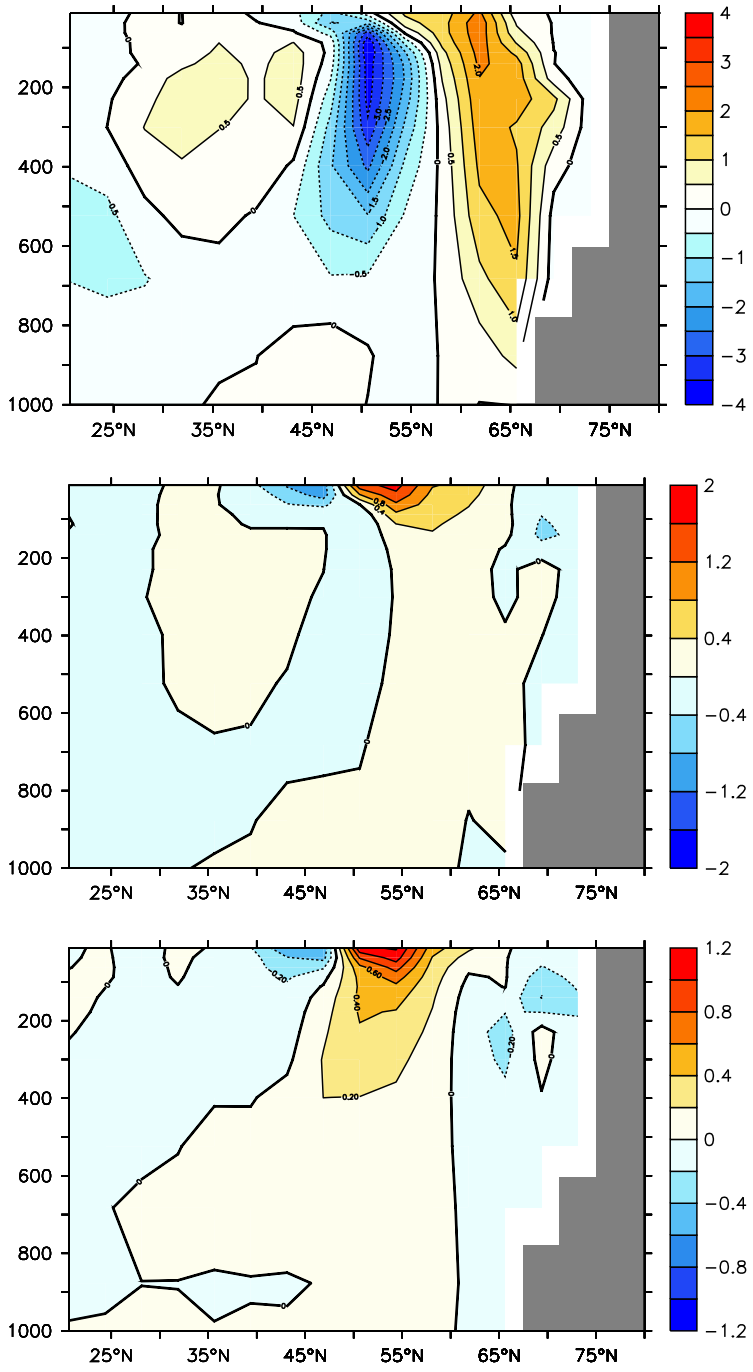

Figure S8: Difference 'after' minus 'before' meltwater pulse, averaged annually and between 40°W and 20°W: temperature (in °C, upper), salinity (in psu, middle), and density (in kg m^{-3}, lower). The largest difference in salinity is seen on the surface due to changes in the advection. In contrast, temperature changes change primarily in subsurface waters because of stronger isopycnal mixing and convection.

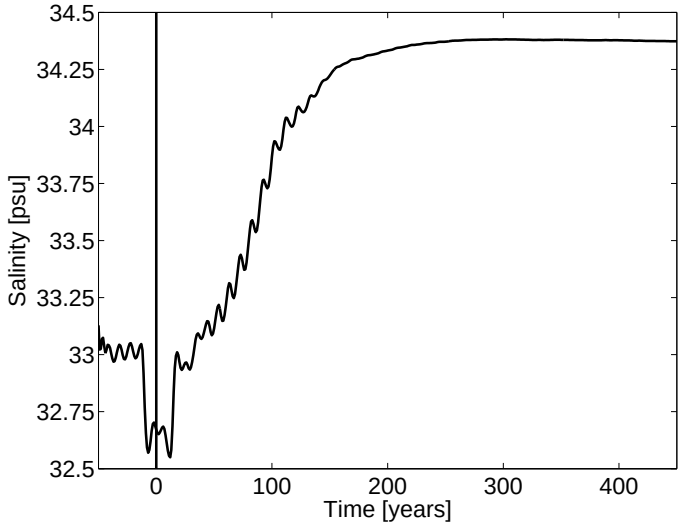

Figure S9: Temporal evolution of annual average sea surface salinity in the center of the subpolar gyre, averaged between 50°N and 60°N and 40°W and 20°W (red rectangle in fig. S7) and filtered with a 25-year running mean. The vertical line indicates the simulated lake Agassiz drainage.

Table S1: List of marine sediment cores used in this study. Magnitude (ΔSST), start of the SPG transition and proxy method are shown where applicable.

Abbreviation in Fig. 1	Full name	ΔSST (°C)	Start (yr BP)	Method	References
HU13	HU90–013–013P	-3	8,200	dinocyst assemblages	*Hillaire-Marcel et al.* (2001) *Solignac et al.* (2004) *de Vernal and Hillaire-Marcel* (2006)
HU21	HU84–030–021TWC&P	-5	8,500	dinocyst assemblages	*de Vernal and Hillaire-Marcel* (2006)
HU94	HU91–045–094P	-5	7,800	dinocyst assemblages	*Hillaire-Marcel et al.* (2001) *Solignac et al.* (2004) *de Vernal and Hillaire-Marcel* (2006)
OCE326 –GGC26	OCE326–GGC26	-3	8,000	alkenones	*Keigwin et al.* (2005) *Sachs* (2007)
LO09-14	LO09-14 LBC/GGC/GC	+2.5	8,000	diatoms	*Andersen et al.* (2004)
ODP984	ODP Site 984	+1.5	8,000	Mg/Ca	*Came et al.* (2007)
MD2251	MD99–2251			sortable silt	*Ellison et al.* (2006)
MD2665	MD03–2665			δ^{13}C & grain size	*Kleiven et al.* (2008)
NEAP4k	NEAP4k			sortable silt	*Hall et al.* (2004)

References

Andersen, C., N. Koc, and M. Moros (2004), A highly unstable Holocene climate in the subpolar North Atlantic: evidence from diatoms, *Quaternary Science Reviews*, *23*, 2155–2166.

Bauer, E., A. Ganopolski, and M. Montoya (2004), Simulation of the cold climate event 8200 years ago by meltwater outburst from Lake Agassiz, *Paleoceanography*, *19*, PA3014.

Born, A., A. Levermann, and J. Mignot (2009), Sensitivity of the Atlantic ocean circulation to a hydraulic overflow parameterisation in a coarse resolution model: Response of the subpolar gyre, *Ocean Modelling*, *27 (3-4)*, 130–142.

Born, A., K. H. Nisancioglu, and P. Braconnot (2010a), Sea ice induced changes in ocean circulation during the Eemian, *Climate Dynamics*, *online*, doi: 10.1007/s00382-009-0709-2.

Born, A., K. H. Nisancioglu, B. Risebrobakken, and A. Levermann (2010b), Late Eemian warming in the Nordic Seas as seen in proxy data and climate models, *Paleoceanography*, *in revision*.

Came, R. E., D. W. Oppo, and J. F. McManus (2007), Amplitude and timing of temperature and salinity variability in the subpolar North Atlantic over the past 10 k.y., *Geology*, *35*, 315–318.

de Vernal, A., and C. Hillaire-Marcel (2006), Provincialism in trends and high frequency changes in the northwest North Atlantic during the Holocene, *Global and Planetary Change*, *54*, 263–290.

Eden, C., and J. Willebrand (2001), Mechanism of Interannual to Decadal Variability of the North Atlantic Circulation, *Journal of Climate*, *14*, 2266–2280.

Ellison, C. R. W., M. R. Chapman, and I. R. Hall (2006), Surface and Deep Ocean Interactions During the Cold Climate Event 8200 Years Ago, *Science*, *312*, 1929–1932.

Fichefet, T., and M. A. M. Maqueda (1997), Sensitivity of a global sea ice model to the treatment of ice thermodynamics and dynamics, *Journal of Geophysical Research*, *102*, 12,609.

Häkkinen, S., and P. B. Rhines (2004), Decline of subpolar North Atlantic circulation during the 1990s, *Science*, *304*, 555–559.

Hall, I. R., G. Bianchi, and J. R. Evans (2004), Centennial to millenial scale Holocene climate-deep water linkage in the North Atlantic, *Quaternary Science Reviews*, *23*, 1529–1536.

Hasumi, H., and N. Suginohara (1999), Effects of locally enhanced vertical diffusivity over rough bathymetry on the world ocean circulation, *Journal of Geophysical Research*, *104*, 23,364–23,374.

Hillaire-Marcel, C., A. de Vernal, A. Bilodeau, and A. J. Weaver (2001), Absence of deep-water formation in the Labrador Sea during the last interglacial period, *Nature*, *410*, 1073–1077.

Hillaire-Marcel, C., A. de Vernal, and D. J. W. Piper (2007), Lake Agassiz Final drainage event in the northwest North Atlantic, *Geophysical Research Letters*, *34*, L15,601.

Hofmann, M., and M. A. M. Maqueda (2006), Performance of a second-order moments advection scheme in an Ocean General Circulation Model, *Journal of Geophysical Research*, *111*, C05,006.

Jongma, J., M. Prange, H. Renssen, and M. Schulz (2007), Amplification of Holocene multicentennial climate forcing by mode transitions in North Atlantic overturning circulation, *Geophysical Research Letters*, *34*, L15,706.

Kalnay, E., and coauthors (1996), The NCEP/NCAR 40-year reanalysis project, *Bull. Amer. Meteor. Soc.*, *77*, 437–471.

Keigwin, L. D., J. P. Sachs, Y. Rosenthal, and E. A. Boyle (2005), The 8200 year B.P. event in the slope water system, western subpolar North Atlantic, *Paleoceanography*, *20*, PA2003.

Kleinen, T., T. J. Osborn, and K. R. Briffa (2009), Sensitivity of climate response to variations in freshwater hosing location, *Ocean Dynamics*, *59(3)*, 509–521, doi: 10.1007/s10236-009-0189-2.

Kleiven, H. F., C. Kissel, C. Laj, U. S. Ninnemann, T. O. Richter, and E. Cortijo (2008), Reduced North Atlantic Deep Water Coeval with the Glacial Lake Agassiz Fresh Water Outburst., *Science*, *319*, 60–64.

Ledwell, J. R., E. T. Montgomery, K. L. Polzin, L. C. S. Laurent, R. W. Schmitt, and J. M. Toole (2000), Evidence for enhanced mixing over rough topography in the abyssal ocean, *Nature*, *403*, 179–182.

LeGrande, A. N., and G. A. Schmidt (2008), Ensemble, water isotope-enabled, coupled general circulation modeling insights into the 8.2 ka event, *Paleoceanography*, *23*, PA3207.

LeGrande, A. N., G. A. Schmidt, D. T. Shindell, C. V. Field, R. L. Miller, D. M. Koch, G. Faluvegi, and G. Hoffmann (2006), Consistent simulations of multiple proxy responses to an abrupt climate change event, *Proceedings of the National Academy of Sciences (US)*, *103*, 837–842.

Levermann, A., and A. Born (2007), Bistability of the Atlantic subpolar gyre in a coarse-resolution model, *Geophysical Research Letters*, *34*, L24,605.

Marzeion, B., A. Levermann, and J. Mignot (2010), Sensitivity of North Atlantic subpolar gyre and overturning to stratification-dependent mixing: response to global warming, *Climate Dynamics*, *online*, doi:10.1007/s00382-008-0521-4.

Mignot, J., A. Levermann, and A. Griesel (2006), A decomposition of the Atlantic meridional overturning circulation into physical components using its sensitivity to vertical diffusivity., *Journal of Physical Oceanography*, *36*, 636–650.

Montoya, M., and A. Levermann (2008), Surface wind stress threshold for glacial Atlantic overturning, *Geophysical Research Letters*, *35*, L03,608.

Montoya, M., A. Griesel, A. Levermann, J. Mignot, M. Hofmann, A. Ganopolski, and S. Rahmstorf (2005), The Earth System Model of Intermediate Complexity

CLIM*BER*-3α. Part I: description and performance for present-day conditions, *Climate Dynamics*, *25*, 237–263.

Montoya, M., A. Born, and A. Levermann (2010), Reversed North Atlantic gyre dynamics in glacial climate, *Climate Dynamics*, *online*, doi:10.1007/s00382-009-0729-y.

Petoukhov, V., A. Ganopolski, V. Brovkin, M. Claussen, A. Eliseev, C. Kubatzki, and S. Rahmstorf (2000), CLIM*BER*-2: a climate system model of intermediate complexity. Part I: model description and performance for present climate, *Climate Dynamics*, *16*, 1.

Prather, M. J. (1986), Numerical advection by conservation of second-order moments, *Journal of Geophysical Research*, *91*, 6671–6681.

Renssen, H., H. Goosse, and T. Fichefet (2005), Contrasting trends in North Atlantic deep-water formation in the Labrador Sea and Nordic Seas during the Holocene, *Geophysical Research Letters*, *32*, L08,711.

Sachs, J. P. (2007), Cooling of Northwest Atlantic slope waters during the Holocene, *Geophysical Research Letters*, *34*, L03,609.

Solignac, S., A. de Vernal, and C. Hillaire-Marcel (2004), Holocene sea-surface conditions in the North Atlantic–contrasted trends and regimes in the western and eastern sectors (Labrador Sea vs. Iceland Basin), *Quaternary Science Reviews*, *23*, 319–334.

Treguier, A. M., S. Theetten, E. P. Chassignet, T. Penduff, R. Smith, L. Talley, J. O. Beismann, and C. Böning (2005), The North Atlantic Subpolar Gyre in Four High-Resolution Models, *Journal of Physical Oceanography*, *35*, 757–774.

Wiersma, A. P., H. Renssen, H. Goosse, and T. Fichefet (2006), Evaluation of different freshwater forcing scenarios for the 8.2 ka BP event in a coupled climate model, *Climate Dynamics*, *27*, 831–849.

Winsor, P., L. Keigwin, S. J. Lentz, and D. C. Chapman (2006), The pathways and impact of fresh water discharge through Hudson Strait 8200 years ago, *Geophysical Research Abstracts*, *8*, 11,007.

Wu, P., and R. A. Wood (2008), Convection induced long term freshening of the subpolar North Atlantic Ocean, *Climate Dynamics*, *31*, 941–956.

Paper V

Reversed North Atlantic gyre dynamics in present and glacial climate[1]

Montoya, M., A. Born and A. Levermann (2010)

Climate Dynamics, doi:10.1007/s00382-009-0729-y

[1]Reproduced with permission of the publisher

Clim Dyn
DOI 10.1007/s00382-009-0729-y

Reversed North Atlantic gyre dynamics in present and glacial climates

Marisa Montoya · Andreas Born · Anders Levermann

Received: 29 July 2009 / Accepted: 19 December 2009

Abstract The dynamics of the North Atlantic subpolar gyre (SPG) are assessed under present and glacial boundary conditions by investigating the SPG sensitivity to surface wind-stress changes in a coupled climate model. To this end, the gyre transport is decomposed in Ekman, thermohaline, and bottom transports. Surface wind-stress variations are found to play an important indirect role in SPG dynamics through their effect on water-mass densities. Our results suggest the existence of two dynamically distinct regimes of the SPG, depending on the absence or presence of deep water formation (DWF) in the Nordic Seas and a vigorous Greenland–Scotland ridge (GSR) overflow. In the first regime, the GSR overflow is weak and the SPG strength increases with wind-stress as a result of enhanced outcropping of isopycnals in the centre of the SPG. As soon as a vigorous GSR overflow is established, its associated positive density anomalies on the southern GSR slope reduce the SPG strength. This has implications for past glacial abrupt climate changes, insofar as these can be explained through latitudinal shifts in North Atlantic DWF sites and strengthening of the North Atlantic current. Regardless of the ultimate trigger, an abrupt shift of DWF into the Nordic Seas could result both in a drastic reduction of the SPG strength and a sudden reversal in its sensitivity to wind-stress variations. Our results could provide insight into changes in the horizontal ocean circulation during abrupt glacial climate changes, which have been largely neglected up to now in model studies.

The authors are grateful to Didier Roche and two anonymous reviewers for helpful comments on the manuscript. M. M. was funded by MCINN projects CGL2008-06558-C02-C01/CLI and HA2007-0056, and MARM project 200800050084028. A.B. was funded by the Marie Curie Actions project NICE (MRTN-CT-2006-036127).

M. Montoya (✉)
Dpto. Astrofísica y Ciencias de la Atmósfera,
Facultad de Ciencias Físicas, Universidad Complutense de Madrid, Ciudad Universitaria, Madrid, Spain
e-mail: mmontoya@fis.ucm.es

A. Born
Bjerknes Centre for Climate Research, Bergen, Norway

A. Born
Geophysical Institute, University of Bergen, Bergen, Norway

A. Levermann
Earth System Analysis, Potsdam Institute for Climate Impact Research, Potsdam, Germany

A. Levermann
Institute of Physics, Potsdam University, Potsdam, Germany

1 Introduction

The North Atlantic subpolar gyre (SPG) is an important component of the global ocean circulation and plays a crucial role in climate variability (Treguier et al. 2005). Its dynamics have received renewed attention in the last years, since a decline in its strength in the nineties as observed from satellite altimeter data was associated with a reduction in the Atlantic meridional overturning circulation (AMOC) (Häkkinen and Rhines 2004). Through its modulation of the North Atlantic Current, the SPG has been found to exert a strong control on the surface salinity of the northeastern North Atlantic on interannual to interdecadal timescales, suggesting that the recent high salinities recorded in this region have been a consequence of the former SPG strength decline (Hátún et al. 2005). This decline has subsequently been found to reflect decadal variability, rather than a long term trend (Böning et al. 2006). The former mechanism has recently been found to

Published online: 12 January 2010

operate also at millennial timescales throughout the Holocene (Thornalley et al. 2009). Although far from being well understood, the relationship between the SPG and the AMOC suggests the potential of SPG changes to monitor AMOC changes (Böning et al. 2006; Häkkinen and Rhines 2004; Zhang 2008).

While surface wind-stress has large influence on its strength and variability (Böning et al. 2006; Curry et al. 1998), the SPG circulation is also partly controlled by baroclinic adjustments and therefore by the density structure in the subpolar North Atlantic (Eden and Willebrand 2001; Greatbatch et al. 1991; Mellor et al. 1982; Myers et al. 1996; Penduff et al. 2000). This has shown to have two important consequences for its dynamics. Firstly, model results have recently suggested the existence of at least two stable SPG states as a consequence of positive feedbacks involving the transport of temperature and salinity toward the centre of the gyre and the interaction with the Greenland-Scotland ridge (GSR) overflow (Levermann and Born 2007). In addition, the SPG strength has proved to be strongly sensitive to deep convection (Born et al. 2009b; Treguier et al. 2005). Recently, improving the representation of water masses in the Nordic Seas and the subpolar North Atlantic has shown to result in a substantial strengthening of the SPG in climate simulations (Born et al. 2009a).

Despite these recent efforts, a complete understanding of the SPG dynamics remains elusive. Here we address this issue by analysing quantitatively the sensitivity of the SPG to the surface wind-stress in idealised climate simulations both under present and glacial boundary conditions. Surface wind-stress variations are found to play an indirect role in the SPG dynamics through their effect on water-mass densities, while the existence of a GSR overflow appears to have a dramatic impact on the SPG strength as well as on its dynamics.

The paper is organised as follows: in Sect. 2 the model and experimental setup are described. In Sect. 3 the SPG strength response to wind-stress changes is investigated by analysing the components of the vertically integrated momentum equations (Ekman, thermohaline, and bottom transports), and the impact of surface wind-stress changes on the SPG strength through changes in the water-mass densities is described. Finally, in Sect. 4 the main conclusions are summarised.

2 Model and experimental setup

The model used in this study is the CLIMBER-3α coupled climate model (Montoya et al. 2005). Its atmospheric component is a statistical-dynamical model (Petoukhov et al. 2000). The oceanic component contains the GFDL MOM-3 ocean general circulation model, with a horizontal resolution of 3.75° and 24 vertical levels, and the ISIS thermodynamic-dynamic snow and sea-ice model (Fichefet and Maqueda 1997). The version used herein includes a few modifications with respect to the standard configuration described by Montoya et al. (2005) in order to improve the model's performance for preindustrial climate: isopycnal diffusivity was doubled to $\kappa_h = 2{,}000\ \mathrm{m^2\ s^{-1}}$ and bathymetry amids the Indonesian islands was slightly deepened. As a consequence, the Indonesian throughflow increased from about 7 Sv ($1\ \mathrm{Sv} = 10^6\ \mathrm{m^3\ s^{-1}}$) in the previous version to 10 Sv, which is in the range of observations for present-day climate (Wijffels et al. 2008), the surface salinity distribution and the stratification in the deep ocean improved (not shown), and the strength of the AMOC increased from about 12 to 17 Sv, comparable to current estimates (Ganachaud and Wunsch 2000; Talley et al. 2003).

Climate simulations were performed both for present (preindustrial) and glacial boundary conditions (Montoya and Levermann 2008). Preindustrial boundary conditions consist of the present-day Earth geography and ice-sheet distribution, vegetation (disregarding land-use changes due to human activities), insolation, and atmospheric CO_2 concentration (280 ppmv), as described by Montoya et al. (2005). For glacial boundary conditions, the PMIP2 specifications (http://pmip2.lsce.ipsl.fr) for the Last Glacial Maximum (LGM, ca. 21,000 years before present) were imposed, namely: changes in insolation, a reduced equivalent atmospheric CO_2 concentration of 167 ppmv to account for the lowered CH_4, N_2O, and CO_2 concentrations, the ICE-5G ice-sheet reconstruction (Peltier 2004), and land-sea mask changes plus a global increase of salinity by 1 psu to account for the $\sim$120 m sea-level lowering. Oceanic bathymetry, vegetation, and river-runoff routing were unchanged with respect to the Holocene simulation.

An important issue when assessing the glacial ocean circulation is the fact that glacial winds are poorly constrained at present. This issue is critical, since surface winds force the ocean circulation both directly and indirectly, by enhancing vertical mixing and altering the density structure (Kuhlbrodt et al. 2007; Toggweiler and Samuels 1998; Wunsch 1998; Wunsch and Ferrari 2004). Stronger glacial meridional surface temperature gradients and evidence mainly from ice-core data for greatly increased dust and sea-salt concentrations have led to the general assumption of considerably stronger than present surface winds, possibly by more than 50% (Crowley and North 1991 and references therein). However, enhanced aerosol concentrations also reflect changes in the sources such as enhanced aridity. Models furthermore show enhanced westerlies but not uniformly enhanced surface

winds (e.g. Hewitt et al. 2003; Otto-Bliesner et al. 2006). Recently, it has been claimed that, because westerly winds respond mainly to changes in the thermal contrast in the mid-atmosphere rather than to changes at the surface, and because the mid-atmosphere thermal contrast increases with the atmospheric CO_2 concentration, lower than present glacial CO_2 atmospheric levels should have led to weaker than present glacial westerly winds (Toggweiler and Russell 2008).

In order to take this uncertainty into account, Montoya and Levermann (2008) integrated the model to equilibrium with the Trenberth et al. (1989) surface wind-stress climatology multiplied globally by varying factors $\alpha \in [0.5, 2]$ (hereafter, LGMα). To assess the potential of multiple stable states, two different initial conditions were used: equilibrium simulations with either $\alpha = 1$ (LGM1.0) or $\alpha = 2$ (LGM2.0). The resulting LGM equilibrium simulations for a given α value are denoted LGMα-weak and LGMα-strong. The simulated glacial AMOC strength was found to increase continuously with surface wind-stress up to $\alpha_c \equiv 1.7$ (Fig. 1a, see also Montoya and Levermann (2008)). For $\alpha \lesssim \alpha_c \equiv 1.7$, deep water formation (DWF) takes place south of the GSR. At $\alpha = \alpha_c \equiv 1.7$ a threshold is found, associated with a drastic AMOC increase of more than 10 Sv, a northward shift of DWF north of the GSR, and a strengthening of the GSR overflow (Fig. 1b). In the vicinity of this threshold ($\alpha \simeq 1.7 - 1.75$) the AMOC exhibits two stable states, with weak and strong circulation, respectively.

To assess whether this behaviour is unique to the LGM, similar simulations with varying surface wind-stress were carried out for the Holocene (hereafter, HOLOα). Note since in these DWF in the Nordic Seas already takes place for $\alpha = 1$ (Fig. 1b), only reduced wind-stress with $\alpha \in [0.25, 1]$ was considered. In this case, contrarily to the LGM, the overflow increases continuously with wind-stress (Fig. 1b) and the AMOC strength increase with wind-stress is roughly linear (Fig. 1a).

The dynamical mechanism behind the non-linear behaviour found in the LGM runs is based on an altered salinity distribution in the North Atlantic. Enhanced surface wind-stress increases the horizontal gyre circulation both in the subtropics and the subpolar region. As a consequence, more salt is transported from the tropics to the North Atlantic in the upper ocean layers. Higher subtropical sea surface temperatures (SSTs) also result in enhanced evaporation and thereby higher subtropical surface salinities, but the relevant mechanism at high northern latitudes is the increased salt transport (Montoya and Levermann 2008). For $\alpha \leq \alpha_c$ the AMOC increase is thus gradual in response to a gradual increase in gyre salinity transport. In this regime, deep convection and DWF are confined to the region south of the Greenland–Scotland ridge. For $\alpha > \alpha_c$ the gyre salinity transport to the Nordic Seas is sufficient to induce DWF there and strengthen the AMOC. The enhanced overturning triggers a positive salt-advection feedback (Rahmstorf 1996). More salt is transported from the south toward high northern latitudes by the AMOC and, consequently, salinity increases in the Nordic Seas and the overturning further strengthens.

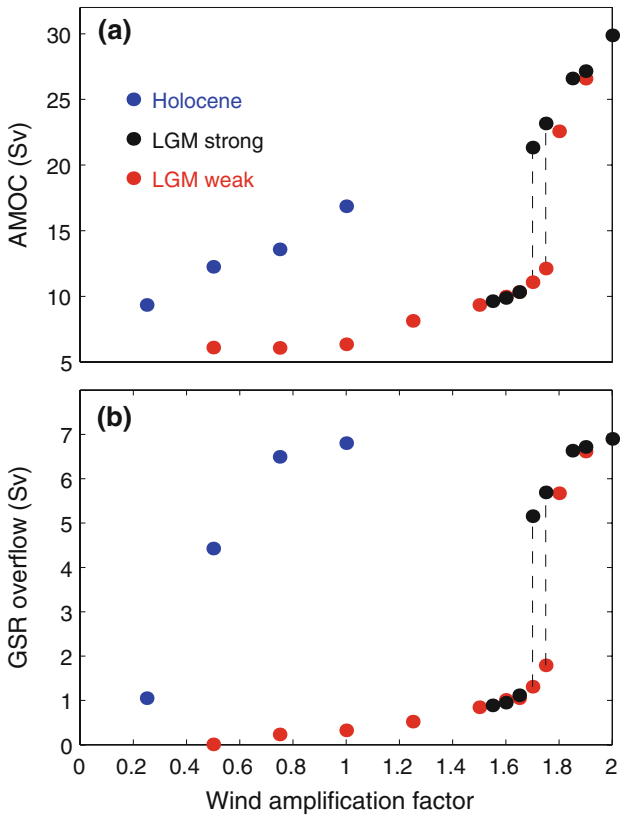

Fig. 1 **a** AMOC strength (see also Montoya and Levermann 2008) and **b** GSR overflow as a function of wind-stress enhancement factor α for the LGM (*black*, *red*) and Holocene (*blue*), in Sv. *Black* and *red dots* indicate LGM equilibrium simulations starting from LGM2.0 (LGMα-strong) and LGM1.0 (LGMα-weak), respectively. The glacial AMOC strength increases continuously with surface wind-stress up to $\alpha_c \equiv 1.7$. For $\alpha \leq \alpha_c$, DWF takes place south of the GSR. At $\alpha = \alpha_c$ a threshold is found associated with a drastic AMOC increase of more than 10 Sv, a northward shift of DWF north of the GSR, and a strengthening of the GSR overflow. In the vicinity of this threshold ($\alpha \simeq 1.7$) the AMOC exhibits two stable states, with weak and strong circulation, respectively. The Holocene, in contrast, shows a roughly linear increase of the AMOC strength with wind-stress in response to the more gradual GSR overflow increase

These results show the GSR overflow and AMOC exhibit very different sensitivities to surface wind-stress changes in the LGM and HOLO runs. As mentioned previously (Sect. 1), baroclinic adjustments following changes in the GSR overflow have been shown to play a very important role in SPG dynamics (Born et al. 2009a; Levermann and Born 2007). Herein, the sensitivity of the

SPG strength to surface wind-stress is investigated in the aforementioned runs.

3 Results

3.1 SPG strength variation with surface wind-stress

Due to its explicit free surface the ocean model used herein does not have a well defined vertically integrated (barotropic) streamfunction. Born et al (2009a) thus calculated the SPG strength by integrating the vertically integrated zonal transport M_x meridionally between the southern Greenland coast and the SPG centre (hereafter $\overline{M}_x$), which in turn is defined so that the former integral is maximum.

Using the same procedure, $\overline{M}_x$ is found to increase monotonically with increasing surface wind-stress in the LGM runs, while it does not show a clear behaviour in the HOLO runs (Fig. 2). Nevertheless, changes in AMOC strength and GSR overflow in response to wind-stress variations impact strongly on the flow path in the subpolar North Atlantic, most notably in the LGM runs. This is illustrated by analysing the water-mass flow in the subpolar North Atlantic without and with a strong GSR overflow (Fig. 3). Without a strong GSR overflow most of the sinking takes place at the southern rim of the SPG, south of 40°N, and the upper ocean provides the bulk of the SPG

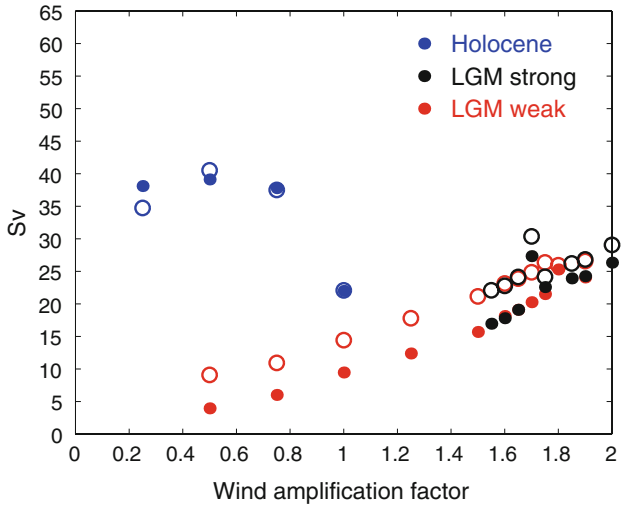

Fig. 2 Magnitude of the zonal transport $\overline{M}_x$ between the southern Greenland coast and the centre of the SPG, integrated vertically within the whole water column, as a function of wind-stress enhancement factor α for the LGM (*black*, *red*) and Holocene (*blue*), in Sv (*closed circles*). *Black* and *red dots* indicate LGM equilibrium simulations starting from LGM2.0 (LGMα-strong) and LGM1.0 (LGMα-weak), respectively. Also shown is the sum of the three terms in the r.h.s. of Eqs. 1 and 4–6 for M_x shown in Fig. 4b–d (*open circles*)

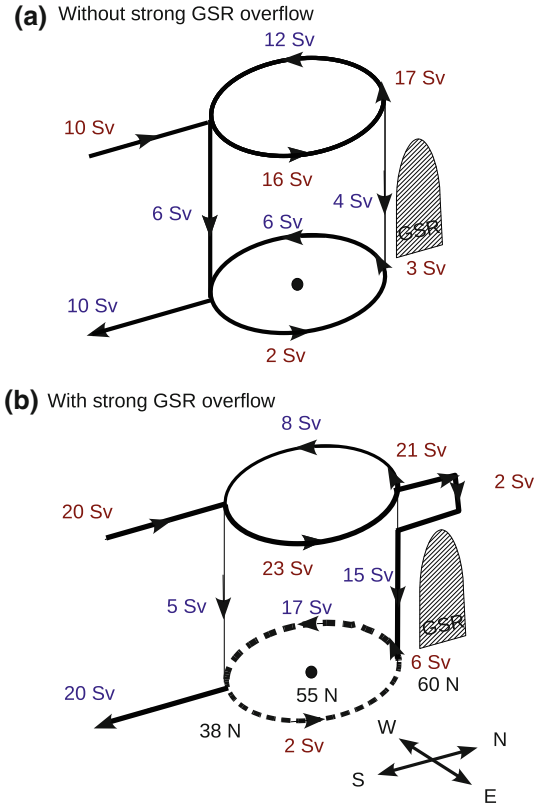

Fig. 3 Schematic figure indicating the flow of water masses in the subpolar North Atlantic **a** in LGM1.7-weak, without a strong GSR overflow, and **b** in LGM1.7-strong, with a strong GSR overflow. The main flow paths are represented by *thick lines* with *arrows*. The *upper* and *lower branches* represent the flows integrated vertically in the upper 1,000 m and in the deep ocean as well as zonally, east and west of the SPG centre (located at ca. 34°W and 55°N), at different latitudes: 38°N, the SPG centre (ca. 55°N), and 60°N. Eastward and northward flows are represented in *red*, while westward and southward flows are in *blue* (see text for a more detailed explanation)

flow. As an example, in LGM1.7-weak $\overline{M}_x$ is ca. 20 Sv. Of these, about 17 and 3 Sv flow westward within and below the upper 1,000 m, respectively (Fig. 3a). A similar amount (18 Sv) is obtained when integrating the meridional, vertically integrated transport M_y zonally between the coast of North America and the SPG centre (hereafter $\overline{M}_y$). Of these, about 12 and 6 Sv flow southward in the upper 1,000 m and in the deep ocean, respectively. In LGM1.7-strong, which shows a vigorous GSR overflow (Fig. 3b), the upper AMOC inflow is strongly intensified. Most of this water circulates in the eastern section of the North Atlantic (northward branch of SPG), sinks in the Nordic Seas and flows south in the western branch of the SPG. The total southward transport increases up to ca. 25 Sv, but only 8 Sv take place in the upper 1,000 m while about 17 Sv flow south in the deep ocean. Thus, the upper southward and deep northward flows are strongly diminished.

As the GSR overflow and the AMOC strengthen with wind-stress, the upper northward flow is intensified mainly in the northeastern North Atlantic, reflecting a strengthening of the North Atlantic Current. North Atlantic Deep Water (NADW) formation increases, and its southward flow is enhanced mainly along the deep western boundary, while the recirculation toward the basin interior is strongly diminished (Fig. 3b). Accordingly, variations in the total horizontal transport around the SPG centre reflect to a large extent AMOC changes. To isolate exclusively the flow which recirculates within the subpolar North Atlantic in the whole water column, AMOC variations must be subtracted. Thus, the SPG strength is estimated as the difference between $\overline{M}_x$ and the maximum AMOC strength at the latitude of the SPG centre. The idea behind this is that in the extreme case in which the upper flow is northward at all longitudes and returns southward along the western boundary current we cannot truly speak of a gyre. Instead the circulation is fully represented by the AMOC. Note as long as changes in the AMOC strength are not very large the usual definition of the SPG strength is fully appropriate, and the SPG strength variations are consistent with those used herein (e.g. Born et al. 2009a; Levermann and Born 2007).

For any given value of the wind-stress, the SPG is found to be considerably stronger in the Holocene than in the LGM (Fig. 4a). In addition, it shows a qualitatively different sensitivity to surface wind-stress under each of these climatic conditions. In the Holocene it generally decreases with increasing wind-stress. In the LGM, for $\alpha < 1.7$, it increases roughly linearly with wind-stress extrapolating to zero for $\alpha = 0$, only decreasing abruptly once the GSR overflow is initiated for $\alpha > 1.7$. Thus, a threshold is found in the SPG strength at the same value as in the AMOC and the GSR overflow (see Fig. 1 and Montoya and Levermann 2008). Note that the SPG strength in the LGM runs vanishes for high α values, reflecting the fact that, as mentioned above, the upper and deep circulation are northward and southward, respectively, practically everywhere and thus the circulation is well represented by the AMOC.

3.2 Flow decomposition

In order to gain further insight into the former behaviour, the contributions to the SPG strength are analysed (see e.g. Born et al. 2009a; Mellor et al. 1982). Ignoring frictional terms, the vertically integrated zonal and meridional time-independent transports are given by (see Appendix):

$$fM_x = -Hg\partial_y\eta + H\int_{-H}^{0}\partial_y b dz + \int_{-H}^{0} z\partial_y b dz + \rho_0^{-1}\tau_{0y} \quad (1)$$

$$fM_y = Hg\partial_x\eta - H\int_{-H}^{0}\partial_x b dz - \int_{-H}^{0} z\partial_x b dz - \rho_0^{-1}\tau_{0x}, \quad (2)$$

where M_x and M_y are the zonal and meridional vertically integrated transports, respectively, f is the Coriolis parameter, H the ocean depth, g local gravity, η the sea-

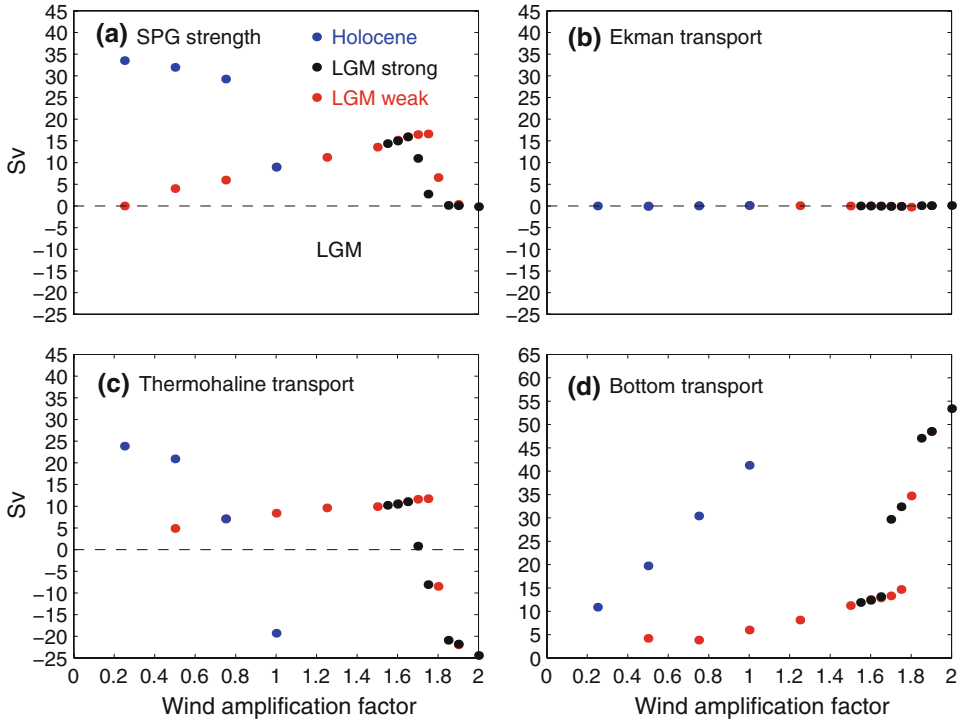

Fig. 4 Relevant components of North Atlantic volume transport as a function of wind-stress enhancement factor α for the LGM (*black*, *red*) and Holocene (*blue*): **a** SPG strength, **b** Ekman transport, **c** thermohaline transport, and **d** bottom transport contributions to the SPG strength as in Eqs. 1 and 4–6 for M_x. Note here the magnitudes of the former terms are represented. *Black* and *red dots* indicate LGM equilibrium simulations starting from LGM2.0 (LGMα-strong) and LGM1.0 (LGMα-weak), respectively (in Sv)

surface elevation, ρ_0 the average density, τ_{0x} and τ_{0y} the surface wind stresses, and

$$b = g\frac{\rho_0 - \rho}{\rho_0} \tag{3}$$

the buoyancy. Identification of the Ekman, thermohaline, and bottom velocities as defined by Fofonoff (1962) (see also Mellor et al. 1982) allows decomposing Eqs. 1 and 2 into their respective vertically integrated Ekman, thermohaline and bottom transports:

$$f[M_{xe}, M_{ye}] = \left[\rho_0^{-1}\tau_{0y}, -\rho_0^{-1}\tau_{0x}\right] \tag{4}$$

$$f[M_{xt}, M_{yt}] = \left[\int_{-H}^{0} z\partial_y b dz, -\int_{-H}^{0} z\partial_x b dz\right] \tag{5}$$

$$f[M_{xb}, M_{yb}] = \left[-Hg\partial_y\eta + H\int_{-H}^{0}\partial_y b dz, Hg\partial_x\eta - H\int_{-H}^{0}\partial_x b dz\right]. \tag{6}$$

As explained in Sect. 3.1, the SPG strength (Fig. 4a) is calculated by subtracting the AMOC strength from the integral of M_x from the coast of Greenland to the SPG centre ($\overline{M}_x$). The corresponding integrals of the r.h.s. terms in Eq. 1 are shown in Fig. 4b–d. The direct contribution of the wind-stress through the Ekman transport is found to be negligible (Fig. 4b), in agreement with Mellor et al. (1982). This result might seem trivial given that, according to Sverdrup balance, the curl of the surface wind-stress rather than its local value drives the overall gyre transport. However, high-resolution models indicate that the SPG does not obey simple Sverdrup dynamics (Bryan et al. 1995; Treguier et al. 2005). The SPG strength (Fig. 4a) instead closely follows the variation of the thermohaline transport (Fig. 4c). Without overflow (LGM runs for $\alpha < \alpha_c \equiv 1.7$) the thermohaline transport and the SPG strength slowly increase with increasing α. Once a relatively strong overflow sets in (HOLO runs and LGM runs for $\alpha > \alpha_c \equiv 1.7$), both decrease abruptly with increasing α. The bottom transport (Fig. 4d) instead follows the variations in the AMOC and GSR overflow (Fig. 1), increasing monotonically with α both under present and glacial boundary conditions, and showing a threshold at $\alpha = \alpha_c \equiv 1.7$ above which their sensitivity to wind-stress variations increases considerably. The dynamics underlying the SPG and the AMOC are thus very different, supporting their conceptual distinction. Finally, note the sum of the (meridionally integrated) Ekman, thermohaline and bottom transports on the r.h.s. of Eq. 1 gives roughly the same result as the vertically integrated zonal transport $\overline{M}_x$ on the l.h.s. (Fig. 2, open and closed circles, respectively).

The existence of a GSR overflow thus clearly determines the effect of wind-stress changes on the SPG strength and AMOC through its effect on the thermohaline and bottom transport. We can distinguish two regimes, one with suppressed GSR overflow, corresponding to the LGM runs for $\alpha < \alpha_c \equiv 1.7$, and one with active GSR overflow, corresponding to the Holocene runs and the LGM runs for $\alpha > \alpha_c \equiv 1.7$. Without overflow the thermohaline transport slowly increases with α, leading to an increase in SPG strength. The same applies to the bottom transport. Once a relatively strong overflow sets in, the thermohaline transport, and thus the SPG strength, decreases abruptly with increasing α, while the bottom transport increase with α proceeds faster.

3.3 Wind-induced density changes

In order to assess how wind-stress changes affect the thermohaline transport and thus the SPG strength within each regime, that is, with and without a strong overflow, the meridional density gradient weighted by depth ($z \cdot \partial_y\rho$), which constitutes the core of the thermohaline transport (Eq. 1), is considered in the subpolar North Atlantic. Figure 5 shows its zonal average over the SPG centre (40°W–20°W) for several of the former experiments. Superimposed are the contours of the isopycnals, averaged zonally in the same region, whose slope is indicative of the SPG strength.

Increasing the wind-stress from LGM1.0 to LGM1.7-weak leads to enhanced northward salt transport as well as upwelling and outcropping of isopycnals in the centre of the SPG in LGM1.7-weak relative to LGM1.0 (Fig. 5a, b), and thereby a more efficient mixing of heat to depth and out of the SPG centre. This leads to cooling (Fig. 6), an increase in density in the SPG centre (Fig. 5c), and thereby to a stronger gyre (Eq. 1). This mechanism points to the positive feedback between temperature and the SPG strength (Levermann and Born 2007). North (south) of the SPG centre, the meridional density gradient weighted by depth ($z \cdot \partial_y\rho$) is negative (positive), indicating westward and eastward flow north and south of the SPG centre, respectively (Fig. 5c).

In LGM1.7-strong, DWF in the Nordic Seas is enhanced relative to LGM1.7-weak (Fig. 5d–f). The enhanced overflow thus translates into a density increase mainly south of the GSR. This results in a positive anomalous meridional density gradient and thus eastward anomalous circulation in this area, explaining the SPG strength reduction with increasing wind-stress. Thus, density changes associated with the overflow on the southern GSR slope play a major role in the SPG strength reduction once the second regime is entered.

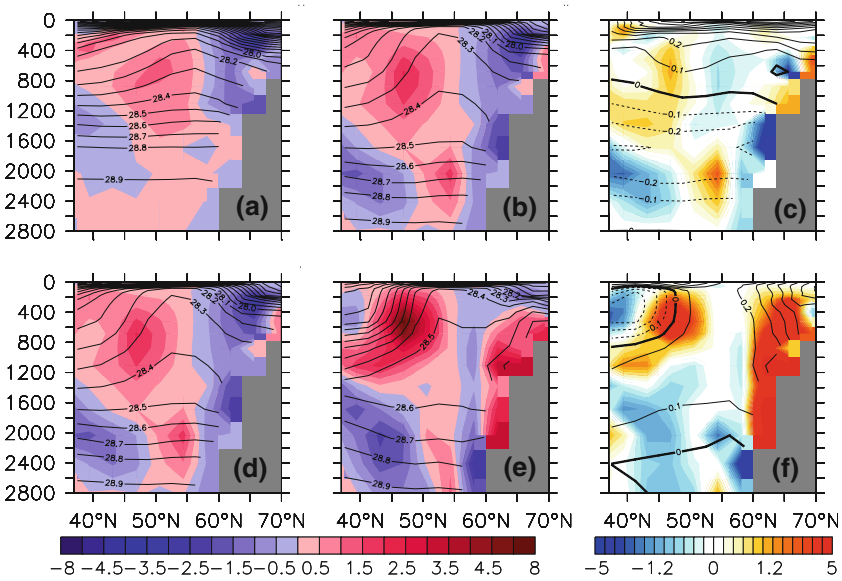

Fig. 5 Meridional density gradient weighted by depth ($z \cdot \partial_y \rho$), averaged over the SPG centre (40°W–20°W), for **a** LGM1.0, **b** LGM1.7-weak, and **c** LGM1.7-weak minus LGM1.0; **d–f** same fields for LGM1.7-weak, LGM1.7-strong, and LGM1.7-strong minus LGM1.7-weak, in 10^{-4} kg m^{-3}. Note here $0 \leq z \leq H$. Thus positive anomalies correspond to positive values in the core of the thermohaline term (Eqs. 1 and 5). Superimposed contours show the corresponding isopycnals (*black*, in 10^{-4} kg m^{-3})

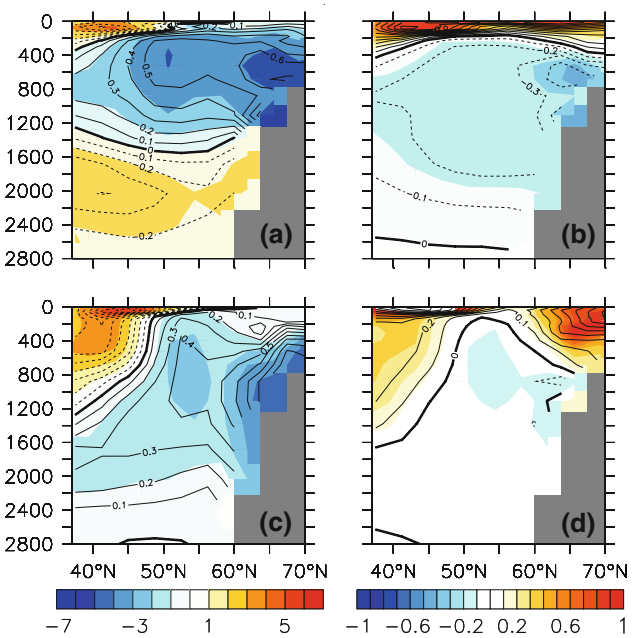

Fig. 6 Difference between LGM1.7-weak and LGM1.0 (LGM1.7-weak minus LGM1.0) **a** temperature (in K) and **b** salinity (in psu) averaged over the SPG centre (40°W–20°W); **c, d** same fields for LGM1.7-strong minus LGM1.7-weak. Superimposed contours show the corresponding contributions of temperature and salinity changes to density changes shown in contours in Fig. 5c, f

The latter mechanism explains as well the decrease in the SPG strength with increasing α in the the HOLO runs (Fig. 4a). Note that this decrease is fastest from $\alpha = 0.75$ to $\alpha = 1$, which yields the low SPG strength value for present-day winds (HOLO1.0). This might seem contradictory with the fact that the GSR overflow increase actually proceeds more slowly for $\alpha \geq 0.75$. Yet, the SPG strength goes in parallel with the decrease in the thermohaline transport (Fig. 4c). Comparison of the $z \cdot \partial_y \rho$ anomaly for HOLO0.75 relative to HOLO0.5 (Fig. 7c) and HOLO1.0 relative to HOLO0.75 (Fig. 7f) reveals density changes along the southern GSR slope result in a stronger SPG reduction in the latter case. A further decomposition of these density changes into temperature and salinity shows these are mainly caused by colder North Atlantic temperatures being entrained by the overflow along the GSR slope (Fig. 8c; note that temperature anomalies along the GSR slope are larger than in Fig. 8a). This implies that not only the magnitude of the overflow, but also the water-mass characteristics are important in setting the SPG circulation response.

To summarise, in the absence of a strong overflow, a wind-stress increase results in a reduction of the upper ocean temperature as a consequence of enhanced outcropping of isopycnals. The latter leads to a density increase in the SPG centre relative to its rim, and thus to a stronger SPG (Fig. 9). In the presence of a significant GSR overflow, wind stress enhances downward transport of cold water masses into GSR slope water, which reduces the density gradient across the SPG and thereby its strength. As a result, the sensitivity to wind-stress in glacial and interglacial times is opposite.

4 Conclusions and discussion

We have investigated the sensitivity of the SPG strength to wind-stress changes under present and glacial climates. Two regimes can be distinguished, depending on the existence of a vigorous GSR overflow. In the first one, GSR overflow is weak and the SPG strength increases with wind-stress as a result of enhanced outcropping of

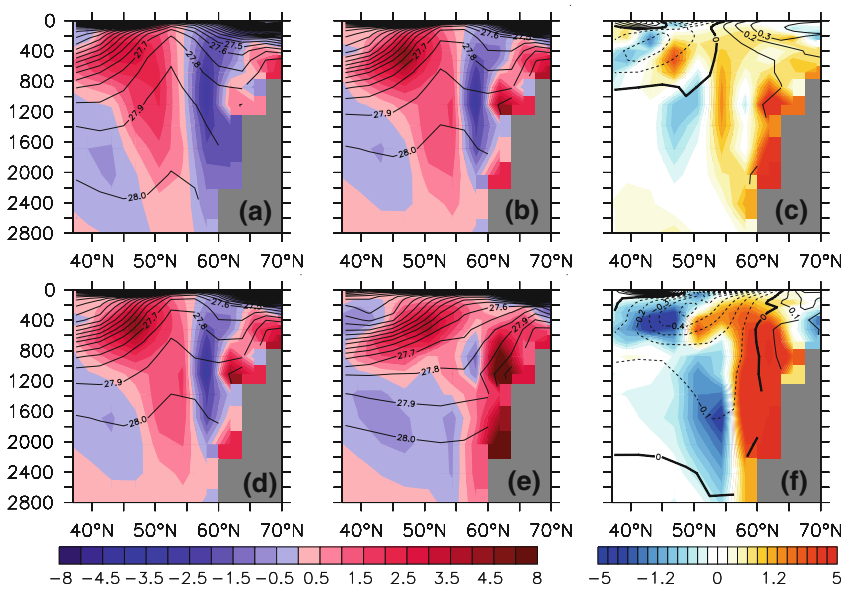

Fig. 7 As Fig. 5 but for **a** HOLO0.5, **b** HOLO0.75, and **c** HOLO0.75 minus HOLO0.5; **d**–**f** same fields for HOLO0.75, HOLO1.0, and HOLO1.0 minus HOLO0.75, in 10^{-4} kg m^{-3}. Superimposed contours show the corresponding isopycnals (*black*, in 10^{-4} kg m^{-3})

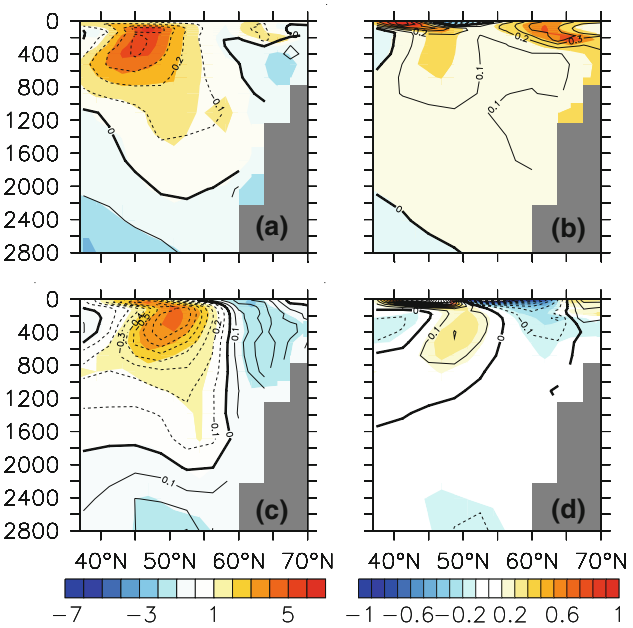

Fig. 8 As Fig. 6 but for HOLO0.75 minus HOLO0.5 (**a, b**) and HOLO1.0 minus HOLO0.75 (**c, d**). Superimposed contours show the corresponding contributions of temperature and salinity changes to density changes shown in contours in Fig. 7c, f

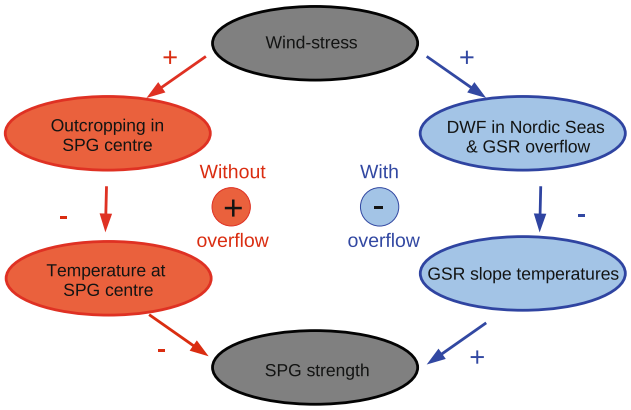

Fig. 9 Mechanisms describing how a wind-stress increase affects the SPG strength through its effect on North Atlantic water-mass densities with and without a strong overflow over the GSR. *Signs between ellipses* indicate how a given magnitude responds to variations in the previous one within the schematic. Without a strong overflow (*red*), a wind-stress increase results in enhanced outcropping of isopycnals in the SPG centre and thus cooling there. This leads to a density increase in the centre of the SPG and thus to a stronger SPG. In the presence of an overflow (*blue*), wind-stress enhances downward transport of cold water masses into GSR slope water which reduces the density gradient across the SPG and thereby its strength

isopycnals. As soon as DWF in the Nordic Seas and a vigorous GSR overflow are established, positive density anomalies on the southern slope of the GSR resulting from the overflow reduce the SPG strength. This reduction is abrupt in the LGM in response to the abrupt onset of DWF, and smooth in the Holocene following the more gradual GSR overflow increase there.

This study was motivated by two previous results. First, Montoya and Levermann (2008) found a threshold in the AMOC as well as in the GSR overflow with respect to wind-stress in glacial climate simulations. Second, Born et al. (2009a) analysed the impact of the representation of the overflows over the GSR in coarse resolution models. Using a hydraulic flow parametrisation, they found that an improved representation of water masses in the Nordic Seas and the subpolar North Atlantic resulted in a stronger SPG. By contrast, an artificial deepening of the topography resulted in a weaker SPG as a result of its stronger GSR overflow and associated water masses. Taken together, these two studies prompted us to analyse the behaviour of the SPG in the aforementioned runs. Our results thus fully

agree with the finding of Born et al. (2009a) indicating that the GSR overflow interacts strongly with the SPG, and that a stronger GSR overflow leads to a weaker SPG, but furthermore indicate the existence of two dynamical regimes, depending on the existence of DWF in the Nordic Seas and a vigorous GSR overflow. Note that AMOC variations are small in the study by Born et al. (2009a) and thus not corrected for in the SPG definition. The generalisation presented here is thus fully consistent.

It is conceivable that our results could be affected by the model's specific configuration, deficiencies, and resolution. An imperfect representation of water masses in the North Atlantic and interaction with the boundaries in the presence of the high viscosity required in such coarse resolution models are likely to impact the SPG circulation. Indeed, the present-day SPG in our model is too weak, and deep convection is shifted from the Labrador Sea to the Irminger Sea. As a consequence, the SPG does not enter Labrador Sea. However, the large-scale circulation under concern in this study is simulated consistently: convection occurs inside the SPG and a cyclonic rim current embraces the deep convection area. The central issue here is the existence of different regimes in the absence and presence of a strong GSR overflow. The governing mechanisms in each of these regimes are simple enough and well understood. Thus, we are confident that the main conclusions presented here are robust and not severely affected by the former features.

Our experimental setup, consisting in multiplying the wind-stress by a constant factor, is highly idealised. Changes in the surface wind-patterns should be the focus of future work. However, our main result is the existence of different dynamical regimes depending on the presence or absence of deep water formation north of the GSR and a vigorous overflow, and the role of wind-stress changes here is merely to trigger the latter. We thus expect our results to be robust against more realistic forcings.

Our findings might be helpful in understanding paleoclimatic records. Abrupt climatic changes of the last glacial period, so called Dansgaard–Oeschger events, have been explained through latitudinal shifts in North Atlantic DWF sites and strengthening of the North Atlantic current (Ganopolski and Rahmstorf 2001; Rahmstorf 2002). While interstadials are associated with DWF in the Nordic Seas and the existence of an overflow over the GSR, during stadials DWF takes place south of the GSR with no overflow. Thus, reversed SPG strength sensitivities to wind forcing are expected in each of these phases. Regardless of their ultimate trigger, glacial abrupt climate changes could result both in a drastic reduction of the SPG strength and a sudden change in its sensitivity to wind-stress variations. SPG dynamics have recently been found to play an important role throughout the Holocene by driving millennial variability in the Atlantic inflow to the Nordic Seas (Thornalley et al. 2009). Our results furthermore imply they could play a relevant role in past glacial abrupt climate changes.

Model studies on glacial abrupt climate changes have up to now mainly focused on the AMOC, largely neglecting changes the horizontal circulations, such as those associated with the gyres. Our study could provide insight as to how the latter might have been affected during such abrupt changes, and may be tested through comparison against paleodata.

Appendix

Ignoring frictional terms, the zonal and meridional time-independent momentum equations are:

$$fu = -g\partial_y\eta + \partial_y \int_z^0 b'dz' + \rho_0^{-1}\partial_z\tau_{zy} \tag{A1}$$

$$-fv = -g\partial_x\eta + \partial_x \int_z^0 b'dz' + \rho_0^{-1}\partial_z\tau_{zx}, \tag{A2}$$

with u and v being the zonal and meridional velocity components, f the Coriolis parameter, g local gravity, η the sea-surface elevation, ρ_0 the average density, τ_{zx} and τ_{zy} the turbulent Reynolds stresses, and

$$b = g\frac{\rho_0 - \rho}{\rho_0} \tag{A3}$$

the buoyancy.

Splitting the second term on the right hand side (r.h.s.) of Eqs. A1 and A2 we have:

$$fu = -g\partial_y\eta + \partial_y \int_{-H}^0 bdz - \partial_y \int_{-H}^z b'dz' + \rho_0^{-1}\partial_z\tau_{zy} \tag{A4}$$

$$-fv = -g\partial_x\eta + \partial_x \int_{-H}^0 bdz - \partial_x \int_{-H}^z b'dz' + \rho_0^{-1}\partial_z\tau_{zx}, \tag{A5}$$

where H is the ocean depth.

Here we can identify the Ekman, thermohaline and bottom velocity as defined by Fofonoff (1962) and Mellor et al. (1982):

$$f[u_e, v_e] = \left[\rho_0^{-1}\partial_z\tau_{zy}, -\rho_0^{-1}\partial_z\tau_{zx}\right] \tag{A6}$$

$$f[u_t, v_t] = \left[-\partial_y \int_{-H}^z b'dz', \partial_x \int_{-H}^z b'dz'\right] \tag{A7}$$

$$f[u_b, v_b] = \left[-g\partial_y \eta + \partial_y \int_{-H}^{0} b dz, g\partial_x \eta - \partial_x \int_{-H}^{0} b dz \right]. \quad \text{(A8)}$$

We now define the vertically integrated zonal and meridional transports:

$$M_x = \int_{-H}^{0} u dz; \quad M_y = \int_{-H}^{0} v dz. \quad \text{(A9)}$$

Integrating vertically Eq. A4 we have:

$$fM_x = -g \int_{-H}^{0} \partial_y \eta dz + \int_{-H}^{0} dz \partial_y \int_{-H}^{0} b dz - \int_{-H}^{0} dz \partial_y \int_{-H}^{z} b' dz' + \rho_0^{-1} \int_{-H}^{0} \partial_z \tau_{zy} dz. \quad \text{(A10)}$$

The third term on the r.h.s. can be rewritten as follows using Leibnitz's rule:

$$\int_{-H}^{0} dz \partial_y \int_{-H}^{z} b' dz' = \partial_y \int_{-H}^{0} dz \int_{-H}^{z} dz' b' - \int_{-H}^{0} dz b \partial_y 0 + \int_{-H}^{-H} dz b \partial_y (-H) = \partial_y \int_{-H}^{0} dz \int_{-H}^{z} dz' b'. \quad \text{(A11)}$$

Thus:

$$fM_x = -Hg\partial_y \eta + H\partial_y \int_{-H}^{0} b dz + \partial_y \int_{-H}^{0} z b dz + \rho_0^{-1} \tau_{0y} \quad \text{(A12)}$$

$$fM_y = Hg\partial_x \eta - H\partial_x \int_{-H}^{0} b dz - \partial_x \int_{-H}^{0} z b dz - \rho_0^{-1} \tau_{0x}, \quad \text{(A13)}$$

where τ_{0x},τ_{0y} are the zonal and meridional component of the surface wind-stress, respectively.

A further simplification can be made by applying again Leibnitz's rule on the second and third term of the r.h.s.:

$$H\partial_y \int_{-H}^{0} b dz = H \int_{-H}^{0} \partial_y b dz + H b_{-H} \partial_y H \quad \text{(A14)}$$

$$\partial_y \int_{-H}^{0} z b dz = \int_{-H}^{0} z \partial_y b dz - H b_{-H} \partial_y H, \quad \text{(A15)}$$

where b_{-H} is the buoyancy at the bottom of the ocean. Substituting into Eqs. A12 and A13, the last term on the r.h.s. cancels out, yielding

$$fM_x = -Hg\partial_y \eta + H \int_{-H}^{0} \partial_y b dz + \int_{-H}^{0} z \partial_y b dz + \rho_0^{-1} \tau_{0y} \quad \text{(A16)}$$

$$fM_y = Hg\partial_x \eta - H \int_{-H}^{0} \partial_x b dz - \int_{-H}^{0} z \partial_x b dz - \rho_0^{-1} \tau_{0x}. \quad \text{(A17)}$$

The vertically integrated Ekman, thermohaline and bottom transports are thus:

$$f[M_{xe}, M_{ye}] = \left[\rho_0^{-1} \tau_{0y}, -\rho_0^{-1} \tau_{0x} \right] \quad \text{(A18)}$$

$$f[M_{xt}, M_{yt}] = \left[\int_{-H}^{0} z \partial_y b dz, - \int_{-H}^{0} z \partial_x b dz \right] \quad \text{(A19)}$$

$$f[M_{xb}, M_{yb}] = \left[-Hg\partial_y \eta + H \int_{-H}^{0} \partial_y b dz, Hg\partial_x \eta - H \int_{-H}^{0} \partial_x b dz \right], \quad \text{(A20)}$$

as discussed by Mellor et al. (1982). Equations A16 and A17, and their decomposition into Eqs. A18–A20 constitute our final equations.

Note that usually the surface elevation is unknown, which precludes calculating the transport directly from Eqs. A16 and A17. As explained by Mellor et al. (1982) this problem can be circumvented by rewriting these equations in terms of the potential energy at depth H $\rho_0 \phi$ and the bottom pressure $\rho_0 P_b$:

$$\phi \equiv \int_{-H}^{0} z b dz \quad \text{(A21)}$$

$$P_b \equiv g\eta - \int_{-H}^{0} b dz. \quad \text{(A22)}$$

These are related to the second and third terms on the r.h.s. of Eqs. A16 and A17 in the following manner:

$$\partial_y \phi = \partial_y \int_{-H}^{0} z b dz = \int_{-H}^{0} z \partial_y b dz - H b_{-H} \partial_y H; \quad \text{(A23)}$$

$$-H\partial_y P_b = -Hg\eta + \partial_y \int_{-H}^{0} b dz = -Hg\eta + \int_{-H}^{0} \partial_y b dz + H b_{-H} \partial_y H. \quad \text{(A24)}$$

Since the last term on the r.h.s. cancels out, Eqs. A16 and A17 can also be written as:

$$M_x = \frac{1}{f}\left\{-H\partial_y P_b + \partial_y \phi + \frac{\tau_{0y}}{\rho_0}\right\} \tag{A25}$$

$$M_y = \frac{1}{f}\left\{H\partial_x P_b - \partial_x \phi - \frac{\tau_{0x}}{\rho_0}\right\}. \tag{A26}$$

Cross-differentiating and adding up Eqs. A25 and A26 yields the equation for the advection of planetary potential vorticity, in which the bottom pressure term has been eliminated:

$$\begin{aligned}\mathbf{M}\cdot\nabla\left(\frac{f}{H}\right) =& H^{-2}(\partial_y H\partial_x\phi - \partial_x H\partial_y\phi) \\ &+ \partial_x\left(\frac{\tau_{0y}}{\rho_0 H}\right) - \partial_y\left(\frac{\tau_{0x}}{\rho_0 H}\right),\end{aligned} \tag{A27}$$

which allows estimating the flow by evaluating the r.h.s. of Eq. A27; the reader is referred to Mellor et al. (1982) and Mellor (1996) for a more detailed explanation of the exact procedure. In our case, however, because we are handling model output, all quantities are available and the transport can be computed directly from Eqs. A16 and A17.

References

Böning C, Scheinert M, Dengg J, Biastoch A, Funk A (2006) Decadal variability of subpolar gyre transport and its reverberation in the North Atlantic overturning. Geophys Res Lett 33:L21S01

Born A, Levermann A, Mignot J (2009a) Sensitivity of the Atlantic circulation to a hydraulic overflow parameterization in a coarse resolution model. Ocean Modelling 27:132–140

Born A, Nisancioglu K, Braconnot P (2009b) Sea ice induced changes in ocean circulation during the Eemian. Climate Dynamics. doi: 10.1007/s00382-009-0709-2

Bryan F, Böning C, Holland W (1995) On the midlatitude circulation in a high-resolution model of the North Atlantic. J Phys Oceanogr 25(3):289–305

Crowley TJ, North GR (1991) Paleoclimatology. Oxford University Press, New York, p 349

Curry R, McCartney M, Joyce T (1998) Oceanic transport of subpolar climate signals to mid-depth subtropical waters. Nature 391:575–577

Eden C, Willebrand J (2001) Mechanism of interannual to decadal variability of the North Atlantic circulation. J Clim 14:2266–2280

Fichefet T, Maqueda MAM (1997) Sensitivity of a global sea ice model to the treatment of ice thermodynamics and dynamics. J Geophys Res 102:12609–12646

Fofonoff NP (1962) The Sea. In: Hill MN (ed) Dynamics of ocean currents, vol I. Interscience, New York

Ganachaud A, Wunsch C (2000) Improved estimates of global ocean circulation, heat transport and mixing from hydrographic data. Nature 48: 453–457

Ganopolski A, Rahmstorf S (2001) Rapid changes of glacial climate simulated in a coupled climate model. Nature 409:153–158

Greatbatch R, Fanning A, Goulding A, Levitus S (1991) A diagnosis of interpentadal circulation changes in the North Atlantic. J Geophys Res 96:22009–22023

Häkkinen S, Rhines PB (2004) Decline of subpolar North Atlantic circulation during the 1990s. Science 304:555–559

Hátún H, Sando A, Drange H, Hansen B, Valdimarsson H (2005) Influence of the Atlantic subpolar gyre on the thermohaline circulation. Science 309:1841–1844

Hewitt CD, Stouffer RJ, Broccoli AJ, Mitchell JFB, Valdes PJ (2003) The effect of ocean dynamics in a coupled GCM simulation of the Last Glacial Maximum. Clim Dyn 20:203–218

Kuhlbrodt T, Griesel A, Montoya M, Levermann A, Hofmann M, Rahmstorf S (2007) On the driving processes of the Atlantic meridional overturning circulation. Rev Geophys 45:RG2001

Levermann A, Born A (2007) Bistability of the subpolar gyre in a coarse resolution climate model. Geophys Res Lett 34:L24605

Mellor GL (1996) Introduction to physical oceanography. Princeton University

Mellor G, Mechoso C, Keto E (1982) A diagnostic calculation of the general circulation of the Atlantic Ocean. Deep Sea Res 29:1171–1192

Montoya M, Griesel A, Levermann A, Mignot J, Hofmann M, Ganopolski A, Rahmstorf S (2005) The Earth system model of intermediate complexity CLIMBER-3α. Part I: description and performance for present day conditions. Clim Dyn 25:237–263

Montoya M, Levermann A (2008) Surface wind-stress threshold for glacial atlantic overturning. Geophys Res Lett 35:L03608. doi: 10.1029/2007GL032,560

Myers P, Fanning A, Weaver A (1996) Jebar, bottom pressure torque, and gulf stream separation. J Phys Oceanogr 26:671–683

Otto-Bliesner B, Brady E, Tomas R, Levis S, Kothavala Z (2006) Last Glacial Maximum and Holocene climate in CCSM3. J Clim 19:2526–2544

Peltier WR (2004) Global glacial isostasy and the surface of the ice-age Earth: the ICE-5G(VM 2) model and GRACE. Annu Rev Earth Planet Sci 32(1):111–149

Penduff T, Barnier B, de Verdière AC (2000) Self-adapting open boundaries for a sigma coordinate model of the eastern North Atlantic. J Geophys Res 105:11279–11298

Petoukhov V, Ganopolski A, Brovkin V, Claussen M, Eliseev A, Kubatzki C, Rahmstorf S (2000) CLIMBER-2: a climate system model of intermediate complexity. Part I: model description and performance for present climate. Clim Dyn 16:1–17

Rahmstorf S (1996) On the freshwater forcing and transport of the Atlantic thermohaline circulation. Clim Dyn 12:799–811

Rahmstorf S (2002) Ocean circulation and climate during the past 120,000 years. Nature 419:207–214

Talley LD, Reid JL, Robbins PE (2003) Data-based meridional overturning streamfunctions for the global ocean. J Clim 16:3213–3226

Thornalley D, Elderfield H, McCave N (2009) Holocene Oscillations in the temperature and salinity of the surface subpolar North Atlantic. Nature 457:711–714

Toggweiler J, Russell J (2008) Ocean circulation in a warming climate. Nature 451:286-288

Toggweiler JR, Samuels B (1998) On the ocean's large scale circulation in the limit of no vertical mixing. J Phys Oceanogr 28:1832–1852

Treguier AM, Theetten S, Chassignet E, Penduff T, Smith R, Talley L, Beismann J, Böning C (2005) The North Atlantic subpolar gyre in four high-resolution models. J Clim 35:757–774

Trenberth K, Olson J, Large W (1989) A global ocean wind stress climatology based on ECMWF analyses. Tech. Rep. NCAR/TN-338+STR, National Center for Atmospheric Research, Boulder, Colorado, USA

Wijffels SE, Meyers G, Godfrey JS (2008) A 20-yr average of the Indonesian throughflow: regional currents and the interbasin exchange. J Phys Oceanogr 38:1965–1978

Wunsch C (1998) The work done by the wind on the oceanic general circulation. J Phys Oceanogr 28:2332–2340

Wunsch C, Ferrari R (2004) Vertical mixing, energy and the general circulation of the oceans. Annu Rev Fluid Mech 36:281–314

Zhang R (2008) Coherent surface-subsurface fingerprint of the Atlantic meridional overturning circulation. Geophys Res Lett 35:L20705

Paper VI

The Atlantic subpolar gyre as a stochastically forced oscillator

Born, A. and J. Mignot (2010)

(manuscript in preparation)

The Atlantic Subpolar Gyre as a stochastically forced oscillator

Andreas Born[1]**,**

Bjerknes Centre for Climate Research, Bergen, Norway

Geophysical Institute, University of Bergen, Bergen, Norway

Juliette Mignot,

LOCEAN, Universite Pierre et Marie Curie, Paris, France

July 8, 2010

[1] Corresponding author: andreas.born@bjerknes.uib.no

Abstract

Internal variability of the Atlantic subpolar gyre is investigated in a 600 year control experiment of a comprehensive coupled climate model. The ocean circulation shows irregular oscillations of decadal time scale with most spectral power between 15 and 25 years. Positive feedback mechanisms destabilize the gyre circulation and lead to internal ocean oscillations. This involves periodically enhanced deep convection in the subpolar gyre center and enhanced air-sea thermal coupling. Anomalies in the large-scale atmospheric circulation are transferred into the ocean on the ocean's intrinsic time scale, triggering the destabilizing feedbacks and exciting the oscillator stochastically. A better understanding of oscillatory mechanisms of the ocean holds considerable potential for decadal predictions.

1 Introduction

The North Atlantic ocean circulation is an important modulator of global climate, mainly because of its northward transport of heat. Changes in this transport have a wide range of consequences on various time scales ranging from the impact on ice sheets during the last glacial (Ganopolski and Rahmstorf, 2001; Born et al., 2010a), abrupt cooling events during the early Holocene (Alley and Ágústsdóttir, 2005; Wiersma et al., 2006) to effects on fisheries in recent decades (Hátún et al., 2009). Many observational and modeling studies describe decadal to multidecadal variability in the Atlantic Ocean, sometimes referred to as the Atlantic Multidecadal Oscillation (Delworth and Mann, 2000; Kerr, 2000; Dijkstra et al., 2006).

Anomalous freshwater input into the North Atlantic and adjacent Nordic Seas is considered critical for the observed variations as it weakens the deep thermohaline circulation. These anomalies are often imposed onto the ocean circulation, e.g. by melting ice sheets or increased advection of sea ice, but internal variability, the generation of anomalies by the circulation itself, has also been found in a number of studies (Delworth et al., 1993; Pohlmann et al., 2004; Jungclaus et al., 2005; Danabasoglu, 2008; Keenlyside et al., 2008; Guemas and Salas-Melia, 2008). The latter leads to a oscillatory behavior that recently raised hope for much needed climate predictions on decadal time scale (Latif et al., 2006; Smith et al., 2007; Goddard et al., 2009). In this context, but also on longer time-scales, many studies identified the important role of the Atlantic subpolar gyre (SPG) (see Yoshimori et al. (2010) for an overview). This circulation system was found to redistribute freshwater anomalies in the North Atlantic and Nordic Seas (Hátún et al., 2005; Wu and Wood, 2008) and to advect salinity anomalies into the Labrador Sea convection region (Delworth et al., 1993). Similar mechanisms potentially decouple the ocean circulation from atmospheric forcing and thus develop independently (Lohmann et al., 2009b,a). Idealized modeling showed that the gyre circulation introduces instabilities of regular duration that provide potential for predictions (Spall, 2008).

On a more conceptual level, these characteristics of the large scale gyre circulation were formulated as positive feedback mechanisms and their usefulness demonstrated in paleo applications (Levermann and Born, 2007; Born et al., 2010b; Born and Levermann, 2010; Born et al., 2010c): First, a stronger SPG transports more saline

subtropical water into the subpolar North Atlantic (salt feedback). This increases the density gradient between the center and the relatively light exterior of the gyre. Sea surface elevation drops through pressure adjustments in the water column and the geostrophic response strengthens the gyre. Secondly, isopycnal mixing is intensified owing to the enhanced isopycnal outcropping associated to a stronger SPG. This results in cooling and again increases the density in the center of the SPG and therewith its strength (temperature feedback).

The original formulation of these feedback mechanisms is based on simulations with a coarse resolution model with a simplified, statistical-dynamical atmosphere model that does not produce internal variability. Thus, in this model, two SPG regimes exist that are stable over several centuries. It is the aim of the present study to further investigate these feedback mechanisms in the presence of variability of a comprehensive atmosphere-ocean general circulation model. The text is organized as follows. The coupled climate model is described in Section 2. Output from the model is analyzed in Section 3. We summarize and discuss in Section 4.

2 Model description

The simulations analyzed here have been carried out with the high resolution version of Institut Pierre Simon Laplace coupled model version 4 (IPSL CM4), comprising ocean, sea ice, atmosphere and land surface components (Marti et al., 2010). The dynamical core of the ocean model is based on the OPA system (Madec et al., 1997). The configuration used here (ORCA2) uses a horizontal resolution based on a 2 degree Mercator mesh, enhanced to 0.5 degree meridional resolution near the equator for a better representation of the equatorial wave channel and with two poles over the continents in the Northern Hemisphere in order to avoid a singularity in the Arctic Ocean. There are 31 unevenly spaced levels in the vertical. A free surface formulation is used for the upper boundary (Roullet and Madec, 2000), and a diffusive boundary parametrization is used for the bottom (Beckmann, 1998). Isopycnal diffusion uses an eddy diffusivity coefficient of 2,000 $m^2 s^{-1}$. The eddy induced velocity parametrization follows Gent and McWilliams (1990), using a coefficient that depends on the growth rate of baroclinic instabilities (usually between 15 and 3,000

$m^2 s^{-1}$).

The dynamic sea ice model (LIM2, Fichefet and Maqueda (1999, 1997)) uses the horizontal ocean grid to compute ice rheology and advection. Thermodynamics are computed in three vertical layers, the uppermost for snow. Ice growth and melting are determined by an energy balance at both the snow-ice and water-ice boundary and in leads. Internal forces follow a viscous-plastic law (Hibler, 1979). The model features parametrizations for the trapping of shortwave radiation by brine pockets, leads in the ice, as well as an implicit representation of subgrid variations in snow and ice thickness.

The atmosphere is simulated by a comprehensive general circulation model (LMDZ, Hourdin et al. (2006)) with a resolution of 2.5 zonally and 1.875 meridionally on 19 vertical levels. Precipitation over land is returned to the ocean by means of a river routing scheme implemented in the land surface model (ORCHIDEE, Krinner et al. (2005)).

This model has been used in several studies of past climate states (Braconnot et al., 2008; Zheng et al., 2008; Born et al., 2010b), present day climate sensitivity to anomalous freshwater forcing (Swingedouw et al., 2007b), and future projections (Swingedouw et al., 2007a; IPCC, 2007).

3 Results

3.1 Periodicity of the subpolar gyre

We analyzed a 600 year control run with fixed preindustrial boundary conditions. It follows a 250 year spin-up initialized with climatological hydrography an ocean at rest. This experiment exhibits pronounced variations in the subpolar gyre index, defined as the absolute value of the local minimum of the depth integrated stream function (Fig. 1). The average strength of the gyre is 21.5 Sv with a standard deviation of 2.0 Sv. Most spectral power of these variations is found in the decadal band between 15 and 25 years. Periods of strong cyclonic circulation follow events of enhanced deep convection in the gyre's center, equivalent to Labrador Sea convection,

with approximately 8 years lag (Fig. 2).

Since the following analysis concerns decadal variability, all time series are filtered with a 15-year running average unless stated otherwise. This interval was chosen to remove faster variations of large amplitude but short enough to not affect the 20-year band. This smoothing procedure reduces the degrees of freedom of the time series because two independent signals have to be spaced at least half of the averaging interval, 7.5 yr. However, the presence of decadal variations implies that signals spaced about 20 years are still correlated. Significance tests shown throughout this study thus assume a number of degrees of freedom of 600 yr/20 yr = 30. We use the two-sided Student's t test.

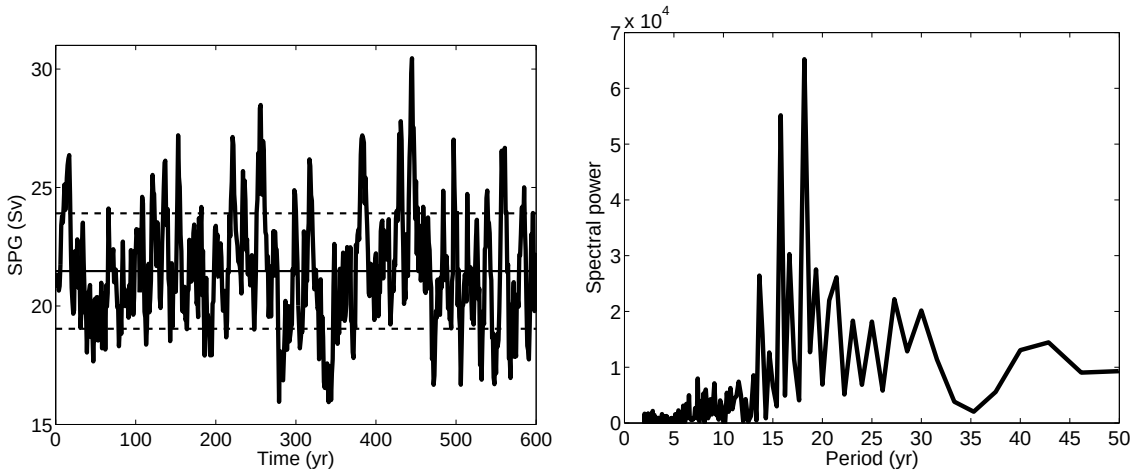

Figure 1: **Left**: Time series of the SPG index. Thin lines mark average value (thin solid) and standard deviations (dashed). **Right**: Frequency spectrum of the SPG index [add noise bounds]. Most spectral power is found between 15 to 25 years.

3.2 Positive feedback mechanisms

Regression of the density of the upper 1000 m in the SPG center on the SPG index shows that maxima in circulation strength are associated with higher densities in the water column, consistent with findings in earlier studies (Häkkinen and Rhines, 2004; Levermann and Born, 2007; Lohmann et al., 2009b) (Fig. 3, left). Thus, baroclinic adjustments influence the SPG on decadal time scales. Decomposition of the density into temperature and salinity contributions shows that higher densities

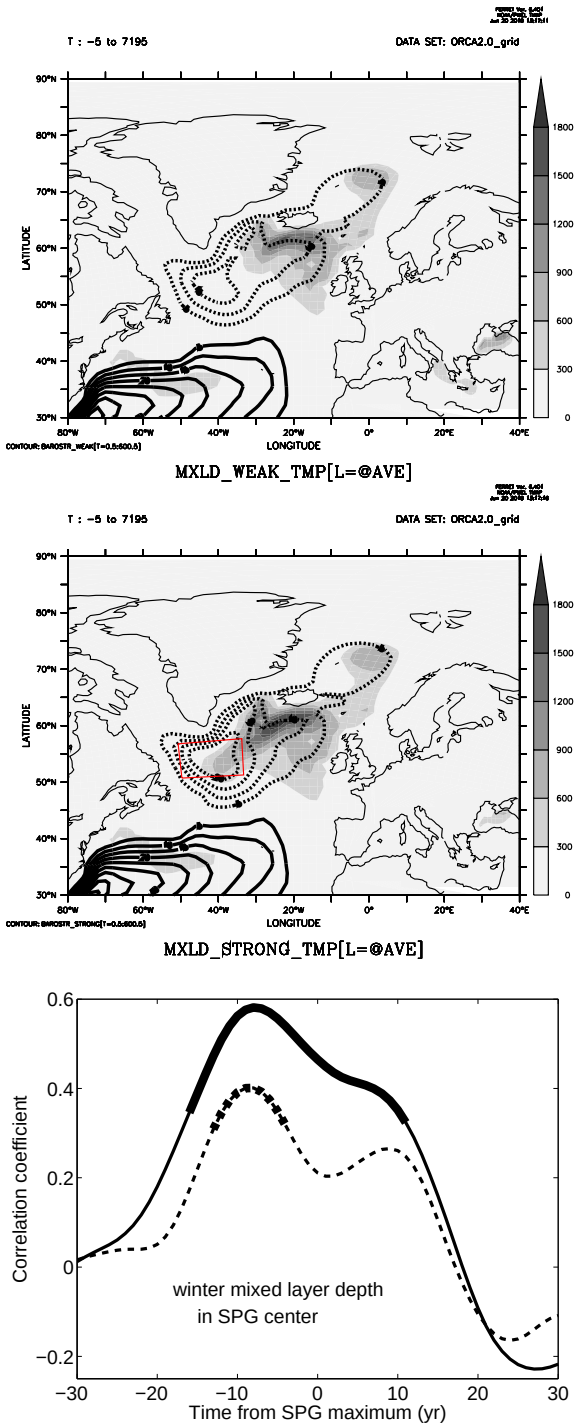

Figure 2: **Upper**: Composite depth integrated stream function for SPG index weaker than one standard deviation (contours, spacing 5 Sv, negative dashed) and composite mixed layer depth leading by 8 years (shading). **Middle**: As before but for SPG index stronger than one standard deviation. Red box shows SPG center region used subsequently. **Lower**: Correlation of mixed layer depth in the SPG center with the normalized SPG index, 15-year (solid) and 5-year running average (dashed). Correlations significant at the 95% level are shown as bold lines.

are the result of a cooling of the upper 1000 m, with salinity mostly counteracting. This cooling is the delayed response to enhanced deep convection which occurs discontinuously in the SPG center (Fig. 3, right). The 7 years lag is owed to the thermal inertial of the water column.

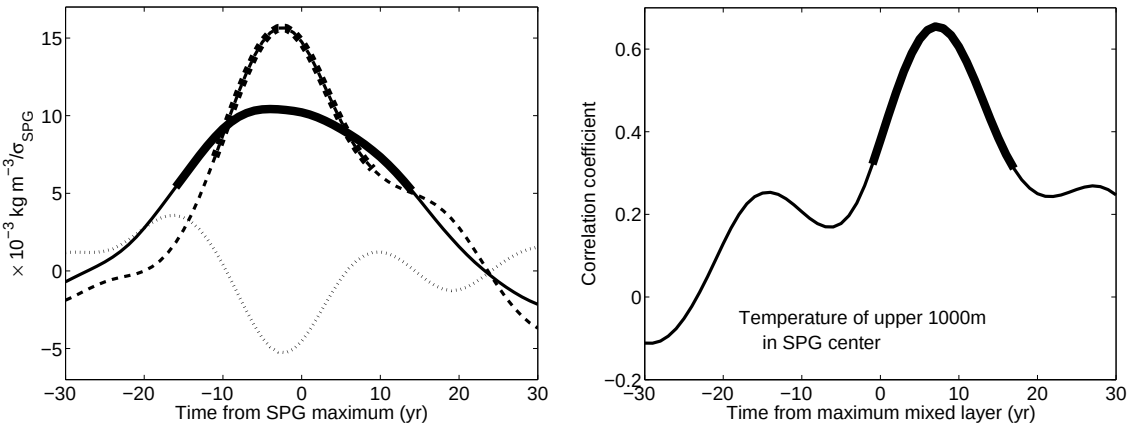

Figure 3: **Left**: Regression of density in the SPG center, averaged over the upper 1000 m, on normalized SPG index (solid), decomposed into temperature (dashed) and salinity (dotted) contributions. **Right**: Correlation of 1000 m temperature in the SPG center with the normalized mixed layer depth (solid). Above 95% significance is shown as bold lines. Density correlates with the SPG, mostly due to cooling of the water column. Highest densities and lowest temperatures occur approximately coeval with the SPG maximum at zero lag. Cooling is a response with a 7 years delay to more intense deep convection.

To find the cause for deep convection and destabilizing surface anomalies, the regression of the 50 m surface density on the SPG index is analyzed (Fig. 4). Density changes by surface freshwater flux are calculated assuming fixed average temperatures and anomalous salinities

$$\Delta S = \frac{F_{anom}}{H}(S - S_0) \tag{1}$$

where F_{anom} is the anomalous freshwater flux, S_0 the average salinity of the target region, S the salinity of the freshwater flux, 0 in the case of air-sea exchange, 4 psu for sea ice, and H the average depth of the mixed layer, taken here as 50 m. The winter mixed layer depth in this region exceeds this value by far in some years

which is potentially important for assessing the impact of surface fluxes. However, the fluxes used in this analysis are annual averages and H is chosen to be consistent. The impact of this simplification is discussed below. Increasing H in equation (1) would increase ΔS to unrealistically small values. Using a time-dependent H would dominate the ΔS variability and mask the impact F_{anom}.

Similarly, density changes due to anomalous heat flux Q_{anom} use anomalous temperatures

$$\Delta T = \frac{\int^{1year} dt\ Q_{anom}}{H c_p \rho} \tag{2}$$

with the anomalous heat flux integrated over one year, corresponding to the temporal resolution of the analyzed data, the specific heat capacity c_p and density ρ of water.

Surface density shows a broad peak around the SPG maximum. In contrast to the intermediate water column, density changes at the surface are due to salinity anomalies while contributions by temperature are not significant. However, the direct effect of freshwater exchange with the atmosphere can not explain the density anomaly due to salinity. Relatively large density variations could be caused by surface heat flux but are mostly below the significance level and apparently contradict small variations in the temperature component of the surface density. This is because the calculation used here to assess the impact of surface fluxes (equation (1)) assumes a homogeneously mixed surface layer of 50 m. This is a good assumption for the usually well stratified upper ocean but fails in the presence of deep convection. High surface heat loss associated with deep convection removes heat not only from the upper 50 m, which is why the surface density anomaly is not as large as expected for the heat flux. Although high surface heat flux only occurs during times of strong convection and is therefore considered a consequence of ocean-internal processes rather than actively controlling the chain of events, the periodically enhanced thermal air-sea coupling allows atmospheric variability to influence the subpolar gyre.

The salinity anomaly that releases deep convection events is not caused by direct surface freshwater forcing but is the result of oceanic processes. Anomalous salinities due to lateral advection, eddy transport, surface freshwater flux and sea ice are calculated according to equation (1). The impact of vertical salt transport is a complicated function of several numerical parametrizations and can not be analyzed directly from the model output. It is thus taken as the residual of a salinity budget that can be calculated based on the above contributions and the salinity simulated by the model. Note that absolute values are not accurate because the salinity budget is not closed when calculated from annual average data. However, the resulting time series of vertical salt transport correlates well with the deep convection time series with r=+0.74 at lag -1 year (>99% significant, not shown).

Most other processes can be neglected so that the evolution of surface salinity over a quasi-oscillation cycle is adequately represented as a balance of lateral advection and vertical transport by convection. At the SPG maximum, enhanced lateral advection of salt results in rising salinities in the SPG center the following 10 years (Fig. 4, right). This is consistent with the strong ∼20 year quasi-cyclicity found in the frequency spectrum (Fig. 1). 10 years after the SPG maximum marks the subsequent minimum and weak salt advection.

High salinities are eroded by convection. This process begins 10 years before the SPG maximum, coeval with the maximum mixed layer depth, and continuously reduces the surface salinity throughout the duration of the convective event (Fig. 2, lower). Assuming a quasi-cyclic behavior of 20 years, the surface salinity maximum caused by anomalously strong salt advection 10 years after the SPG maximum is equivalent to the rise in salinity 10 years before the SPG maximum that is eroded by convection. Advection and convection balance. In the case of perfect cyclicity, both salinity maxima would be equal and this change in perspective unnecessary. Here, however, oscillations occur on time scales other than 20 years because the proposed oceanic oscillator is influenced by atmospheric noise.

The following chain of events can be inferred from the above analysis (Fig. 5). Strong SPG circulation starts accumulating salt in the center of the gyre through lateral advection. This is the salt feedback of Levermann and Born (2007). Freshwater flux by eddies, sea ice, evaporation and precipitation are small. After approx-

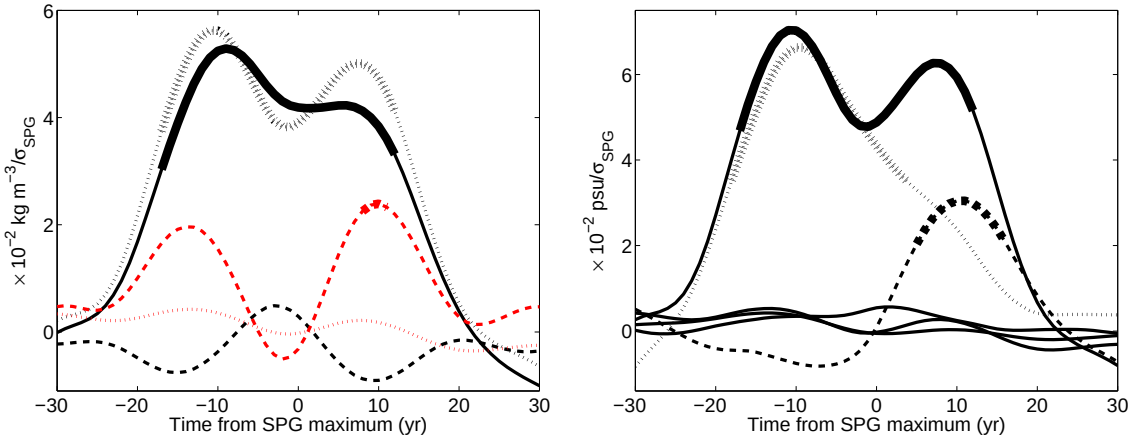

Figure 4: **Left**: Regression of 50 m surface density (black solid) on normalized SPG index, decomposed into temperature (black dashed) and salinity (black dotted) contributions. Red curves show 50 m density changes due to surface heat flux (red dashed) and surface freshwater flux (red dotted). **Right**: Regression of 50 m surface salinity (thick solid) on normalized SPG index, decomposed into major contributions from lateral advection (dashed) and convection (dotted). Negligible contributions are shown as thin solid lines: evaporation minus precipitation, sea ice and eddy salt transport. Correlations significant at the 95% level are shown as bold lines.

imately 10 years, salt advection increased density enough for the water column to become unstable and deep convection begins. Convection causes the intermediate depth water column to start cooling through heat loss at the surface, the temperature feedback. This process takes about 10 years as well due to the large thermal inertia of the water column. Cooling results in higher densities that yield a stronger SPG. The characteristic time scale of 20 years is the approximate sum of the two slowest processes.

3.3 Closing the oscillation cycle

While all these processes work to strengthen the SPG, deep convection also erodes the surface salinity anomaly and thus terminates the deep convection event. This occurs before the slow accumulation of salt at the surface can counteract. Hence, the oscillations can be understood as a balance between lateral salt advection and vertical salt export by convection. Advection can only accumulate salt during times of relatively weak convection. When increasing salinities release a convective event, the

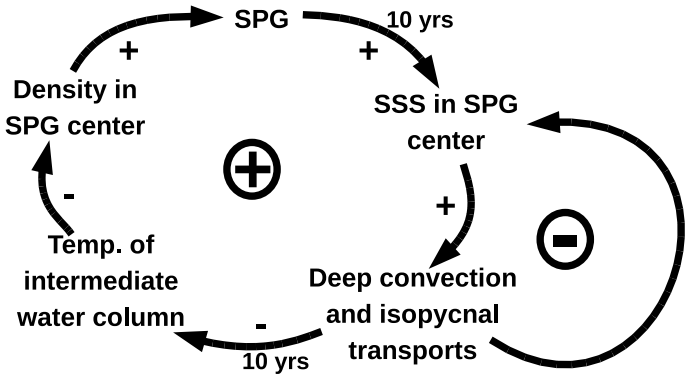

Figure 5: Summary of the mechanisms causing the nonlinearity.

salinity anomaly is removed but cooling of the intermediate water column provides the grounds for a later SPG maximum with renewed salt transport.

Even on the long time scales investigated here, the SPG index correlates with the time series of the North Atlantic Oscillation (NAO) with r=+0.47 (>95% significant), NAO leading by 5 years. The NAO, however, does not show spectral power on long time scales (not shown). This controversy is reconciled by interpreting the SPG as a low-pass frequency filter. Due to the ocean oscillatory mechanism outlined above, deep convection in the SPG center is enhanced periodically with a characteristic time scale of approximately 20 years (Fig. 2, lower). While the stronger surface heat loss during periods of deep convection is primarily a result of the oceanic oscillator, it is modulated by large scale atmospheric conditions. Thus, periodically enhanced thermal air-sea coupling allows large scale atmospheric conditions to influence the evolution of the SPG on one particular decadal time scale set by the ocean - a stochastically forced oscillator.

4 Summary and Discussion

Self-amplifying feedbacks have been found to destabilize the SPG, producing oscillations of irregular period in the decadal band. This allows for a revised description of feedbacks previously found in a coarse resolution model (Levermann and Born, 2007). Both salt advection into the SPG center and cooling due to convection and isopycnal transports intensify with stronger circulation. However, in the framework

of decadal variability, only the temperature signal results in higher densities of the intermediate water column that intensify the cyclonic circulation. Salt advection alone does not form a positive feedback loop with the SPG, but plays an important role because it takes place close to the surface and thus releases more intense convection events, the prerequisite for effective cooling. Thus, intensification of the SPG circulation is the result of the interplay between more intense salt advection at the surface causing stronger deep convection, and the enhanced cooling of intermediate waters resulting from convection intensifying salt advection. This view is consistent with the original conceptual description of the SPG feedbacks but adds significant detail on the respective roles of temperature and salinity anomalies for the dynamic system.

The rapid oscillations suggest that the dynamic system is close to a threshold in preindustrial climate where relatively weak salinity anomalies due to advection can release convection periodically, thereby influencing the intermediate depth density distribution and result in large amplitude variability of the SPG. Modeling work suggests that present day variability in the region can only be simulated qualitatively if the SPG is close to a dynamic threshold (Levermann et al., 2010). Changing the freshwater balance of the subpolar North Atlantic, for example by changes in Arctic sea ice export, stabilizes one or the other SPG mode. This has been found in two experiments with the same climate model, albeit with lower atmospheric resolution, under different orbital configurations (Born et al., 2010b).

The appreciation of convection-advection related feedbacks has led to a new understanding of the SPG in recent years, assigning to it the role of an independent dynamical component of the climate system instead of merely following atmospheric forcing. By modulating Labrador Sea deep convection and thus the strength of atmosphere-ocean coupling, the dynamics of the SPG must be considered a key to understanding past and future climate variability and changes. Indeed, recent analyses of marine sediments revealed that variations in SPG circulation occurred throughout the last 12,000 years, as observed both in Greenland fjords (Ren et al., 2009; Kuijpers et al., 2009), the eastern North Atlantic (Thornalley et al., 2009) and in North American slope waters (Sachs, 2007).

Acknowledgments

We gratefully acknowledge Sébastien Denvil for access to the model data as well as discussions with Jürgen Bader. The climate simulations were originally carried out in the framework of the EC-FP6 project 'ENSEMBLES'. A.B. was funded by the Marie Curie Actions project NICE (MRTN-CT-2006-036127) and the Research Council of Norway project TOPPNICE. This is publication no. XXXX from the Bjerknes Centre for Climate Research.

References

Alley, R. B. and Áugústsdóttir, A. M. (2005). The 8k event: cause and consequences of a major Holocene abrupt climate change. *Quaternary Science Reviews*, 24:1123–1149.

Beckmann, A. (1998). *The representation of bottom boundary layer processes in numerical ocean circulation models. In: E.P. Chassignet and J. Verron, Editors: Ocean modeling and Parametrization*, pages 135–154. Kluwer Academic Publishers, Dordrecht.

Born, A., Kageyama, M., and Nisancioglu, K. H. (2010a). Warm Nordic Seas delayed glacial inception in Scandinavia. in preparation.

Born, A. and Levermann, A. (2010). The 8.2 ka event: Abrupt transition of the subpolar gyre toward a modern North Atlantic circulation. *Geochemistry, Geophysics, Geosystems*, 11:Q06011.

Born, A., Nisancioglu, K. H., and Braconnot, P. (2010b). Sea ice induced changes in ocean circulation during the Eemian. *Climate Dynamics*, online.

Born, A., Nisancioglu, K. H., Risebrobakken, B., and Levermann, A. (2010c). Late Eemian warming in the Nordic Seas as seen in proxy data and climate models. *Paleoceanography*, in revision.

Braconnot, P., Marzin, C., Grégoire, L., Mosquet, E., and Marti, O. (2008). Monsoon response to changes in Earth's orbital parameters: comparisons between simulations of the Eemian and of the Holocene. *Climate of the Past*, 4:281–294.

Danabasoglu, G. (2008). On Multidecadal Variability of the Atlantic Meridional Overturning Circulation in the Community Climate Model Version 3. *Journal of Climate*, 21:5524–5544.

Delworth, T. L., Manabe, S., and Stouffer, R. J. (1993). Interdecadal variations of the thermohaline circulation in a coupled ocean-atmosphere model. *Journal of Climate*, 6:1993–2011.

Delworth, T. L. and Mann, M. E. (2000). Observed and simulated multidecadal variability in the Northern Hemisphere. *Climate Dynamics*, 16:661–676.

Dijkstra, H. A., te Raa, L., Schmeits, M., and Gerrits, J. (2006). On the physics of the Atlantic Multidecadal Oscillation. *Ocean Dynamics*, 56:36–50.

Fichefet, T. and Maqueda, M. A. M. (1997). Sensitivity of a global sea ice model to the treatment of ice thermodynamics and dynamics. *Journal of Geophysical Research*, 102:12,609.

Fichefet, T. and Maqueda, M. A. M. (1999). Modelling the influence of snow accumulation and snow-ice formation on the seasonal cycle of the Antarctic sea-ice cover. *Climate Dynamics*, 15:251–268.

Ganopolski, A. and Rahmstorf, S. (2001). Simulation of rapid glacial climate changes in a coupled climate model. *Nature*, 409:153–158.

Gent, P. R. and McWilliams, J. C. (1990). Isopycnal mixing in Ocean Circulation Models. *Journal of Physical Oceanography*, 20:150–155.

Goddard, L., Baethgen, W., Kirtman, B., and Meehl, G. (2009). The Urgent Need for Improved Models and Predictions. *EOS*, 90:343.

Guemas, V. and Salas-Melia, D. (2008). Simulation of the Atlantic Meridional Overturning Circulation in an Atmosphere-Ocean Global Coupled Model. Part I : A mechanism governing the variability of ocean convection in a preindustrial experiment. *Climate Dynamics*, 31:29–48.

Häkkinen, S. and Rhines, P. B. (2004). Decline of subpolar North Atlantic circulation during the 1990s. *Science*, 304:555–559.

Hátún, H., Payne, M. R., and Jacobsen, J. A. (2009). The North Atlantic subpolar gyre regulates the spawning distribution of blue whiting (Micromesistius poutassou). *Canadian Journal of Fisheries and Aquatic Sciences*, 66 (5):759–770.

Hátún, H., Sandø, A. B., Drange, H., Hansen, B., and Valdimarsson, H. (2005). Influence of the Atlantic Subpolar Gyre on the Thermohaline Circulation. *Science*, 309:1841–1844.

Hibler, W. D. (1979). A Dynamic Thermodynamic Sea Ice Model. *Journal of Physical Oceanography*, 9:815–846.

Hourdin, F., Musat, I., Bony, S., Braconnot, P., Codron, F., Dufresne, J., Fairhead, L., Filiberti, M., Friedlingstein, P., Grandpeix, J., Krinner, G., Levan, P., Li, Z., and Lott, F. (2006). The LMDZ4 general circulation model: climate performance and sensitivity to parametrized physics with emphasis on tropical convection. *Climate Dynamics*, 27(7-8):787–813.

IPCC (2007). *Climate Change 2007: The Physical Science Basis. Contribution of Working Group I to the Fourth Assessment Report of the Intergovernmental Panel on Climate Change. [S. Solomon and D. Qin and M. Manning and Z. Chen and M. Marquis and K. B. Averyt and M. Tignor and H. L. Miller (eds.)]*. Cambridge University Press, Cambridge, United Kingdom and New York, NY, USA.

Jungclaus, J. H., Haak, H., Latif, M., and Mikolajewicz, U. (2005). Arctic-North Atlantic interactions and multidecadal variability of the meridional overturning circulation. *Journal of Climate*, 18:4013–4031.

Keenlyside, N. S., Latif, M., Jungclaus, J., Kornblueh, L., and Roeckner, E. (2008). Advancing decadal-scale climate prediction in the North Atlantic sector. *Nature*, 453:84–88.

Kerr, R. A. (2000). A north atlantic climate pacemaker for the centuries. *Science*, 288:1984–1986.

Krinner, G., Viovy, N., de Noblet-Ducoudre, N., Ogee, J., Polcher, J., Friedlingstein, P., Ciais, P., Sitch, S., and Prentice, I. C. (2005). A Dynamic Global Vegetation Model for Studies of the Coupled Atmosphere - Biosphere System. *Global Biogeochemical Cycles*, 19(1):GB1015.

Kuijpers, A., Malmgren, B. A., and Seidenkrantz, M.-S. (2009). Termination of the Medieval Warm Period: linking subpolar and tropical North Atlantic circulation changes to ENSO. *PAGES news*, 17(2):76–77.

Latif, M., Collins, M., Pohlmann, H., and Keenlyside, N. (2006). A review of predictability studies of the Atlantic sector climate on decadal time scales. *Journal of Climate*, 19 (23):5971–5987.

Levermann, A. and Born, A. (2007). Bistability of the Atlantic subpolar gyre in a coarse-resolution model. *Geophysical Research Letters*, 34:L24605.

Levermann, A., Mengel, M., and Born, A. (2010). Dynamic threshold may enhance variability of subpolar gyre. *in prep.*

Lohmann, K., Drange, H., and Bentsen, M. (2009a). A possible mechanism for the strong weakening of the North Atlantic subpolar gyre in the mid-1990s. *Geophysical Research Letters*, 36:L15602.

Lohmann, K., Drange, H., and Bentsen, M. (2009b). Response of the North Atlantic subpolar gyre to persistent North Atlantic oscillation like forcing. *Climate Dynamics*, 32:273–285.

Madec, G., Delecluse, P., Imbard, M., and Lévy, C. (1997). *OPA version 8.1 Ocean General Circulation Model Reference Manual*. Institut Pierre-Simon Laplace, Note du Pôle de modélisation n^{o}11.

Marti, O., Braconnot, P., Dufresne, J.-L., Bellier, J., Benshila, R., Bony, S., Brockmann, P., Cadule, P., Caubel, A., Codron, F., de Noblet, N., Denvil, S., Fairhead, L., Fichefet, T., Foujols, M.-A., Friedlingstein, P., Goosse, H., Grandpeix, J.-Y., Guilyardi, E., Hourdin, F., Idelkadi, A., Kageyama, M., Krinner, G., Lévy, C., Madec, G., Mignot, J., Musat, I., Swingedouw, D., and Talandier, C. (2010). Key features of the IPSL ocean atmosphere model and its sensitivity to atmospheric resolution. *Climate Dynamics*, 34:1–26.

Pohlmann, H., Botzet, M., Latif, M., Wild, M., and Tschuck, P. (2004). Estimating the long-term predictability potential of a coupled AOGCM. *Journal of Climate*, 17:4463–4472.

Ren, J., Jiang, H., Seidenkrantz, M.-S., and Kuijpers, A. (2009). A diatom-based reconstruction of Early Holocene hydrographic and climatic change in a southwest Greenland fjord. *Marine Micropaleontology*, 70:166–176.

Roullet, G. and Madec, G. (2000). Salt conservation, free surface, and varying levels: A new formulation for ocean general circulation models. *Journal of Geophysical Research*, 105:23927–23942.

Sachs, J. P. (2007). Cooling of Northwest Atlantic slope waters during the Holocene. *Geophysical Research Letters*, 34:L03609.

Smith, D. M., Cusack, S., Colman, A. W., Folland, C. K., Harris, G. R., and Murphy, J. M. (2007). Improved Surface Temperature Prediction for the Coming Decade from a Global Circulation Model. *Science*, 317:796–799.

Spall, M. A. (2008). Low-frequency interaction between horizontal and overturning gyres in the ocean. *Geophysical Research Letters*, 35:L18614.

Swingedouw, D., Braconnot, P., Delecluse, P., Guilyardi, E., and Marti, O. (2007a). Quantifying the AMOC feedbacks during a $2\times CO_2$ stabilization experiment with land-ice melting. *Climate Dynamics*, 29:521–534.

Swingedouw, D., Braconnot, P., Delecluse, P., Guilyardi, E., and Marti, O. (2007b). The impact of global freshwater forcing on the thermohaline circulation: adjustment of North Atlantic convection sites in a CGCM. *Climate Dynamics*, 28:291–305.

Thornalley, D. J. R., Elderfield, H., and McCave, I. N. (2009). Holocene oscillations in temperature and salinity of the surface North Atlantic. *Nature*, 457:711–714.

Wiersma, A. P., Renssen, H., Goosse, H., and Fichefet, T. (2006). Evaluation of different freshwater forcing scenarios for the 8.2 ka BP event in a coupled climate model. *Climate Dynamics*, 27:831–849.

Wu, P. and Wood, R. A. (2008). Convection induced long term freshening of the subpolar North Atlantic Ocean. *Climate Dynamics*, 31:941–956.

Yoshimori, M., Raible, C. C., Stocker, T. F., and Renold, M. (2010). Simulated decadal oscillations of the Atlantic meridional overturning circulation in a cold climate state. *Climate Dynamics*, 34:101–121.

Zheng, W., Braconnot, P., Guilyardi, E., Merkel, U., and Yu, Y. (2008). ENSO at 6ka and 21ka from ocean-atmosphere coupled model simulations. *Climate Dynamics*, 30(7-8):745–762.